UNIVERSITY OF CALIFORNIA SAN DIEGO

Thrombomodulin Binding to Thrombin Reveals the Backbone Dynamics Required for the Serine Protease Catalytic Mechanism

A dissertation submitted in partial satisfaction of the

requirements for the degree Doctor of Philosophy

in

Chemistry

by

Riley Bryant Peacock

Committee in charge:

Professor Elizabeth A. Komives, Chair
Professor Michael Burkart
Professor Edward Dennis
Professor Susan Taylor
Professor Joann Trejo

2020

The dissertation of Riley Bryant Peacock is approved, and it is acceptable in quality and form for publication on microfilm and electronically:

_____

_____

_____

_____

_____

Chair

University of California San Diego

2020

DEDICATION

I dedicate this work to my many teachers,

and to the giants -large and small- whose backs I will always stand on.

TABLE OF CONTENTS

LIST OF ABBREVIATIONS

Å	Angstrom
ABE1	Anion Binding Exosite 1
ABE2	Anion Binding Exosite 2
D	Dalton
DSC	Differential Scanning Calorimetry
EDTA	Ethylenediaminetetraacetic Acid
EGF-like	Epidermal Growth Factor-like
EGRCK	D-Glu-Gly-Arg chloromethylketone
FPLC	Fast Protein Liquid Chromatography
HSQC	Heteronuclear Single Quantum Coherence
$k$ex	Rate constant for exchange
k_a	Association rate constant
K_a	Association equilibrium constant
k_d	Dissociation rate constant
K_d	Dissociation equilibrium constant
NMR	Nuclear Magnetic Resonance
PDB	Protein Data Bank
PPACK	D-Phe-Pro-Arg chloromethylketone
TCEP	tris-carboxyethylphosphine
TFA	Trifluoroacetic Acid
TM	Thrombomodulin

TM45	The fourth and fifth EGF-like domains of thrombomodulin
TM456	The fourth, fifth and sixth EGF-like domains of thrombomodulin
TM56	The fifth and sixth EGF-like domains of thrombomodulin
PAR	Protease activated receptor
CT	Chymotrypsin
Seq	Sequential
AMD	Accelerated Molecular Dynamics
HDXMS	Hydrogen Deuterium Exchange Mass Spectrometry
WT	Wild Type
CPMG	Curr-Purcell-Meiboom-Gill

LIST OF FIGURES

LIST OF TABLES

ACKNOWLEDGEMENTS

I thank my parents, Cheryl and Michael, for each being my deepest examples of resilience, and for instilling in me the self-confidence and drive to achieve any goal I set my mind to. I thank my partner, Lara, for being a bottomless source of love and support through the darkness and the light. I thank my friends and loved ones for keeping me human as I pursued my endeavors. I thank my mentor, my colleague, and my friend Dr. Elizabeth (Betsy) Komives. If not for you, I would not have had this opportunity to become so strong. My only hope is that I can pay forward to others the great fortune you have all bestowed upon me.

Chapter II, in full, is a reprint that the dissertation author was the principal researcher and author of. The material has been submitted to *PNAS*. **Peacock RB**, McGrann T, Tonelli M, Komives EA. (2020). Serine Protease Dynamics Revealed by NMR Analysis of the Thrombin-Thrombomodulin Complex. *PNAS*. (Submitted)

Chapter III, in full, is a reprint that the dissertation author was the principal researcher and author of. The material appears in *Biochemistry*. **Peacock RB**, Davis JR, Markwick PRL, Komives EA. (2018). Dynamic Consequences of Mutation of Tryptophan 215 in Thrombin. *Biochemistry*. 57(18):2694-2703.

Chapter IV, in full, is a reprint that the dissertation author was the principal researcher and author of. The material has been submitted to *Biochemsitry*. Peacock RB, McGrann T, Zaragoza S, Komives EA. (2020). Mutation of W215A/E217A in Thrombin Interrupts the Allosteric Activity of Thrombomodulin. *Biochemistry*. (Submitted).

VITA

2015 Bachelors of Science, Chemistry and Biochemistry, Gonzaga University, Spokane, WA

2017 Masters of Science, Chemistry, University of California San Diego, CA

2020 Doctorate of Philosophy, Chemistry, University of California San Diego, CA

PUBLICATIONS

Peacock RB, McGrann T, Tonelli M, Komives EA. Serine Protease Dynamics Revealed by NMR Analysis of the Thrombin-Thrombomodulin Complex. PNAS. 2020 (submitted).

Peacock RB, McGrann T, Zaragoza S, Komives EA. Mutation of W215A/E217A in Thrombin Interrupts the Allosteric Activity of Thrombomodulin. Biochemistry. 2020 (submitted).

Markwick PRL, **Peacock RB**, Komives EA. Accurate Prediction of Amide Exchange in the Fast Limit Reveals Thrombin Allostery. Biophys J. 2019 Jan 8;116(1):49-56.

Peacock RB, Davis JR, Markwick PRL, Komives EA. Dynamic Consequences of Mutation of Tryptophan 215 in Thrombin. Biochemistry. 2018 May 8;57(18):2694-2703.

FIELDS OF STUDY

Major Field: Biochemistry

Studies in Biochemistry and Biophysics

Professor Elizabeth A. Komives

HONORS AND AWARDS

2017-2018	NIH Molecular Biophysics Training Grant Trainee, University of California San Diego
2016	Teaching Assistant Excellence Award, University of California San Diego
2015	Teaching Assistant Excellence Award, University of California San Diego
2015	American Institute of Chemists Outstanding Chemistry Senior Award, Gonzaga University
2011-2015	Ignatian Leaders Scholarship, Gonzaga University

ABSTRACT OF THE DISSERTATION

Thrombomodulin Binding to Thrombin Reveals the Backbone Dynamics Required for the Serine Protease Catalytic Mechanism

by

Riley Bryant Peacock

Doctor of Philosophy in Chemistry

University of California San Diego, 2020

Professor Elizabeth A. Komives, Chair

The serine protease thrombin plays an essential regulatory role in blood clotting. Prothrombin is converted to the active α-thrombin in response to tissue damage, allowing the enzyme to cleave procoagulative substrates such as fibrinogen and PAR, enabling the formation of the clot. On the other hand, when thrombin binds its protein cofactor thrombomodulin (TM), the enzyme loses substrate specificity for procoagulative substrates, and engages the anticoagulative pathway by selectively

targeting the substrate protein C for proteolytic activation. Despite decades of study, the mechanism by which TM enables thrombin to cleave protein C has yet to be fully characterized, indicating a need for further investigation. Crystallographic evidence shows no notable difference between the thrombin and thrombin-TM structures, suggesting the influence of TM is dynamic in nature. The work presented in this thesis uses two biophysical techniques, hydrogen-deuterium exchange mass spectrometry (HDXMS) and nuclear magnetic resonance spectrometry (NMR) to report the effects of TM on thrombin dynamics.

In Chapter II, HDXMS and NMR were used to evaluate the regions of thrombin effected by the presence of TM. The results show two paths of communication between the active site and TM binding site of thrombin, as well as large scale conformational changes throughout all of thrombin. From these data we generated a model of the dynamic influence of TM on thrombin that describes the global protein dynamics necessary for the execution of the serine protease catalytic mechanism.

Chapter III presents a study of the dynamics of the W215A thrombin mutant using HDXMS. Previous studies have shown that mutations at Trp 215 impart dramatic changes to the substrate specificity of thrombin, and the W215A mutation appeared to favor protein C activation over procoagulative substrate activation. We found that alterations to the hydrophobic environment at and around Trp 215 increased the dynamics of the surrounding thrombin loops, as well as the N-terminus of the thrombin heavy chain over 10 Å away from the sites of mutation.

In Chapter IV, the dynamics of the W215A/E217A mutant was investigated in the presence and absence of TM through HDXMS. The W215A/E217A mutant heavily prefers protein C over procoagulative thrombin substrates, causing us to ask whether TM binding recovers the destabilizing effects of these mutations. We found that TM was capable of stabilizing parts of the W21A/E217A thrombin mutant, but could not recover the increased dynamics of the primary substrate recognition pocket. These results suggest that the primary cause of the decreased activity of the W215A/E217A mutant towards procoagulative substrates results from the mutation of Trp 215, which is not important recognition element for protein C binding but is so for procoagulative substrates.

Chapter I

Introduction

A. Thrombin as a Regulator of Blood Clotting

Blood clotting is a key defense mechanism evolved by deuterostomes[1]. As a result, vascular injury, tissue factor and factor VIIa interact to form a protein complex with full protease activity, leading to the proteolytic cleavage -and thereby activation- of other serine proteases in the blood. The ultimate protease activated by the resulting clotting cascade is the zymogenic enzyme prothrombin, which converts to α-thrombin after being cleaved at two distinct locations[2, 3]. Prothrombin circulates in the blood as a readily-available inactive enzyme that undergoes a structural reorganization upon activation that results in the catalytically-active α-thrombin species[4], which will be referred to as simply "thrombin" from here on out.

Similar to the other proteases that participate in the clotting cascade, thrombin activates its protein substrates via proteolytic cleavage. Thrombin engages its procoagulative function by participating in the activation of upstream members of the clotting cascade -thereby generating more thrombin- and by activating key proteins that are directly involved in the formation of the clot. For example, the thrombin-mediated proteolytic conversion of fibrinogen to fibrin and the cleavage of protease activated receptors (PAR) on the surface of platelets allows for the formation of insoluble clot containing fibrin mesh and platelets at the site of the wound[2]. However, once thrombin associates with its protein cofactor thrombomodulin (TM), it loses affinity for procoagulative substrates, and instead engages an anticoagulative function by increasing the activity of thrombin towards protein C by a factor of over 1000[5]. Activated protein C cleaves -and thereby deactivates- essential cofactors of the coagulation cascade, resulting in a decrease in

the generation of more thrombin. Thus, the substrate targets of thrombin have direct effects on both the propagation and silencing of the coagulative response, categorizing thrombin as a key regulatory element of blood clotting.

B. The Dynamic Structure and Function of Thrombin

Thrombin is a protease from the chymotrypsin family, which share a similar protein fold, as well as the canonical His57$_{CT}$-Asp102$_{CT}$-Ser195$_{CT}$ catalytic triad endogenous to all serine proteases[4]. Because of these homologous characteristics, serine proteases are thought to all utilize the same catalytic steps to achieve their proteolytic function[6]. An aligned catalytic triad allows the electron-rich carboxylate sidechain of Asp 102$_{CT}$ to pull at the proton involved in the imidazole group of His 57$_{CT}$, increasing the pKa of the imidazole ring of His 57$_{CT}$. The proton of the Ser 195$_{CT}$ hydroxyl group is abstracted by the nitrogen moiety in the imidazole ring of His 57$_{CT}$, causing the Ser 195 sidechain to increase in nucleophilicity. The resulting Ser 195 hydroxylate group is primed to attack the backbone carbonyl carbon of a substrate protein bound at the protease active site, resulting in a tetrahedral intermediate species involving a covalent bond linking the substrate to the enzyme. The collapse of this intermediate allows the N-terminal substrate fragment to be released from the protease, leaving behind a relatively stable acyl enzyme intermediate species that is unable to bind nor cleave additional substrate molecules.

To return to a catalytically functional state, a water molecule from the solvent must enter to protease active site and attack the acyl enzyme carbonyl carbon forming a second tetrahedral intermediate[6]. The collapse of this intermediate could

result in either the release of the water molecule or the release of the C-terminal substrate fragment. The mechanistic barriers to the productive release of the C-terminal substrate fragment are significantly more limiting than those acting on the initial attack by Ser 195 and the subsequent release of the N-terminal substrate fragment, which is why this is considered the rate limiting step in the peptide cleavage reaction catalyzed by serine proteases.

Though different proteases have evolved to cleave proteins at distinct peptide sequence recognition sites dictated by the amino acid identities that form their S1-S4 polypeptide binding sites, all serine proteases share a common substrate binding site located in the cleft that forms between the N-terminal and C-terminal β-barrels that make up the core of these proteins. Thrombin specifically recognizes and cleaves the amide bond C-terminal to the basic amino acid, arginine, in the peptide sequence[4]. However, thrombin also demonstrates additional elements of substrate specificity through the utilization of a distal, secondary site on the enzyme that coordinates substrate binding in conjunction with the primary binding located at the active site. This secondary binding site is named the anion binding exosite 1 (ABE1) because it contains many positively charged amino acids. ABE1 is formed by two regions of thrombin referred to as the 30_{CT} and $70s_{CT}$ loops.

In addition to the loops that make up ABE1, thrombin contains a number of loops thought to be involved in substrate binding and enzymatic regulation. The $30s_{CT}$ and $70s_{CT}$ loops make up ABE1, the $60s_{CT}$ loop is adjacent to His 57_{CT}, the 90s loop is adjacent to Asp 102_{CT}, the $140s_{CT}$ loop appears to be involved in substrate recognition, the $170s_{CT}$ loop appears to contribute to the stabilization and

formation of the primary substrate pocket, and the 180s$_{CT}$ and 220s$_{CT}$ loops are involved in chelating a sodium ion and the formation of the S1 pocket[2, 4, 7-11]. Despite these observations, our understanding of the roles played by each of these loops is rather limited. The loops of thrombin are particularly interesting regions because they each contain sequence insertions that are only found in thrombin[12, 13].

In addition to the theories regarding how the loops of thrombin regulate substrate interactions, biophysical experiments have shown these loops to be particularly dynamic, and the particular behavior of these dynamics appear to be dependent on the molecules and ions that interact with thrombin[8, 14-20]. These studies have revealed the dynamic motions exhibited by the loops that contribute to the formation of the thrombin active site are linked to the dynamics of ABE1. Thus, the sequence insertions that structurally distinguish thrombin from other serine proteases are likely evolutionary developments that not only participate in substrate recognition, but also help shape the thrombin conformational landscape to enable allosteric communication between the primary and secondary substrate binding sites.

C. Thrombomodulin as a Modulator of Thrombin Activity

All of the procoagulative substrates of thrombin bind simultaneously to both the primary substrate binding site at the active site and to ABE1[2]. However, protein C -anticoagulative thrombin substrate- binds at the primary active site only when TM is present[21]. The commonly accepted explanation for why thrombin loses

specificity towards procoagulative substrates when TM is present is that these proteins share a common binding site at ABE1, but TM binding is able to out-compete other proteins as TM also binds to ABE1 and with higher affinity (~1 nM) than procoagulative substrates (e.g. fibrin: ~1 μM)[22]. However, it is less clear why thrombin shows very poor activity towards protein C in the absence of TM, yet demonstrates an >1000x increase in protein C activation when TM is present[21].

TM is a glycoprotein found on the endothelial surface of blood vessels. Though TM has six EGF-like domains, only domains 5 and 6 are involved in the binding interaction with thrombin. However, to invoke the full boost in thrombin activity towards protein C, the 4th EGF-like domain must also be present[23, 24]. Though a crystal structure of thrombin bound to the 4th, 5th, and 6th domains of TM (TM456) exists, the thrombin conformation when TM456 is bound is indistinguishable from that of thrombin alone[4, 25]. Thrombin and thrombin-TM456 alike required the presence of peptide-like active site inhibitors that covalently modify the active site Ser 195$_{CT}$ to allow for X-ray crystallography to be performed on wild-type (WT) thrombin.

Accelerated molecular dynamics (AMD) simulations have shown that the bound TM456 induces strongly correlated motions between TM and the thrombin active site [16], and hydrogen-deuterium exchange mass spectrometry (HDXMS) experiments on the thrombin-TM456 complex have been used to observe TM-induced changes in thrombin dynamics across the enzyme[18]. HDXMS is a powerful technique for studying protein dynamics[26], but provides limited information for singular domain proteins like thrombin as this method cannot report on regions that

are not solvent exposed, such as the hydrophobic protein core. Thus, the motivation behind my thesis work and graduate training has been to utilize HDXMS in conjunction with nuclear magnetic resonance (NMR) to characterize the effect of TM binding on the dynamics of thrombin in order to identify the mechanism behind the TM-induced catalytic boost thrombin exhibits towards protein C.

Chapter II

Serine protease dynamics revealed by NMR analysis of the thrombin-thrombomodulin complex

Serine protease dynamics revealed by NMR analysis of the thrombin-thrombomodulin complex

Riley B. Peacock[1], Taylor McGrann[1] Marco Tonelli[2], and Elizabeth A. Komives[1*]

[1]Department of Chemistry and Biochemistry, University of California, San Diego, 9500 Gilman Drive, La Jolla, CA 92093-0378.

[2] NMRFAM University of Wisconsin, 433 Babcock Drive, Madison, WI 53706.

*Corresponding author: Elizabeth A. Komives

Department of Chemistry and Biochemistry, University of California, San Diego, 9500 Gilman Drive, La Jolla, CA 92092-0378

Ph: (858) 534-3058

Email: ekomives@ucsd.edu

Keywords: serine protease, protein dynamics, nuclear magnetic resonance, relaxation dispersion, allostery

A. ABSTRACT

Serine proteases catalyze peptide bond cleavage through a multi-step mechanism involving acid-base and covalent catalysis. It has long been assumed that they do this without the need for conformational rearrangement of what appears to be their stable two-β-barrel structure. Unlike the pro-coagulative activity of thrombin which requires fibrinogen engagement at both the allosteric site and the active site, TM binds at the allosteric site enabling thrombin to cleave protein C bound only at the active site. Despite decades of study, one question remains: why is TM binding a requirement for thrombin to cleave protein C? Accelerated molecular dynamics (AMD) simulations predicted that TM binding changes the μs-ms thrombin dynamics in a way that correlates motions of the catalytic triad with other regions of the enzyme. To investigate whether TM changes thrombin dynamics, we performed nuclear magnetic resonance (NMR) and hydrogen deuterium exchange mass spectrometry (HDX-MS) experiments on the thrombin-TM456 complex, and we compared the results to previous studies on apo-thrombin and PPACK-thrombin. Our results show that TM reduces μs-ms motions in the substrate binding (S1) pocket consistent with acceleration of PC binding. TM also induced μs-ms motions in a β-strand connecting the TM binding site to the catalytic aspartate. Finally, TM induced motions that were slow on the NMR timescale in residues along the interface between the two β-barrels, a motion that may be responsible for the slow step involving release of the N-terminal product and entry of the water molecule required for hydrolysis of the acyl-enzyme intermediate.

B. Introduction

Serine proteases provide textbook examples of enzyme catalysis since the first crystal structure of chymotrypsin was solved in 1967[27]. The well-known catalytic triad, the S1 substrate-binding pocket, and the oxy-anion hole provide nucleophilic and acid-base catalysis and the myriad of crystal structures with highly similar structures have led to the idea that serine proteases can do their catalysis without moving. We have been studying the serine protease, thrombin, which catalyzes the last step of the blood-clotting protease cascade. The crystal structure of α-thrombin reveals the canonical chymotrypsin (CT) fold, comprised of an N-terminal and a C-terminal β-barrel, as well as an aligned catalytic triad containing His 57_{CT} (79_{seq}), Asp 102_{CT} (135_{seq}), and Ser 195_{CT} (241_{seq}) [4]. The proteolytic cleavage of the zymogen, prothrombin, generates the new N-terminus of the thrombin heavy chain, which is observed to be inserted into Ile cleft forming a key interaction with Asp 194 and positioning Ser 195 for catalysis [28-30].

Using hydrogen-deuterium exchange mass spectrometry (HDX-MS), we previously showed, however, that the new N-terminal peptide is highly exchanging in the absence of the covalent active site inhibitor D-Phe-Pro-Arg-chloromethylketone (PPACK) [18]. In fact, binding of PPACK reduced exchange throughout the thrombin molecule. Similarly, NMR experiments comparing apo- and PPACK-thrombin showed that the presence of PPACK leads to the appearance of many, strong resonances that are either weak or absent in the apo-thrombin spectrum [14, 17]. A number of thrombin resonances remained absent from HSQC spectra of PPACK thrombin in multiple NMR experiments [15, 19]. These missing resonances

were largely localized to the loop regions of thrombin, which are the main structural elements that distinguish thrombin from CT, suggesting that the thrombin structure remains dynamic even when inhibited at the active site. HDX-MS and accelerated molecular dynamics (AMD) simulations also reported the loops of thrombin to be conformationally dynamic [14, 16-18]. In addition, Carr-Purcell-Meiboom-Gill (CPMG) experiments revealed a large number of backbone NH groups undergo μs-ms motions throughout apo thrombin and a pathway of residues retain these motions in PPACK thrombin [17].

The loops of thrombin have been shown to play important roles in thrombin activity. Residues from the $170s_{CT}$, $180s_{CT}$, and $220s_{CT}$ loops have been implicated in the Na^+-mediated allosteric activation of thrombin through the structuring of the S1 binding site that results from the presence of a Na^+ ion bound in this region [9, 31]. Residues within the $30s_{CT}$ and $70s_{CT}$ loops interact with the thrombin cofactor thrombomodulin (TM). TM binding toggles the substrate specificity of thrombin away from pro-coagulative substrates that encourage clotting once proteolytically cleaved by thrombin, and towards the anticoagulative thrombin substrate protein C, which acts to shut down the clotting cascade once activated by thrombin[32]. Though TM contains multiple domains, the TM456 fragment containing only the 4^{th}, 5^{th}, and 6^{th} EGF-like domains of TM is able to invoke the full anticoagulative activity of thrombin [24, 33]. Interestingly, the active site inhibitor GGACK was required to solve the crystal structure of thrombin bound to TM456 [25]. Surface plasmon resonance reported rapid association and dissociation rates ($6.7x10^6\ M^{-1}\ s^{-1}$ and $0.033\ s^{-1}$ respectively) for the interaction of TM456 with thrombin [34], and Isothermal titration

calorimetry (ITC) showed that TM456-binding is primarily driven by a change in entropy rather than enthalpy [20, 35]. HDX-MS experiments have reported reductions in amide exchange in regions of thrombin distant from the TM-binding site, characterizing TM as an allosteric activator of thrombin [16, 18].

Though multiple studies have investigated the impact of TM binding on thrombin dynamics, there is still no clear explanation as to how TM binding modulates the catalytic activity of the protease. Here we report both HDX-MS and NMR Carr-Purcell-Meiboom-Gill (CPMG) experiments to characterize the dynamic consequences of TM456 binding to thrombin on the μs-ms timescale. HDX-MS can measure changes in the dynamics of solvent-exposed regions of a protein [36, 37], while NMR CPMG experiments give information on the motional dynamics of individual residues [38, 39]. Through the complimentary use of these two biophysical methods, we report the identities of the thrombin residues that facilitate allosteric communication between the TM binding site, the catalytic residues, and the S1 binding pocket. These results show that TM binding remodels thrombin dynamics on multiple timescales.TM promotes thrombin substrate binding while also promoting the conformational flexibility required for the mechanistic steps of the serine protease reaction.

C. RESULTS

Resonance assignments and chemical shift perturbations. We previously reported resonance assignments, backbone dynamics and CPMG analysis of the μs-ms motions for apo thrombin [17] and PPACK thrombin [15, 17]. Here we have analyzed

the complex between apo thrombin and the fully-active fragment of thrombomodulin, TM456 which we previously reported [18]. Here we report a comprehensive experimental analysis of thrombin in complex with TM456 wherein we integrate HDX-MS and NMR data to understand the multiple timescales of motion relevant to the mechanism by which TM alters the catalytic activity of thrombin. For PPACK-thrombin, 82% of the amino acids could be assigned whereas for apo-thrombin only 73% could be assigned. The thrombin-TM456 spectra more closely resembled the apo-thrombin and a similar percentage of amino acids could be assigned. Notably we assigned every single cross peak in the spectra, so missing cross peaks are likely due to conformational heterogeneity. Nine residues- clustered around the N-terminal β-barrel and the S1 pocket- which were missing from the apo-thrombin spectra could be assigned in thrombin-TM456. These nine residues were also observed in PPACK-thrombin HSQC spectra. Interestingly, four assignments were present in the apo-thrombin spectrum that were missing from the thrombin-TM456 spectra, and these were all located within the C-terminal β-barrel.

There were 23 residues with resonances TM456 showing multiple peaks in the thrombin-TM456 spectra, while the resonances for these same assignments in the apo and PPACK spectra were singlets. Often, one peak of the multiplet corresponded to the equivalent resonance in apo-thrombin (Figure 2.1). All of these assignments were verified by backbone walk using HNCA, HNCO, and HNCOCA spectra. The appearance of these multiplet resonances suggested that the presence of TM456 induces motions that are slow on the NMR timescale ($< 80\ s^{-1}$) in these residues.

The TM binding site remains dynamic when TM is present. Despite the stabilization of thrombin afforded by PPACK binding [20], resonances corresponding to the N-terminus of the heavy chain Ile 16_{CT} (37seq) and nearly all of the residues in the $30s_{CT}$ (residues 54 – 61seq) and $70s_{CT}$ (residues 97 – 113seq) loops as well as residues $151\text{-}156_{CT}$ (193-197seq), and the $220s_{CT}$ loop $221\text{-}221A_{CT}$ (268-269seq) were not observed in previous NMR experiments on PPACK-thrombin or apo-thrombin [15, 17]. Cross peaks for these residues were also not observed in the thrombin-TM456 spectrum collected for this study. We were, however, able to learn about the solvent accessibility/dynamics of these loops from HDX-MS, which reported on 99% of the thrombin sequence for experiments on WT-thrombin with TM456 either present or absent (Figure 2.2). The HDX-MS experiments showed a ~3 deuteron decrease in exchange of residues $66\text{-}84_{CT}$ (97-116seq; MH+ 2473.357) in the $70s_{CT}$ loop within 1 min when TM456 was present, consistent with the exclusion of solvent due to TM456 binding [Figure 2.3A-B]. Interestingly, this binding site "protection" was transient, becoming less over the 5 min time course of the HDX experiment suggesting that this region remains dynamic, which is consistent with our inability to observe resonances for the $70s_{CT}$ loop in the NMR. We did observe resonances for Ile 82_{CT} (114seq) and Met 84_{CT} (116seq) in the β-sheet following the $70s_{CT}$ loop and CPMG curves for these two residues showed they are each moving on the μs-ms timescale (Figure 2.3A, C).

The thrombin C-terminal β-barrel becomes more dynamic when TM is bound. Ten residues within the thrombin N-terminal β-barrel experienced more significant motions on the μs-ms timescale when TM456 was present. A subgroup of

these residues was distributed along two antiparallel β-strands that connect the thrombin $70s_{CT}$ and $90s_{CT}$ loops (Figure 2.4A). HDX-MS showed residues 106-114_{CT} (139-147seq; MH+ 1061.654) were more protected from deuterium exchange (by ~1 deuteron) when TM456 was present (Figure 2.4B). Interestingly, CPMG experiments showed that TM456 induces μs-ms motions in four residues within this segment (Figure 2.4C). This subgroup of residues also included Leu 105_{CT} (138seq), suggesting that the dynamic modulation induced by TM456 may be transferred into the catalytic Asp 102_{CT} (189seq) through these antiparallel β-strands. Resonances corresponding to Ile 88 and Tyr 89_{CT} (120-121seq) located directly across from Leu 105_{CT} and Met 106_{CT} in the neighboring β-strand could be assigned in the apo-thrombin spectrum, but were absent in the thrombin-TM456 spectrum supporting the claim that the residues in this region are undergoing μs-ms timescale motions. Although we could assign Asp 102_{CT} (189seq), CPMG analysis could not be performed due to the presence of overlapped resonances. In addition, residues within these same antiparallel β-strands showed peak multiplets (Figure 2.4D). Thus, TM456 appeared stabilize the end of the β-strand leading to the catalytic Asp 102_{CT} (189seq), yet also induced μs-ms dynamic motions within this strand and the neighboring strand. These results provide definitive evidence for dynamic communication between the $70s_{CT}$ loop where TM binds and the catalytic residues in the active site of thrombin.

TM binding allosterically reduces the dynamics of the S1 pocket, and also induces a slow time scale conformational change in the N-terminal β-barrel. In the thrombin-TM456 complex, HDX-MS revealed slowed dynamics of the $170s_{CT}$,

180s$_{CT}$, and 220s$_{CT}$ loops of thrombin despite the >20 Å distance between the TM binding site and these loops. Upon TM456 binding, decreased exchange of ~1 deuteron was observed for the 170s$_{CT}$ loop residues 161-180$_{CT}$ (202-221seq; MH+2343.227) and of ~2 deuterons for the 180s$_{CT}$ loop residues 182-198$_{CT}$ based on subtraction of deuterium uptake into residues 198-207$_{CT}$ (244-255seq; MH+ 1522.762) from uptake into residues 182-207$_{CT}$ (223-255seq; MH+ 3575.589)). Finally, a decreased exchange of ~1.5 deuterons was observed for the 220s$_{CT}$ loop residues 212-227$_{CT}$ (260-275seq; MH+ 1788.801) (Figure 2.5A, C). CPMG analysis identified seven residues within these loops showed significantly decreased μs-ms motions when TM456 was present as compared to apo-thrombin (Figure 2.5B, C).

Val 158$_{CT}$ and Asn 159$_{CT}$ are in the center of the β-strand coming from the 140s$_{CT}$ loop and leading to the 170s$_{CT}$ loop (Figure 2.6A). A stack of three valines (residues 158$_{CT}$ (199seq), 138$_{CT}$ (174seq) and 213$_{CT}$ (261seq)) forms one side of the hydrophobic core of the C-terminal β-barrel (Figure 2.6A). Val 158$_{CT}$ (199seq) moves on the μs-ms timescale in all three thrombin states (Figure 2.6B). Val 138$_{CT}$ (174seq) also showed μs-ms timescale motions in apo thrombin, but this resonance became a doublet in the thrombin-TM456 HSQC spectrum (Figure 2.6C). Finally, V213$_{CT}$ (261seq) is also a doublet only in the thrombin-TM456 HSQC spectrum (Figure 2.6C). Adjacent to Val 158$_{CT}$, Asn 159$_{CT}$ was a doublet only in the HSQC spectrum of the thrombin-TM456 complex, and was moving on the μs-ms timescale in apo-thrombin but not in the thrombin-TM456 complex (Figure 2.6B, C). The core of the C-terminal β-barrel is flanked by Phe 199$_{CT}$ (245seq) which also was a doublet in the thrombin-TM456 HSQC spectrum and showed μs-ms timescale

motions in all three thrombin states (Figure 2.6B, C). Tyr 228$_{CT}$ (276seq) could be assigned to both a doublet resonance and a singlet resonance with notably different chemical shifts (Figure 2.7). Thus, the addition of TM456 causes decreased H/D exchange in the loops around the thrombin S1 pocket, reduces μs-ms timescale motions, and also induces motions that are slow on the NMR timescale in the residues that make up hydrophobic core of the C-terminal β-barrel.

TM induces slow two-state motion of the N-terminus of the heavy chain and the 140s$_{CT}$ loop. HDX-MS showed that residues 16-23$_{CT}$ (36-44seq; MH+ 819.373) at the N-terminus of the thrombin heavy chain experienced a decrease in exchange when TM456 was bound to thrombin (Figure 2.8A). The x-ray crystal structure of thrombin-TM456 (PDB ID: 1DX5[25]), shows the hydrophobic side chains of Val 158$_{CT}$ (199seq) and Val 138$_{CT}$ (174seq) interacting with the side chain of Ile 16$_{CT}$ (36seq) at the N-terminus of the thrombin heavy chain, which inserts into the Ile cleft to form the catalytically active conformation. Adjacent to the new N-terminus belonging to Ile 16$_{CT}$, cross peaks for Val 17$_{CT}$- Ser 20$_{CT}$ (38-41seq) also were doublets in the thrombin-TM456- spectrum (Figure 2.8B). The cross peak for Val 17$_{CT}$ (38seq) could not be assigned in apo-thrombin, but it could be assigned in the thrombin-TM456 spectrum suggesting that it adopts a more defined conformation(s) in the thrombin-TM456 complex. Glu 23$_{CT}$ (44seq) showed motions on the μs-ms timescale in all three thrombin states, providing more evidence that the N-terminus of the heavy chain remains somewhat mobile in the thrombin-TM456 complex.

The 140s$_{CT}$ loop is adjacent to the residues following the N-terminus of the heavy chain, and residues within this loop 139-149A$_{CT}$ (175-186seq, Figure 2.9A)

could not be assigned in any thrombin spectrum. The dynamics of this loop were determined instead from HDX-MS experiments. Residues 145-155$_{CT}$ (181-196seq; MH+ 1714.912) showed nearly complete exchange, consistent with this loop being very dynamic and solvent-exposed whereas residues 132-144$_{CT}$ (168-180seq; MH+ 1378.723) exchanged much less (Figure 2.9B). The deuterium exchange of the 140s$_{CT}$ loop did not change with the addition of TM456. This is consistent with the CPMG data, which showed that residues N149B$_{CT}$ and K149E$_{CT}$- were undergoing μs-ms timescale motions in all thrombin states (Figure 2.9C). In addition, residues 149B-150$_{CT}$ (187-191seq) were all doublets in the thrombin-TM456 HSQC (Figures 2.9D). Thus, the HDX-MS and NMR data suggest that TM456 modulates the slow timescale motions of the N-terminus of the thrombin heavy chain as well as the 140s$_{CT}$ loop despite the TM binding site being located >14 Å from these regions.

D. DISCUSSION

Multiple investigations have shown that thrombin is a highly dynamic enzyme [11, 14, 16, 19], and that it samples multiple conformational states allowing it to bind different substrates and its activity to be allosterically modified by cofactors such as TM to direct catalysis of specific substrates [11, 40-42]. Here we present a combination of HDX-MS and NMR CPMG data that provides a wealth of information regarding the dynamics of the thrombin-TM complex. We had expected to see the TM binding site on thrombin become ordered in the presence of TM based on prior HDX-MS data [17]. However, just as observed in both the apo- and PPACK-

thrombin states, the TM binding site appears to remain largely disordered with TM456 present. No new cross peaks were observed in the thrombin-TM456 spectra, and the HD exchange protection did not persist after 5 min of incubation, consistent with the very rapid binding kinetics previously observed [34]. The thrombin-TM interaction is entirely entropically-driven, consistent with the binding site remaining disordered. CPMG data on thrombin-TM revealed 10 residues that showed increased dynamics and no residues that demonstrated decreased dynamics in the N-terminal b-barrel when compared to apo- and PPACK thrombin. Conversely, nine residues showed decreased dynamics in the C-terminal β-barrel, and none showed increased dynamics. This even exchange of dynamics on the μs-ms timescale likely indicates entropic compensation within thrombin. Thus, the favorable entropy of binding is likely due to release of water molecules from the binding site as originally suggested [43].

Interestingly, the reduction in μs-ms timescale motions observed in the C-terminal β-barrel involves residues in the loops implicated in the formation of the S1 pocket [9, 31]. Six residues within these loops were moving on the μs-ms timescale in apo-thrombin but their motions were quenched by binding PPACK. Remarkably, the motions of all of these residues were also quenched in the thrombin-TM complex, strongly indicating that TM binding over 25 Å away allosterically organizes the S1 pocket. These residues include Asp 189 at the bottom of the S1 substrate binding pocket and the sodium-binding site. The fact that this part of thrombin is significantly rigidified by TM was also observed through crystallographic studies on thrombin-TM in the absence of Na^{+} [42], and explains the insensitivity of the thrombin-

TM complex to Na^+ concentration [44], as well as the increased binding rate of thrombin active-site inhibitors observed when TM is bound [45-49]. In addition, such a pre-formation of this critical substrate-binding pocket would promote rapid binding of substrate, a known feature of how TM accelerates catalysis of protein C cleavage by thrombin. Formation of the first covalently-bound intermediate between thrombin and its substrate is probably mimicked by the PPACK-thrombin complex [14, 16-19], which was observed to have the lowest degree of conformational heterogeneity [14, 17]. A similar conformationally rigid, covalently-bound intermediate species was recently reported for the UMP/CMP kinase from *D. discoideum* [50], suggesting that rigidity may be a common feature of covalently-bound reaction intermediates.

The NMR CPMG data revealed a novel pathway of dynamic motions that link the TM binding site to the catalytic residues through the N-terminal β-barrel. This pathway encompassed the β-strand that connects the $70s_{CT}$ and $90s_{CT}$ loops and the adjacent strand that butts up against the C-terminal helix of thrombin. Community network analysis of accelerated MD simulations had indicated that several small communities of residues were moving independently of one another in this region of apo-thrombin, whereas these communities coalesce into a single community when TM456 binds [16]. We now have evidence that these predicted correlated motions are on the μs-ms timescale. TM456 binding induced μs-ms dynamic motions in the β-strand leading to the catalytic Asp 102_{CT} (189seq) and the neighboring strand. It is interesting to speculate that these motions may be important for catalysis since Asp 102_{CT} must closely approach His 57_{CT} in order to raise its

pKa to promote abstraction of the Ser 195_{CT} proton prior to nucleophilic attack on the substrate carbonyl (Figure 2.10A).

For thrombin to catalyze fibrinogen cleavage, fibrinogen must engage both the anion binding exosite 1 (where TM binds) and the active site [51]. It is thought that TM promotes cleavage of protein C by engaging anion binding exosite 1 in a manner similar to fibrinogen. Thus, one can think of the thrombin-TM456 complex as revealing the catalytically active form of thrombin via engagement of anion binding exosite 1. Remarkably, many cross peaks in the HSQC were doublets only in thrombin-TM456 but not in apo-thrombin or PPACK thrombin. Doublets represent motions that are slow on the NMR time scale, $< 80\ s^{-1}$ yet this is still fairly fast compared to the k_{cat} for protein C cleavage of $5\ s^{-1}$ [24]. It is tempting to speculate that the doublets reveal a thrombin motion that is important for catalysis of the slow steps of peptide bond cleavage. For serine proteases, the slow steps are thought to be release of the first product, the N-terminal portion after cleavage of the scissile bond, and subsequent binding of a water molecule that is required for hydrolysis of the acyl-enzyme intermediate which remains bound in the S1 pocket (Figure 2.10A). When we mapped all of the residues for which doublets are observed onto the structure of thrombin, we saw that they fall all along the interface between the N-terminal and C-terminal β-barrels (Figure 2.10B).

These data support a model of the serine protease reaction coordinate that explains how the conformational heterogeneity induced in thrombin by TM facilitates effective catalysis of protein C activation. TM binding allosterically remodels apo-thrombin dynamics to accomplish three catalytic functions: 1) TM

decreases dynamics in the C-terminal β-barrel forming the S1 pocket to accelerate protein C binding, 2) TM enhances μs-ms timescale motions of the β-strands connecting the TM binding site to the $90s_{CT}$ loop which moves Asp 102_{CT} to promote deprotonation of the catalytic serine, and 3) TM causes motions that are slow on the NMR timescale along the interface between the N-terminal and C-terminal β-barrels (Figure 2.10). This slower motion is likely required for release of the first product and subsequent hydrolysis of the covalently bound acyl-enzyme intermediate.

E. METHODS

Thrombin expression and purification. The S195M mutant thrombin and WT thrombin were expressed and refolded from *E. coli* as previously described [15, 17]. Activation of WT thrombin was facilitated by the addition of *E. carinatus* venom (Sigma-Aldrich Car. #V8250) after dilution to 50 mL with 50 mM Tris/HCl pH 7.4, 20 mM $CaCl_2$, PEG8000 (1 mg/mL), and glycerol (5% v/v) for 2-10 hr at room temperature. To activate S195M thrombin, the protein was concentrated by a factor of 2 using 6 mL 10K MWCO Vivaspin concentrators. The sample was then diluted by a factor of 2 using a solution of 50 mM Tris/HCl pH 7.4, 20 mM $CaCl_2$, 1 mg/mL PEG8000, and 5% (v/v) glycerol before adding the *E. carinatus* venom. After the S195M thrombin sample was left to rock for 3 hr with *E. carinatus* venom, previously purified α-thrombin was added to a molar ratio of 1:30 WT:S195M and was left to rock for 12-16 hr at 28ºC 30ºC to convert the meizothrombin species formed to α-thrombin. After activation, the WT α-thrombin was removed by addition

of biotinyl-PPACK (Haematologic Technologies) followed by addition of streptavidin resin (Thermo Scientific) to capture the biotinyl-PPACK-α-thrombin complex which was then removed using a 0.2 micron syringe filter.

The activated thrombin samples were purified from the pre-thrombin-2 and γ-thrombin on a MonoS 10/100 GL cation exchange column (GE Healthcare Life Sciences) using a gradient of 100 mM – 500 mM NaCl in 25 mM phosphate pH 6.5. The fully-active WT thrombin species (α-thrombin) eluted last off the MonoS column. The S195M α-thrombin species eluted slightly differently from the WT α-thrombin and so could be separated from the small amount of WT α-thrombin used in the activation. Fractions containing the target α-thrombin species were pooled and stored at -80 ^{o}C for no longer than 1 month before use. This method of thrombin purification has been shown to result in >95% α-thrombin, and previous NMR analysis of isotopically labeled thrombin prepared this way demonstrated that the species present was α-thrombin [15, 34].

Production of TM456. The TM456 species used for all thrombin-TM456 experiments was "TM456m" which ends at G449 and has Cys448 changed to Ser and has been previously described[24]. Briefly, expression and purification of this TM variant was carried out in *P. pastoris* via spheroplast transformation of the freshly purified, Bgl II linearized pPic9K expression plasmid containing the TM456m gene into the *P. pastoris* protease resistant strain, SMD1168, to achieve multicopy insertion of the expression plasmid into the chromosomal DNA resulting in stable transformants. Multicopy transformants were selected by replica plating on 2 mg/ml

G418, a kanamycin analog that penetrates *P. pastoris*. The SMD1168 transformants that produced the highest levels of TM expression were stored as glycerol freezes at −80°C.

P. pastoris transformant glycerol stocks were used to start growths in baffled shake-flasks according to previously published methods[24]. The TM proteins are secreted into the media, and initially captured by anion-exchange chromatography using a QAE Sephadex A-50 column. The protein is then further purified on a HiLoad 26/10 Q Sepharose High Performance column followed by reverse-phase C-18 HPLC using an acetonitrile gradient from 10 – 50% in 20mM NH_4OAc pH 5.65. The protein was lyophilized before being reconstituted in MilliQ H_2O and purified by Superdex 75 size-exclusion chromatography in 50 mM Tris 150 mM NaCl pH 7.4. Protein C activation assays (described below) were used at each step in the purification strategy to determine the highest activity fractions to be taken to the next step.

Protein C Activation Assays. Protein C activation assays were performed as previously described [24]. Briefly, a discontinuous assay for TM activation of thrombin towards protein C cleavage was performed by first incubating TM with human α-thrombin before adding human protein C (Hematologic Technologies, Essex Junction, VT). Following a 20 min incubation with protein C, the thrombin was inactivated by addition of heparin/antithrombin-III, and the activated protein C was assayed by addition of the chromagenic substrate, S-2366 (Diapharma, West Chester, OH). The cleavage of the chromogenic substrate results in a linear increase

in absorbance at 405 nm over time, which is proportional to the amount of activated protein C.

Hydrogen-Deuterium Exchange Mass Spectrometry. Purified WT α-thrombin samples were concentrated to 5 µM using pre-rinsed 6 mL 10K MWCO Vivaspin concentrators, spinning at 3000 rpm in 5 min intervals at 4°C. These apo-thrombin samples were passed through a 0.2 micron filter, and 130 µL of each was saved for the HDX-MS experiment. The remaining apo-thrombin samples were then concentrated to 10 µM, and 50 µL was used for peptide identification. To make the α-thrombin-TM456 complex for HDX-MS, purified TM456 was added to purified WT α-thrombin samples at a molar ratio of 1:10 thrombin:TM456, which ensured 99% of thrombin would be bound to TM456. These samples were then concentrated to 5 µM and 10 µM for the HDX-MS and peptide identification MSMS respectively.

HDX-MS was performed using a Waters Synapt G2Si system with HDX technology (Waters Corporation) [52]. Deuterium exchange reaction were prepared using a Leap HDX PAL autosampler (Leap technologies, Carrboro, NC). D_2O buffer was prepared by lyophilizing 1 mL of 250 mM phosphate pH 6.5 along with 850 mM NaCl for the apo-thrombin experiments and 1000 mM NaCl for the thrombin-TM456 experiments, before being resuspended in 10 mL 99.96% D_2O immediately before use. Each deuterium exchange time point (0 min, 30 sec, 1 min, 2 min, and 5 min) was measured in triplicate. For each deuteration time point, 5 µL of protein was held at 25 °C for 5 min before being mixed with 55 µL of D_2O buffer, which ensured a concentration of 100 mM NaCl for both the apo and TM456-bound samples at the

time of the HDX experiments. The deuterium exchange was quenched for 1 min at 1 ^{o}C by combining 50 µL of the deuteration reaction with 50 µL of ice cold 250 mM TCEP pH 2.5. The quenched sample was then injected into a 50 µL sample loop, followed by digestion on an in-line pepsin column (immobilized pepsin, Pierce, Inc.) at 15 ^{o}C. The resulting peptides were captured on a BEH C18 Vanguard pre-column, separated by analytical chromatography (Acquity UPLC BEH C18, 1.7 µM, 1.0 x 50 mm, Waters Corporation) using a 7-85% acetonitrile in 0.1% formic acid over 7.5 min, and electrosprayed into the Waters Synapt G2Si quadrupole time-of-flight mass spectrometer. The mass spectrometer was set to collect data in the Mobility, ESI^{+} mode; mass acquisition range 200-2,000 (m/z); scan time 0.4 s. Continuous lock mass correction was accomplished with infusion of leu-enkephalin every 30 s (mass accuracy of 1 ppm for calibration standard). For peptide identification, the mass spectrometer was set to collect data in MS^{E}, mobility ESI+ mode instead. Peptides masses were identified from triplicated analyses of 10 µM α-thrombin, and data were analyzed using PLGS 2.5 (Waters Corporation). Peptides masses were identified using a minimum number of 250 ion counts for low energy peptides and 50 ion counts for their fragment ions.

The peptides identified in PLGS were then analyzed in DynamX 3.0 (Waters Corporation) to determine deuterium uptake. Additional filters in DynamX 3.0 included a cut-off score of 7, minimum products per amino acid of 0.2, maximum MH+ error tolerance of 5 ppm, retention time standard deviation of 5%, and requiring that the peptide be present in at least 2 of the 3 peptide identification runs. The deuterium uptake for each peptide was calculated by comparing the centroids of

the mass envelopes of the deuterated samples vs. the undeuterated controls. For all HDX-MS data, at least 2 biological replicates were analyzed, each with 3 technical replicates. Data are represented as mean values +/- SEM of 3 technical replicates due to processing software limitations, however biological replicates were highly reproducible due to use of the LEAP robot for all experiments. The deuterium uptake was corrected for back-exchange using a global back exchange correction factor (typically 25%) determined from the average percent exchange measured in disordered termini of various proteins. ANOVA analyses and t tests with a p value cutoff of 0.05 implemented in the program, DECA, were used to determine the significance of differences between HDX data points[53]. The peptides reported on the coverage maps are actually those from which deuterium uptake data were obtained. Deuterium uptake plots were generated in DECA (github.com/komiveslab/DECA) and the data are fitted with an exponential curve for ease of viewing. Data were plotted in DECA as number of deuterons incorporated vs. time (min). The Y-axis limit for each plot reflects the total possible number of amides within the peptide that can exchange. Each plot includes the peptide MH+ value, sequence, and sequential residue numbering.

NMR sample preparation. Purified ^{2}H-^{15}N-S195M and ^{2}H-^{15}N-^{13}C-S195M thrombin was added to separate samples of purified TM456 at a molar ratio of 2:3 thrombin:TM456, which ensured that 99% of thrombin was bound to TM456 at the concentrations used for these experiments. These samples were diluted with 25 mM phosphate pH 6.5 and 50 mM NaCl to adjust the concentrations of NaCl to 150mM,

before the samples were left at 4 °C for 12-16 hr. The ^{2}H-^{15}N-thrombin-TM456 and ^{2}H-^{15}N-^{13}C-thrombin-TM456 samples were then concentrated using 6 mL 3K MWCO Vivaspin concentrators, spinning at 3000 rpm in 15 min intervals at 4°C to 112 µM and 122 µM respectively with 0.05% sodium azide and 10% D_2O present.

NMR resonance assignments. All NMR experiments followed the procedures for resonance assignments previously published[15]. All NMR experiments were acquired on Varian VNMRS (Agilent Technologies, Santa Clara, CA) and Bruker Avance III spectrometers operating at 600, 800 and 900 MHz (^{1}H), and equipped with cryogenic triple-resonance probes. The temperature of the sample was regulated at 298 K for all the experiments. For the sequence specific assignment of backbone resonances, the TROSY version of 2D ^{1}H,^{15}N-HSQC and 3D HNCA, 3D HN(CO)CA and 3D HNCO spectra were recorded. The acquisition parameters for these spectra are reported in Table 3.1. The 3D spectra were recorded using Non-Uniform Sampling (NUS) with sampling rates ranging between 36 and 38%. All spectra were processed using NMRPipe. The 3D spectra recorded using NUS were reconstructed using the SMILE package available in NMRPipe. The Experimental details for all NMR spectra collected can be found in Table 3.1. Some assignments were transferred from the previously assigned PPACK-thrombin[15], and additional assignments were made. Assignment transfers were confirmed with the 3D experimental data.

Twenty-seven residues for which N-H peaks were visible in PPACK-bound thrombin did not have visible peaks in the HSQC-TROSY spectrum of thombin-

TM456. These included residues: 30_{CT} (51_{seq}), 66_{CT} (97_{seq}), 81_{CT} (113_{seq}), 97A-99_{CT} (130-132_{seq}), 139-$149A_{CT}$ (175-186_{seq}), 151-156_{CT} (192-197_{seq}), 192_{CT} (238_{seq}), 196_{CT} (242_{seq}), 221_{CT} (268_{seq}), and $221A_{CT}$ (269_{seq}). Four residues were visible in the HSQC-TROSY spectrum of apo-thrombin, but were not observed in the thrombin-TM456m spectrum. These included residues: 45_{CT} (67_{seq}), 66_{CT} (97_{seq}), 88_{CT} (120_{seq}), and 89_{CT} (121_{seq}). Nine residues were visible in the HSQC-TROSY thrombin-TM456m spectrum that were not observed in the apo-thrombin spectrum. These included residues: 18_{CT} (38_{seq}), 188-191_{CT} (234-237_{seq}), 215_{CT} (263_{seq}), 220_{CT} (267_{seq}), 225_{CT} (273_{seq}), and 226_{CT} (274_{seq}).

Carr-Purcell-Meiboom-Gill Experiments. The effective relative relaxation rated ($R_{2,eff}$) due to contributions from conformational exchange on μs-ms time scales were evaluated with Carr-Purcell-Meiboom-Gill (CPMG) experiments. To identify conformational exchange, spectra were recorded at 600 and 800MHz (1H) using a CPMG relaxation dispersion experiment with TROSY selection. The constant relaxation time for CPMG was set to 40ms and multiple 2D spectra with different CPMG delays were recorded in an interleaved manner. In total, 10 ν_{CPMG} values ranging from 25 to 1000Hz were recorded both at 600 and 800MHz. In addition, 2 ν_{CPMG} values repeated for error estimation. All relaxation dispersion spectra were processed using NMRPipe. The Experimental details for all NMR spectra collected can be found in Table 3.1. For these experiments, Shigemi salt tolerant susceptibility matched slot NMR tubes were used. These tubes only require 170 μL of sample and

need to be properly oriented inside the magnet to optimize S/N and minimize sample heating[54].

The 600 MHz and 800 MHz $R_{2,eff}$ relaxation dispersion data for all apo-thrombin residues with $R_{ex} > 6$ Hz (24 residues) were fit to the Richard-Carver equation[55] by using the software package CPMGFit (http://www.palmer.hs.columbia.edu/software/cpmgfit.html). The fit yielded the global exchange rate, k_{ex}, the populations of the ground state (A) and excited state (B), where $p_A + p_B = 1$ and the residue-specific chemical shift difference between conformational states A and B ($\Delta\omega$). A cut-off of Rex > 6 Hz was used which is equivalent to 2 times the maximal duplicate error. We attempted to fit the thrombin-TM456 CPMG data globally using GLOVE, which minimizes global and local parameters alternately, and incorporates a Monte-Carlo minimization method to allow fitting parameters to pass through local minima[56]. However, none of the residues with $R_{ex} > 6\ s^{-1}$ could be globally fit within an acceptable χ^2 value.

Chapter II, in full, is a reprint that the dissertation author was the principal researcher and author of. The material has been submitted to *PNAS*. **Peacock RB**, McGrann T, Tonelli M, Komives EA. (2020). Serine Protease Dynamics Revealed by NMR Analysis of the Thrombin-Thrombomodulin Complex. *PNAS*. (Submitted)

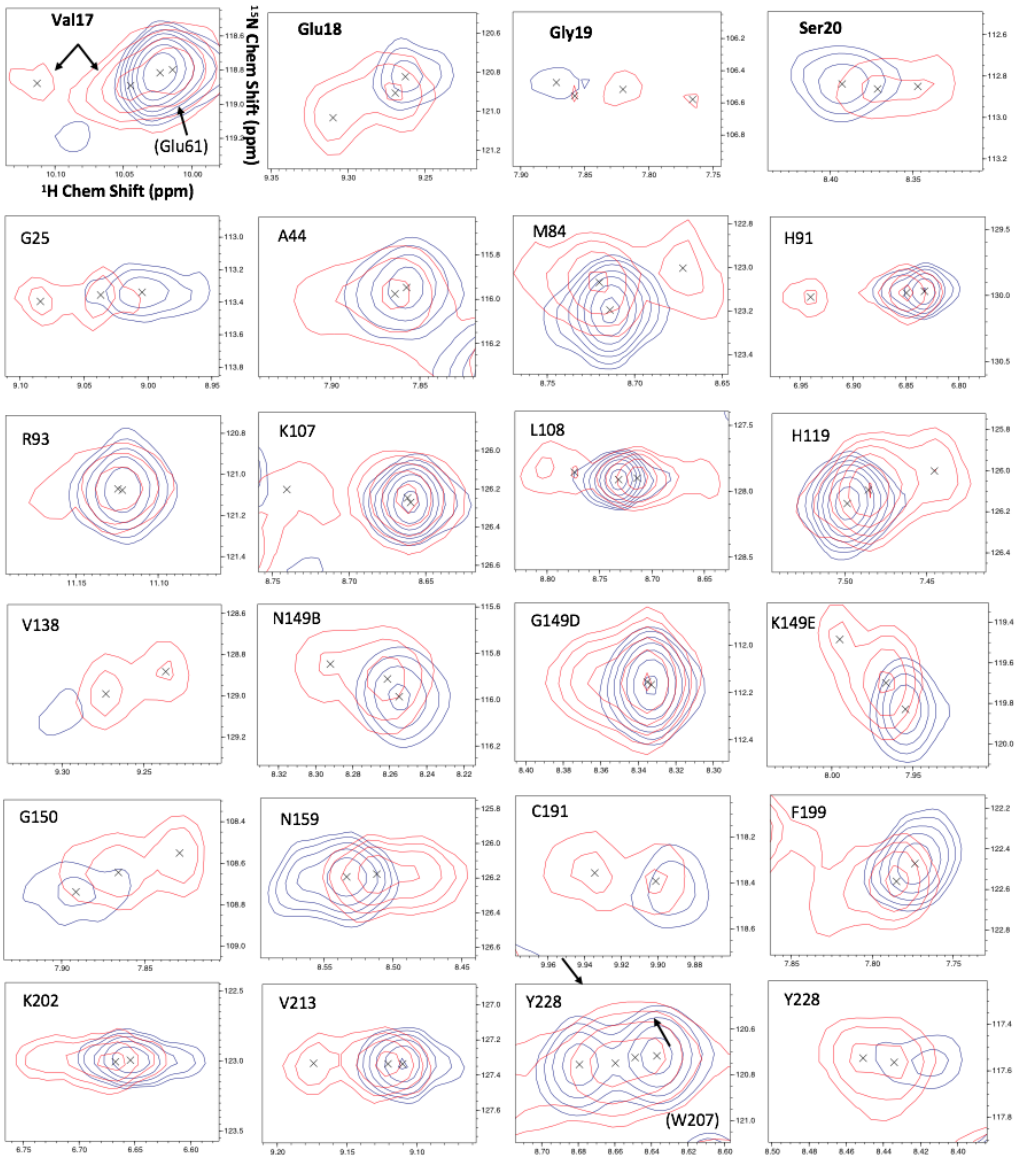

Figure 2.1. All thrombin resonances that appeared as doublets or multiplets in the thrombin-TM456 HSQC spectrum. Residues are numbered according the the CT numbering scheme. The red traces correspond to the thrombin-TM456 HSQC spectrum taken at 800 MHz, while the blue traces correspond to the apo-thrombin spectrum taken at 800 MHz

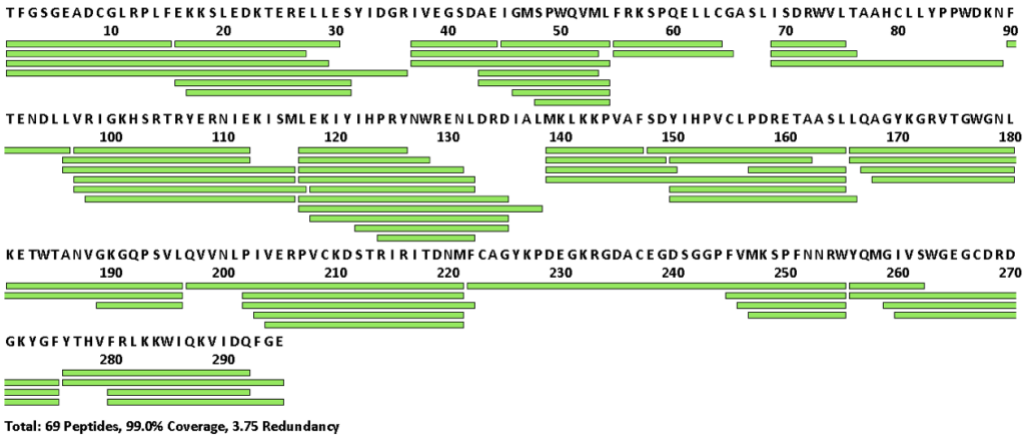

Figure 2.2. Coverage map showing the peptides identified and evaluated during HDX-MS experiments on WT thrombin and thrombin-TM456.

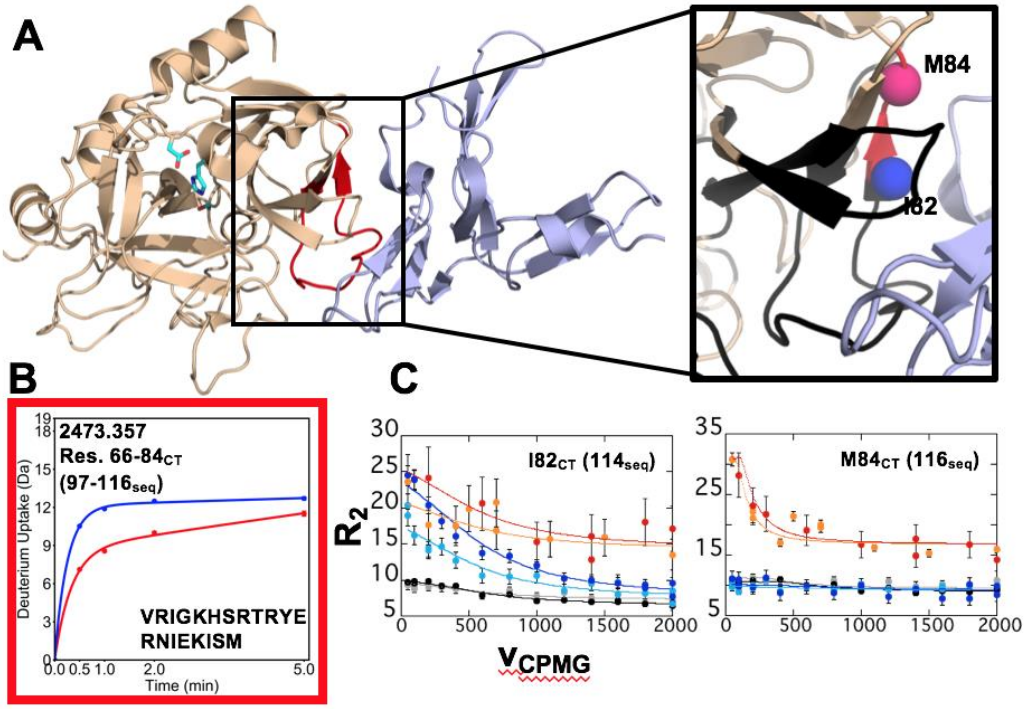

Figure 2.3. A) Crystal structure of thrombin (wheat) bound to TM456 (light blue) [PDB ID: 1DX5]. The side chains of the catalytic triad are shown as cyan sticks. Thrombin residues 66-84_{CT} (97-116_{seq}) of the $70s_{CT}$ loop are colored red (left). A close-up of the $30s_{CT}$ and $70s_{CT}$ loops (right) has residues missing from thrombin-TM456 HSQC colored black, and the amides of residues showing notable CPMG behavior in this region as spheres. CT numbering is used. Pink spheres indicate increased CPMG sensitivity in thrombin-TM456 and blue spheres indicate lesser CPMG sensitivity compared to apo-thrombin. **B)** Relative deuterium uptake plots for the peptide spanning residues 66-84_{CT} (97-116_{seq}; MH+ 2473.357). The blue curve shows the deuterium uptake in apo-thrombin, while the red curve shows that in thrombin-TM456. Error bars are shown. **C)** CPMG plots for residues $I82_{CT}$ (112_{seq}) and $M84_{CT}$ (116_{seq}). The red and orange curves are from spectra collected on thrombin-TM456 at 800 MHz and 600 MHz respectively, the blue and cyan curves are from apo-thrombin at 800 MHz and 600 MHz respectively, and the black and grey curves are from PPACK-thrombin at 800 MHz and 600 MHz respectively. Error bars are shown.

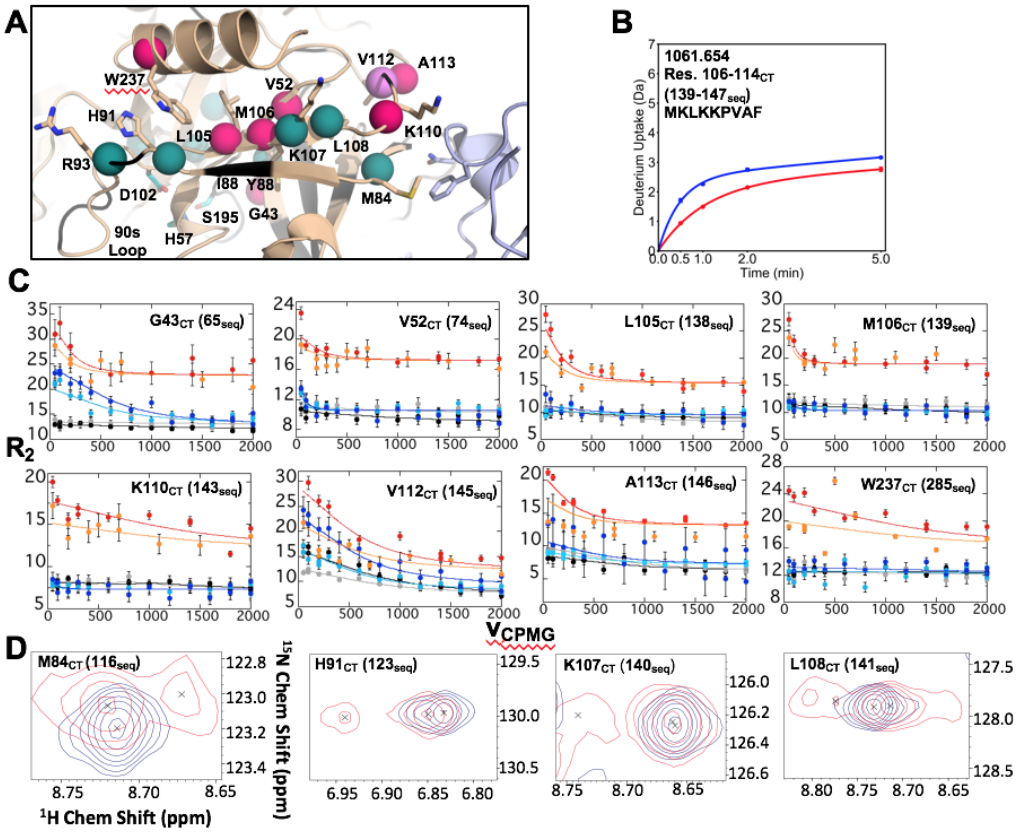

Figure 2.4. A) Crystal structure of thrombin (wheat) bound to TM456 (light blue) [PDB ID: 1DX5]. Residues lacking resonances in the thrombin-TM456 HSQC are colored black. The amides of residues assigned to doublet resonances in the thrombin-TM456 HSQC are shown as teal spheres, the amides of residues showing increased CPMG sensitivity in thrombin-TM456 compared to apo-thrombin are pink spheres, and the amides of residues showing similar CPMG sensitivity between thrombin-TM456 and apo-thrombin are shown as violet spheres. Sidechains are showed for residues of interest, including the catalytic triad (colored cyan). **B)** Relative deuterium uptake plots for the peptide spanning residues 106-114$_{CT}$ (139-147$_{seq}$; MH+ 1061.654). The blue curve shows the deuterium uptake in apo-thrombin, while the red curve shows that in thrombin-TM456. Error bars are shown. **C)** CPMG plots for residues in the thrombin N-terminal β-barrel. The red and orange curves are from spectra collected on thrombin-TM456 at 800 MHz and 600 MHz respectively, the blue and cyan curves are from apo-thrombin at 800 MHz and 600 MHz respectively, and the black and grey curves are from PPACK-thrombin at 800 MHz and 600 MHz respectively. Error bars are shown. **D)** Examples of thrombin-TM456 HSQC (red) doublet resonances compared to apo-thrombin (blue) resonances for residues in the N-terminal β-barrel. All doublet resonances are shown in Figure 2.1.

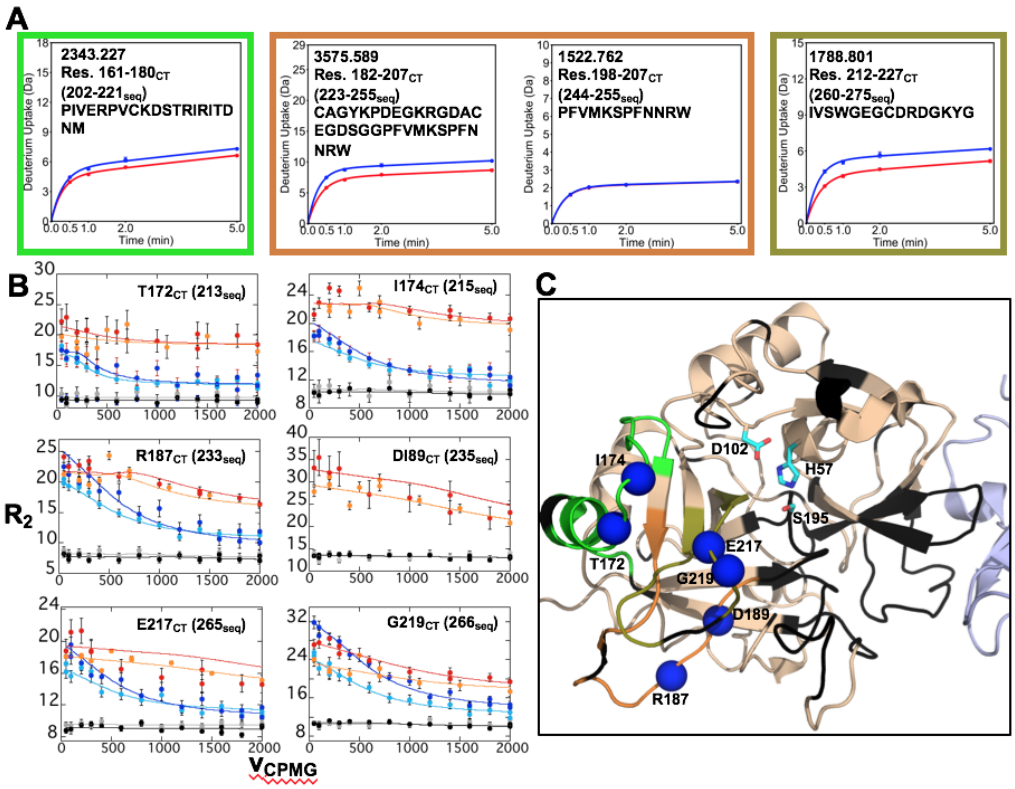

Figure 2.5. A) Relative deuterium uptake plots for the peptide spanning residues 161-180$_{CT}$ (202-221$_{seq}$; MH+ 2343.227), 182-207$_{CT}$ (223-255$_{seq}$; MH+ 3575.589), 198-207$_{CT}$ (244-255$_{seq}$; MH+ 1522.762), and 212-227$_{CT}$ (260-275$_{seq}$; MH+ 1788.801). The blue curve shows the deuterium uptake in apo-thrombin, while the red curve shows that in thrombin-TM456. Error bars are shown. **B)** CPMG plots for residues showing less CPMG sensitivity around the S1 pocket when TM456m is present compared to apo-thrombin. The red and orange curves are from spectra collected on thrombin-TM456 at 800 MHz and 600 MHz respectively, the blue and cyan curves are from apo-thrombin at 800 MHz and 600 MHz respectively, and the black and grey curves are from PPACK-thrombin at 800 MHz and 600 MHz respectively. Error bars are shown. **C)** Crystal structure of thrombin (wheat) bound to TM456 (light blue) [PDB ID: 1DX5]. The residues within the peptides identified in panel (A) are colored accordingly. Residues with missing HSQC resonances are colored black. The sidechains of the catalytic triad are shown as cyan sticks. The amides of residues showing less CPMG sensitivity in thrombin-TM456 compared to apo-thrombin are shown as blue spheres.

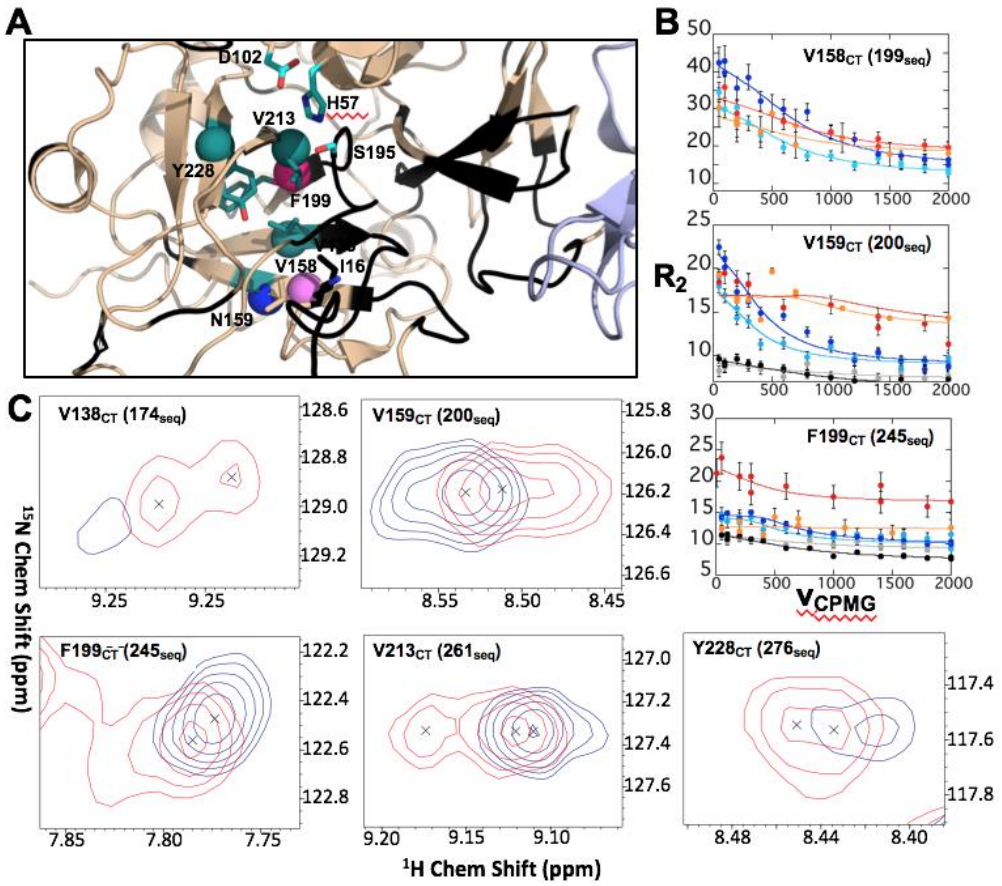

Figure 2.6. A) Crystal structure of thrombin (wheat) bound to TM456 (light blue) [PDB ID: 1DX5] focused on the thrombin C-terminal β-barrel. Residues lacking resonances in the thrombin-TM456 HSQC are colored black. The side chains of the catalytic triad are shown as cyan sticks. Residue Amides assigned to doublet resonances in the thrombin-TM456 HSQC are shown as teal spheres. Pink spheres indicate amides with increased CPMG sensitivity in thrombin-TM456, blue spheres indicate less CPMG sensitivity, and violet spheres indicate similar CPMG sensitivity compared to apo-thrombin. Sidechains are showed for residues of interest. **B)** CPMG plots for residues in the thrombin C-terminal β-barrel. The red and orange curves are from spectra collected on thrombin-TM456 at 800 MHz and 600 MHz respectively, the blue and cyan curves are from apo-thrombin at 800 MHz and 600 MHz respectively, and the black and grey curves are from PPACK-thrombin at 800 MHz and 600 MHz respectively. Error bars are shown. **D)** Examples of thrombin-TM456 HSQC (red) doublet resonances compared to apo-thrombin (blue) resonances for residues in the C-terminal β-barrel. All doublet resonances are shown in Figure 2.1.

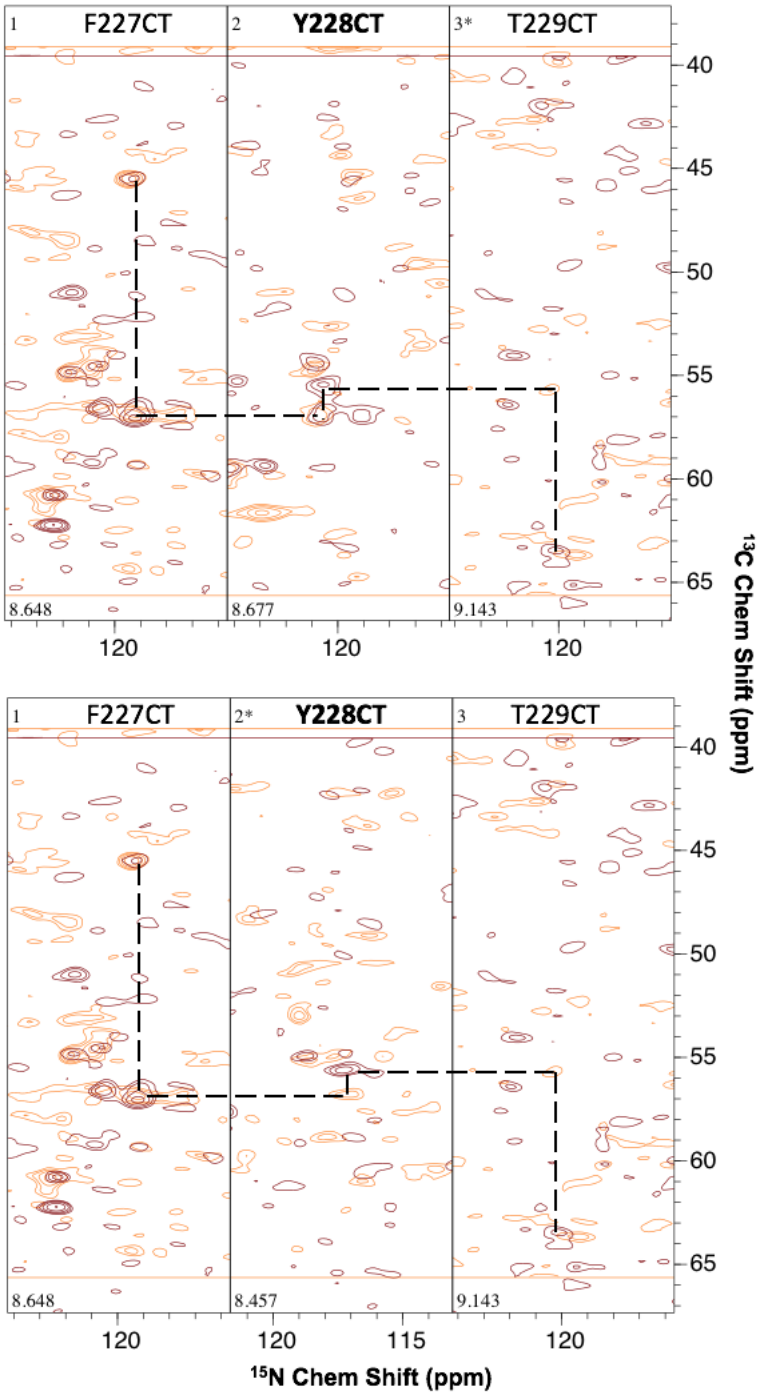

Figure 2.7. Backbone walking from Ca_i to Ca_{-i} HNCA peaks for both residue 228_{CT} assignments. The brown and orange spectra correspond to the HNCA and HN(CO)CA spectra taken at 800 MHz for thrombin-TM456.

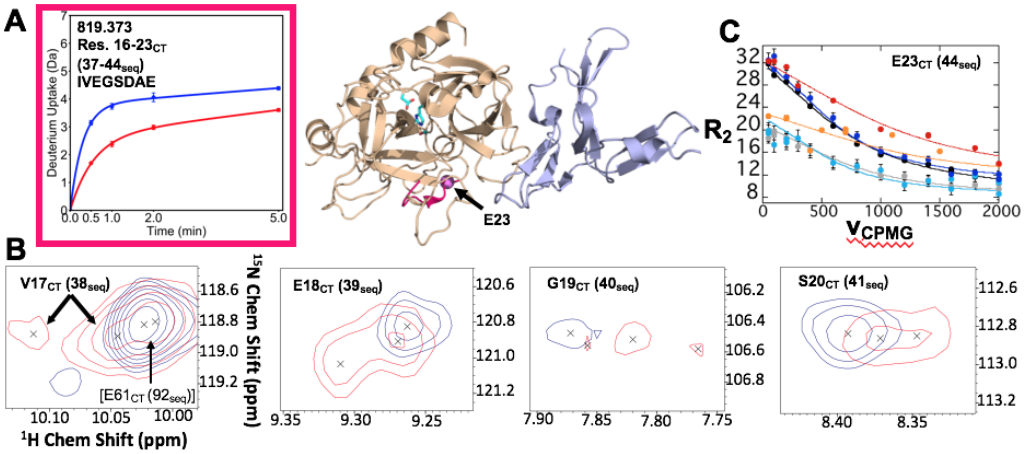

Figure 2.8. A) Crystal structure of thrombin (wheat) bound to TM456 (light blue) [PDB ID: 1DX5]. Residues 16-23_{CT} (37-44_{seq}; MH+ 819.373) are colored hot pink, and the relative deuterium uptake plot for the peptide spanning these residues is shown. HDX error bars are shown in plot. The blue curve shows the deuterium uptake in apo-thrombin, while the red curve shows that in thrombin-TM456. The amide of Glu 23_{CT} (44_{seq}) is shown as a violet sphere as its CPMG sensitivity in thrombin-TM456 was similar to apo-thrombin. Cyan sidechains are shown for the catalytic triad. **B)** Examples of thrombin-TM456 HSQC (red) doublet resonances compared to apo-thrombin (blue) resonances for residues at the N-terminus of the heavy chain. All doublet resonances are shown in Figure 2.1. **C)** CPMG plot for residue 23_{CT} (44_{seq}) with error bars shown. The red and orange curves are from spectra collected on thrombin-TM456 at 800 MHz and 600 MHz respectively, the blue and cyan curves are from apo-thrombin at 800 MHz and 600 MHz respectively, and the black and grey curves are from PPACK-thrombin at 800 MHz and 600 MHz respectively.

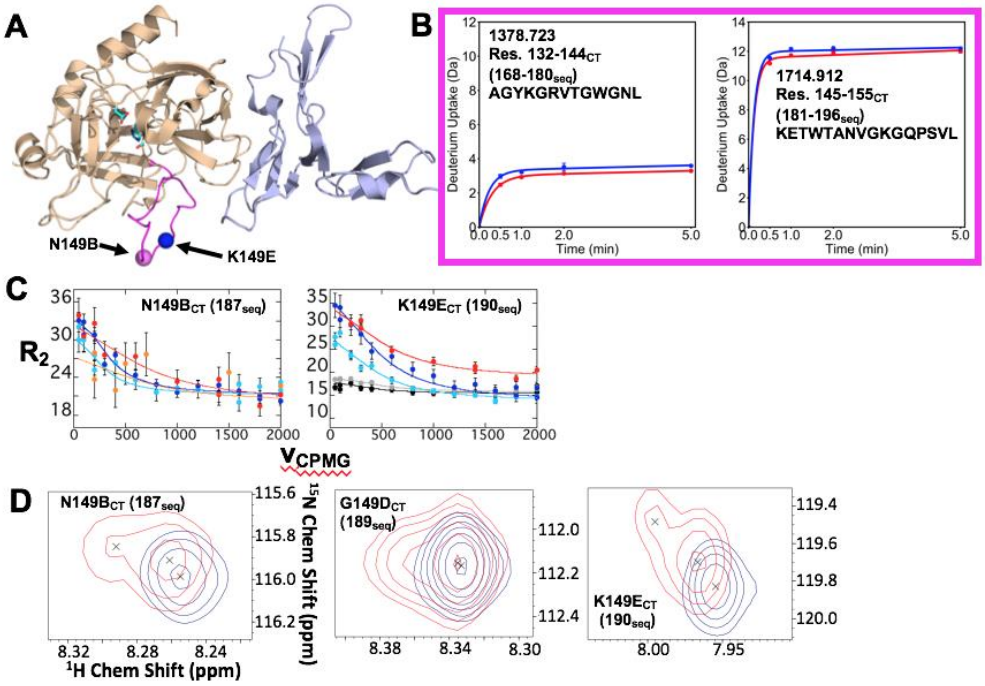

Figure 2.9. A) Crystal structure of thrombin (wheat) bound to TM456 (light blue) [PDB ID: 1DX5]. Residues 140-155$_{CT}$ (176-196$_{seq}$) of the 140s$_{CT}$ loop are colored magenta. The amides of residues showing less CPMG sensitivity in thrombin-TM456 compared to apo-thrombin are shown as blue spheres, and those with similar CPMG sensitivity are shown as violet spheres. Cyan sidechains are showed for the catalytic triad. **B)** Relative deuterium uptake plots for the peptides spanning residues 132-144$_{CT}$ (168-180$_{seq}$; MH+ 1378.723) and 145-155$_{CT}$ (181-196$_{seq}$; MH+ 1714.912). The blue curve shows the deuterium uptake in apo-thrombin, while the red curve shows that in thrombin-TM456. Error bars are shown **C)** CPMG plots for thrombin residues 149B$_{CT}$ (187$_{seq}$) and 149E$_{CT}$ (190$_{seq}$). The red and orange curves are from spectra collected on thrombin-TM456 at 800 MHz and 600 MHz respectively, the blue and cyan curves are from apo-thrombin at 800 MHz and 600 MHz respectively, and the black and grey curves are from PPACK-thrombin at 800 MHz and 600 MHz respectively. CPMG data could not be extracted from the 600 MHz spectra for res 149$_{CT}$ (187$_{seq}$). Error bars are shown. **D)** Examples of thrombin-TM456 HSQC (red) doublet resonances compared to apo-thrombin (blue) resonances for residues in the 140s$_{CT}$ loop. All doublet resonances are shown in Figure 2.1.

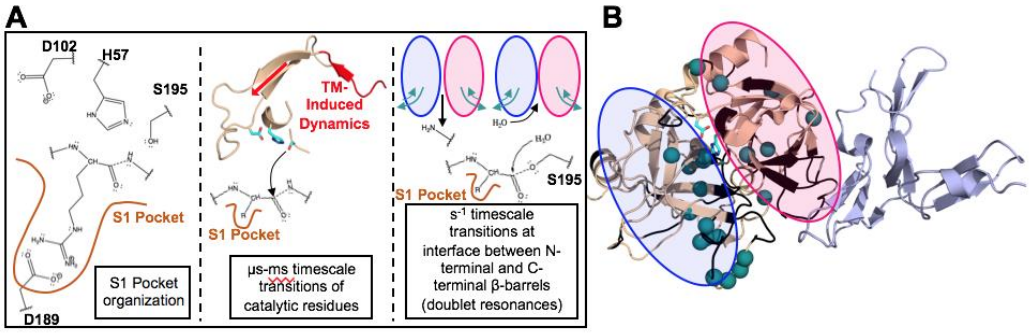

Figure 2.10. A) A model that describes the steps of the serine protease mechanism involving substrate binding (left), the TM-induced motions that promote the nucleophilic attack of Ser 195_{CT}(middle), and the motions of the N-terminal (pink oval) and C-terminal (blue oval) β-barrels required for the release of substrate from Ser 195_{CT}(right). The influence of TM binding to thrombin based on the interpretation of NMR data is included in boxes for each of these steps. B) Crystal structure of thrombin (wheat) bound to TM456 (light blue) [PDB ID: 1DX5]. Residues lacking resonances in the thrombin-TM456 HSQC are colored black. The backbone amides for residues assigned to doublet resonances in the thrombin-TM456 HSQC are shown as teal spheres. The sidechains of the catalytic triad are shown as cyan sticks. The N-terminal and C-terminal β-barrels are highlighted using the pink and blue ovals respectively.

Table 2.1. Experimental details for 3D spectra collected for backbone assignments and 2D relaxation dispersion spectra.

Experiment	# Scans	Spectral Window (ppm) $^{1}H\times(^{13}C\times)^{15}N$	Complex Points $^{1}H\times(^{13}C\times)^{15}N$	Offset (ppm) $^{1}H\times(^{13}C\times)^{15}N$	NUS sampling rate (%)
3D HNCA-TROSY[♦]	64	17.3×31.6×36.6	1024×58×35	4.77, 54.7, 118.1	38
3D HN(CO)CA-TROSY	80	20×26.5×36.2	1024×56×48	4.77, 52.4, 118.6	36
3D HNCO-TROSY	64	20×14.6×36.2	1024×44×44	4.77, 175.5, 118.6	38
2D ^{15}N-HSQC-TROSY[♦]	16	17.3×36.6	1024×128	4.77, 118.1	N/A
2D ^{15}N-CPMG-TROSY	96	16.7×34.6	1024×128	4.77, 118.7	N/A
2D ^{15}N-CPMG-TROSY[♣]	80	16.3×34.6	1024×98	4.77, 118.1	N/A
[a]All spectra were collected with a cryogenic probe at 600, 800[♣] and 900[♦] MHz (^{1}H) at a temperature of 298 K.					

Chapter III

Dynamic Consequences of Mutation of Tryptophan 215 in Thrombin

Dynamic Consequences of Mutation of Tryptophan 215 in Thrombin

Riley Peacock[1], Jessie Davis[1], Phineus R. L. Markwick[2] and Elizabeth A. Komives[1]

[1]Department of Chemistry and Biochemistry, University of California, San Diego, 9500 Gilman Drive, La Jolla, CA 92093-0378 USA.

[2] San Diego Supercomputer Center University of California, San Diego 10100 Hopkins Dr, La Jolla, CA 92093 USA.

Corresponding author: Elizabeth A. Komives

Department of Chemistry and Biochemistry, University of California, San Diego, 9500 Gilman Drive, La Jolla, CA 92092-0378

Ph: (858) 534-3058

Email: ekomives@ucsd.edu

Keywords: serine protease, protein dynamics, hydrogen-deuterium exchange, allostery

A. ABSTRACT

Thrombin normally activates fibrinogen for coagulation, however, binding of thrombomodulin to thrombin alters the catalytic activity of the enzyme toward protein C, triggering the switch from the coagulation to the anticoagulation pathway. The W215A mutant of thrombin was reported to have decreased activity towards fibrinogen without significant loss of activity towards protein C. To understand how mutation of Trp215 may alter thrombin specificity, hydrogen-deuterium exchange experiments (HDXMS), accelerated molecular dynamics (AMD) simulations, and activity assays were carried out to compare the dynamics of W215A with those of wild type (WT) thrombin. Variation in NaCl concentration had no detectable effect on the sodium-binding ($220s_{CT}$) loop, but surface loops that may weakly interact with sodium ions showed increased exchange. The W215A mutant showed significant increases in amide exchange in the $170s_{CT}$ loop consistent with loss of H-bonding in the $170s_{CT}$ loop revealed by AMD simulations. HDXMS experiments revealed that mutation of Phe227, which engages in a pi-stacking interaction with Trp215, also caused significantly increased amide exchange in the $170s_{CT}$ loop, indicating that the Trp215-Phe227 stacking interaction stabilizes the $170s_{CT}$ loop. Activity assays showed only the F227V mutant had wild type catalytic activity, whereas all of the other mutants had markedly lower catalytic activity. Comparison of WT to W215A thrombin HDXMS results showed that besides directly stabilizing the $170s_{CT}$ loop, mutation of Trp215 causes increased amide exchange in the $220s_{CT}$ loop and in the N-terminus of the heavy chain. The AMD simulations also showed that the transient conformation of the W215A thrombin has a distorted catalytic

triad. Taken together, the results explain the reduced pro-coagulant activity of the W215A mutant and demonstrate the allosteric connection between Trp215, the sodium-binding loop and the active site.

B. Introduction

Thrombin is a dual action serine protease that binds and cleaves a variety of substrates [57]. Substrate recognition is dependent on the binding of a consensus sequence at the primary specificity pockets (S1-4) within the active site, as well as binding at distinct exosites located on opposites sides of thrombin. Central to its role in the clotting cascade, thrombin distinguishes between substrates that elicit either a procoagulative or an anticoagulative response. The binding of thrombomodulin (TM) to anion binding site 1 (AEB1) of thrombin shifts the enzyme's specificity away from procoagulative substrates, such as fibrinogen and the protease-activated receptor 1(PAR1), and towards the anticoagulative substrate, protein C (PC) [58]. How TM binding to thrombin alters its substrate specificity is still not fully understood. Comparison of the X-ray crystal structures of apo-thrombin and thrombin bound to TM456, a construct of TM containing only the domains necessary for toggling thrombin's substrate specify, shows no discernable differences between the two structures [25]. Thus, TM-binding affects thrombin in ways that are invisible to X-ray crystallography.

Di Cera determined that mutation of $Trp215_{CT}$ to alanine resulted in significant loss of activity towards procoagulative substrates, yet this mutant retained most of the activity towards PC in the presence of TM [59]. Interestingly, the W215I

mutation resulted in nearly a complete loss of activity of thrombin towards both procoagulative and anticoagulative substrates [60]. Measurements of hirudin binding to three Trp215$_{CT}$ mutants showed that mutations at position 215$_{CT}$ make thrombin much less sensitive to sodium binding, offering an explanation for the decreased activity observed for procoagulative substrates [59, 61]. Saturation mutagenesis of Trp215$_{CT}$ revealed an array of activity profiles that distinguish Trp215$_{CT}$ mutants in their abilities to cleave fibrinopeptide A (FpA), PAR1, and PC [60], suggesting that this residue is involved in key aspects of modulating thrombin's activity. The dramatic effect of mutations at Trp215$_{CT}$ on substrate specificity identifies this residue as one of significant interest, warranting further study of how the characteristics Trp215$_{CT}$ mutants differ from those of WT thrombin.

Thrombin is a highly dynamic enzyme. Studies have demonstrated that the surface loops of thrombin exhibit highly dynamic motions [15, 19]. Previous work from our lab has also connected the dynamic motions of thrombin to key catalytic regions of the protein, providing evidence for dynamic allostery [16, 17]. Here we focus on Trp215$_{CT}$ to gain a clearer picture of how this mutation affects thrombin dynamics and activity. Due to the apparent pi-stacking interaction between Trp215$_{CT}$ and Phe227$_{CT}$ in the X-ray crystal structure of thrombin (Protein Data Base (PDB) ID code 1PPB) [4], we included mutants of Phe227$_{CT}$ in our study as well. We used a combination of activity assays, HDXMS to evaluate the differences in backbone dynamics, and AMD to obtain a molecular mechanism of changes in amide exchange.

HDXMS provides a measure of the backbone dynamics and solvent accessibility changes that occur on physiologically relevant time scales [26]. HDX has already been used to compare the dynamics of apo-thrombin, PPACK-thrombin, and TM-thrombin, revealing changes in surface loop dynamics that directly impact thrombin activity [62, 63]. Thus, HDXMS provides a tool for comparing the backbone dynamics of thrombin mutants with the motions native to WT thrombin. AMD is an efficient and versatile enhanced conformational space sampling algorithm that allows for the accurate study of slow motions in bio-molecular systems up to time-scales several orders of magnitude greater than those accessible using standard classical MD methods, while still affording a fully atomistic representation of the system. The acceleration level used here has previously been shown to afford an increase in the rate of conformational space sampling by 3-4 orders of magnitude [64, 65].

We show that the W215A mutant has markedly increased dynamics in the 170s$_{CT}$ loop, the 220s$_{CT}$ loop, and the N-terminus of the heavy chain and its dynamics are less sensitive to NaCl concentration. Investigation of the pi-stacking interaction between Phe227$_{CT}$ and Trp215$_{CT}$ revealed that this interaction is critical for ordering the 170s$_{CT}$ loop, but Trp215$_{CT}$ alone is responsible for long-range allostery that impacts the 220s$_{CT}$ loop and the N-terminus of the heavy chain. The results of this study clarify the role of sodium and reveal the dramatic changes in thrombin dynamics that result from mutations at both Trp215$_{CT}$ and Phe227$_{CT}$.

C. **Results**

Improved HDXMS of thrombin. In order to determine the effects of sodium concentration and the W215A mutation on thrombin dynamics, HDXMS experiments were carried-out. WT and each mutant thrombin were allowed to exchange into deuterated buffer for 0-5 min followed by quenching in 100mM tris-carboxyethylphosphine, pH 2.5, which improved sequence coverage after pepsin digestion. Fifty-one peptides were reliably identified, which covered 99.0% of the thrombin sequence. Due to the location of the mutations examined, the peptides covering the 220s$_{CT}$ loop varied depending on the mutation (Figure 3.1). To probe the dependence of the thrombin dynamics on NaCl concentration, experiments on WT and W215A thrombin were carried out at 100 mM NaCl and 300 mM NaCl.

The effect of W215A and Salt on the 220s$_{CT}$ Loop. We first analyzed the difference in deuterium uptake of W215A and WT thrombin in 100 mM vs. 300 mM NaCl. As previously reported by Di Cera's group, the W215A mutation renders thrombin much less sensitive to Na^+ ions [59]. The deuterium uptake within the W215A 220s$_{CT}$ loop (residues 260-275; MH+ 1673.760, 1788.801) appeared unaffected by NaCl concentration, resulting in similar uptake values at both NaCl concentrations (Figure 3.2). Interestingly, the 220s$_{CT}$ loop in WT thrombin also showed nearly identical deuterium uptake at 100mM and 300 mM NaCl. The 220s$_{CT}$ loop of the W215A mutant showed notably higher deuterium uptake compared to WT thrombin, by an average of ~2 deuterons at both the high and low salt concentrations. These results indicate that the 220s$_{CT}$ loop is sensitive to dynamic

modulation caused by changes to side chains at the base of the loop, but the loop dynamics appear insensitive to NaCl concentration.

Subtle effects caused by NaCl. Several other functionally interesting regions of thrombin did show a moderate dependence of deuterium uptake on NaCl concentration. The deuterium uptake in regions located near anion binding sites 1 (AEB1) and 2 (AEB2) were affected by the concentration of salt more so than by the W215A mutation. Residues 66-85$_{CT}$ (residues 97-117; MH+ 2586.441) showed a slight increase in deuterium uptake with decreasing salt concentration but residues 66-80$_{CT}$ (residues 97-112; MH+ 2014.105) showed no difference, allowing us to localize the salt effect to residues 81-85$_{CT}$ (residues 113-117) (Figure 3.3). This trend extended through residues 85-102$_{CT}$ (residues 117-135; MH+ 2530.295), which approaches AEB2 and includes Asp102$_{CT}$ of the catalytic triad. Similarly, residues 117-129$_{CT}$ (residues 150-162; MH+ 1513.747) showed no dependence on NaCl concentration, but residues 117-130$_{CT}$ (residues 150-166; MH+ 1897.984) were affected by salt indicating residues 129A-130$_{CT}$ (residues 163-166) of ABE2 also respond to salt concentration. Slight salt effects were observed for other surface loops including the 180s$_{CT}$ loop (residues 223-255; MH+ 3575.589), the 140s$_{CT}$ loop (residues 181-196; MH+ 1714.912), the 30s$_{CT}$ loop (residues 55-64; MH+ 1220.646), and the light chain (residues 1-15; MH+ 1569.737 and residues 16-31; MH+ 1934.008) (Figure 3.4).

The effect of the W215A mutation and NaCl on the 170s$_{CT}$ loop. Unlike the 220s$_{CT}$ loop, both NaCl and the W215A mutation significantly affected deuterium uptake. Three peptides - residues 156-180$_{CT}$ (residues 197-221; MH+ 2896.550),

161-170$_{CT}$ (residues 202-211; MH+ 1155.619), and residues 161-181$_{CT}$ (residues 202-222; MH+ 2490.296) covered the 170s$_{CT}$ loop and portions of the C-terminal β-barrel (Figure 3.5). The combination of the W215A mutation and low NaCl concentration resulted in the highest exchange, and this region of the W215A mutant thrombin incorporated an average of ~4 more deuterons over 5 min as compared to WT thrombin.

The effect of W215A and NaCl on the N-Terminus of the heavy chain. The N-terminus of the heavy chain, residues 16-23$_{CT}$ (residues 37-44; MH+ 819.373) exhibited a slight increase in uptake under lower NaCl as well as in the presence of the W215A mutation (Figure 3.6A). Thus, the dynamics of the N-terminus of the heavy chain are also affected by NaCl and the W215A mutation.

Accelerated MD simulations of the W215A mutant thrombin. In order to complement the experimental HDXMS data, we performed extensive accelerated molecular dynamics (AMD) simulations [66, 67] on both WT thrombin and the W215A mutant (see Methods for details). AMD simulations were performed for 750,000,000 steps using a "real time" time step of 2fs, the equivalent of 1.5μs in a classical MD simulation. Because the acceleration level used here affords an increase in the rate of conformational space sampling by 3-4 orders of magnitude, the simulations presented here probe slow molecular motions occurring on timescales of milliseconds to tens of milliseconds [65].

In agreement with the experimental HDXMS data, comparative analysis of the conformational dynamics from AMD simulations of WT and W215A thrombin revealed, for the most part, very few differences between WT and the W215A

mutant. The most significant difference observed was a transient destabilization of the 170s$_{CT}$ loop (residues 205-223) in the W215A mutant on slow timescales. Mutation of Trp215$_{CT}$ to Ala removes the strong ring-ring stacking interaction between Trp215$_{CT}$ (residue 263) and Phe227$_{CT}$ (residue 275), causing enhanced mobility on slow timescales of residue Phe227$_{CT}$ and its neighbor, Tyr228$_{CT}$ (residue 276). As a result, transient dislocation of H-bond interactions between residues Tyr228$_{CT}$ and Phe181$_{CT}$ (Tyr276:NH-Phe222:CO and Phe222:NH-Tyr276:CO) is observed. The loss of these H-bonds apparently results in transient unfolding of the alpha-helix residues Arg165-Ser171$_{CT}$ (residues 206-212) with further dislocation of the H-bonds between residues Val167$_{CT}$, Glu164$_{CT}$, Lys169$_{CT}$, Arg165$_{CT}$, and Ser171$_{CT}$(residues Val208:NH-Glu205:CO, Lys210:NH-Arg206:CO, and Ser212:NH-Val208:CO). It should be noted that the local unfolding events described above are rare, and approximate free energy statistics obtained from the AMD simulations suggest that the population of this locally unfolded structural motif is less than 10%. These results are consistent with the experimental HDXMS results which showed an increased uptake of four additional deuterons in residues 156-181$_{CT}$ (197-222) for the W215A mutant thrombin (cf. Figure 3.5). The AMD simulation results suggest that the four amide protons are those of residues Arg 165$_{CT}$, Val167$_{CT}$, Lys169$_{CT}$, and Ser171$_{CT}$ (residues Arg206, Val208, Lys210, and Ser212).

In addition to the transient destabilization of the 170s$_{CT}$ loop, the AMD simulations also identified a transient conformation of the W215A mutant which was characterized by a dramatic shift in the side chains of Phe227$_{CT}$ and Ile16$_{CT}$ (residue

37) resulting in a misalignment of the catalytic triad (Figure 3.6B). A full description of the AMD simulations, including a computational analysis of the HDXMS data will be presented elsewhere[68].

Determination of the role of Trp215 in stabilizing the thrombin structure. Because $Trp215_{CT}$ appears to be undergoing pi-stacking with $Phe\ 227_{CT}$ [4], we wondered whether the F227A mutation would have the same effects as the W215A mutation. In addition, the more conservative substitutions W215I and F227V were also prepared and all of the mutants were subjected to HDXMS under conditions where the enzyme appears to be most dynamic (100 mM NaCl). The W215A, W215I, and F227A mutants all showed similarly increased deuterium uptake in residues $156\text{-}180_{CT}$ (residues 197-221; MH+ 2896.550) and residues $161\text{-}181_{CT}$ (residues 202-222 MH+ 2490.296) as compared to WT thrombin (Figure 3.7A). Comparison of the deuterium uptake in the overlapping peptide, residues $161\text{-}170_{CT}$ (202-211; MH+ 1155.619), suggested the increased deuterium uptake was at least partially occurring in the α-helix spanning residues $165\text{-}170_{CT}$ (residues 206-211) in all mutants, however the W215I mutation did not destabilize to the same extent. All of the mutants also showed increased deuterium uptake in the $220s_{CT}$ loop - residues $208\text{-}227_{CT}$ (residues 256-275; MH+ 2152.943, MH+ 2191.954, and MH+ 2267.985 for W215A, F227A, and WT respectively), residues $212\text{-}227_{CT}$ (residues 260-275; MH+ 1673.760, MH+ 1715.806, and MH+ 1788.801 for W215A, W215I, and WT respectively), and residues $212\text{-}228_{CT}$ (residues 260-276; MH+ 1903.864 for F227V) - relative to wild type thrombin (Figure 3.7B), although the increase in uptake for

F227V could not be accurately determined as there was no matching peptide in the WT dataset.

Evidence for exposure of the Trp215 backbone amide. Although increased deuterium uptake in peptides spanning the 220s$_{CT}$ loop was observed for the Trp215$_{CT}$ and Phe227$_{CT}$ mutants, examination of the deuterium uptake into two overlapping peptides spanning residues 208-215$_{CT}$ (residues 256-263) in WT, F227A and F227V allowed assignment of a significant portion of the effect to the backbone amide at position 215$_{CT}$ (residue 263). By subtracting the deuterium uptake into the peptide spanning residues 208-214$_{CT}$ (residues 256-262; MH+ 797.386) from that of the peptide spanning residues 208-215$_{CT}$ (residues 256-263; MH+ 983.466), it was possible to determine that a full additional amide was exchanged into position 215$_{CT}$ in the F227A mutant and a stepwise increase in deuterium uptake with decreasing hydrophobic character in the sidechain of residue 227$_{CT}$ (Figure 3.7C). Thus, the hydrophobicity of the residue at position 227 affects the exchange of the amide group at position 215.

Understanding the HDXMS results in light of thrombin catalytic activity. Because HDXMS showed that mutation of W215A, W215I, F227A, and F227V affected the dynamics of the loops surrounding the thrombin active site, the catalytic activity of these mutants was characterized using chromogenic substrates that target only the active site. The catalytic ability of W215A, W215I, and F227A towards the coagulative substrates fibrinopeptide A (FPA) and protease-activated receptor 1 (PAR1), and the anticoagulative substrate protein C (PC) have already been characterized [60]. When expressing and purifying the various mutants as fusion

constructs containing 18 residues from prothrombin, we noticed that W215A and F227V were able to catalyze the self-cleavage of the propeptide which occurs after cleavage of the activation peptide by ecarin. W215I and F227A required the addition of WT thrombin to affect the self-cleavage. Consistent with its ability to self-cleave, the F227V mutant retained significant activity towards all substrates tested compared to WT thrombin (Table 2.1). Although W215A could self-cleave, its activity was decreased to less than 10% of WT thrombin in chromogenic substrate assays as well as towards fibrinogen. The mutants W215I and F227A, lost their ability to self-activate, and were not studied further due to their lack of observed activity.

We compared two chromogenic substrates, the S-2238, which has a bulky Phe at P3 and is thought to mimic fibrinogen, vs. S-2366, which has a smaller pyroGlu at P3 and is thought to mimic protein C and PAR1. Though WT thrombin was able to cleave both chromogenic substrates, each mutant preferentially cleaved the procoagulant mimicking substrate S-2238, which is best exemplified by F227V (Table 2.1).

D. Discussion

The effect of NaCl on the dynamics of thrombin. Even though the sodium binding site was identified between the 220s$_{CT}$ and 180s$_{CT}$ loops [69, 70], our HDXMS results did not show a difference in dynamics in these loops at NaCl concentrations between 100 mM NaCl and 300 mM NaCl for WT thrombin. In contrast, mutation of Trp215$_{CT}$ did cause a significant increase in the dynamics of the 220s$_{CT}$ loop indicating that its motions can, in fact, be altered. The region of thrombin that

showed the most significant sensitivity to NaCl concentration was the 170s$_{CT}$ loop (residues 197-222; 156-181$_{CT}$), which did not show an appreciable difference in conformation between the sodium-free and sodium bound forms according to crystallographic evidence [9].

Other effects of NaCl concentration observed were almost entirely localized to the surface loops of thrombin, in both WT thrombin and the W215A mutant. Interaction of monovalent ions interact with regions of thrombin distinct from the 220s$_{CT}$ and 180s$_{CT}$ loops was proposed previously based on MD simulations [71] and Xiao et al. showed that the surface loops of thrombin displayed a smaller ensemble of conformations upon interaction with sodium ions [72]. In fact, we show decreased amide exchange in the surface loops at higher NaCl concentrations consistent with these simulation results. Our results also showed a marked sodium-induced stabilization of the 90s$_{CT}$ loop (residues 117-135), which contains Asp102$_{CT}$, and this may actually be the major underlying cause of observed effects of sodium ions on thrombin activity.

The effect of mutations at Trp215 and Phe227 on local structure. Just as a lower concentration of NaCl leads to increased deuterium uptake in the 170s$_{CT}$ loop and the β-strands that flank it, so does the interruption of the pi-stacking interaction between the side chain at positions 215$_{CT}$ and 227$_{CT}$. When the side chain at either position was replaced with Val or Ile, the 170s$_{CT}$ loop was slightly more stabilized than for the alanine mutants. Analysis of the deuterium uptake into residues 156-181$_{CT}$ (residues 197-222) in conjunction with the hydrogen bonds broken during the AMD simulations of W215A localized the amides that are likely undergoing

increased amide exchange in the Trp215$_{CT}$ and Phe227$_{CT}$ mutants to those within the 170s$_{CT}$ loop itself.

Uniqueness of the Trp215$_{CT}$-Phe227$_{CT}$ interaction. Trp215$_{CT}$ is nearly perfectly conserved across the chymotrypsin family of serine proteases, although Phe227$_{CT}$ is not. Val or Ile is found at position 227$_{CT}$ for all members in this family except for thrombin. It was recently shown that the 170s$_{CT}$ loop in murine urokinase-type plasminogen activator (muPA), which contains a Val at position 227$_{CT}$, exists in equilibrium between two distinct, highly dynamic conformations that require the Cys168$_{CT}$-Cys182$_{CT}$ bond to "adopt different rotational conformers to allow" for interconversion [73]. This result is consistent with our observation that the F227V mutant has higher exchange in the 170s$_{CT}$ loop. Conventional molecular dynamics simulations analyzed using a Markov state model showed that trypsin, which also has a Val at position 227$_{CT}$, samples conformational states where the side chain of Trp215$_{CT}$ is rotated towards the active site [74]. In fact, there are many apparently stabilizing interactions that Trp215$_{CT}$ makes with residues in the 170s$_{CT}$ loop including interaction with Ile174$_{CT}$. Additional interactions within the 170s$_{CT}$ loop that don't directly involve Trp215$_{CT}$ include the interaction between Thr172$_{CT}$ and Glu217$_{CT}$. Given that the T172A, I174A, E217A, and F227A all exhibit the same ~10-fold decrease in activity towards FpA and PAR1, while retaining protein C activation [60], we may speculate that these side chains all work together to optimize thrombin's procoagulative function.

The residue at position 215$_{CT}$ may flip into the active site. Multiple other studies have shown that the Trp215$_{CT}$ side chain of thrombin can occlude the active

site upon mutation of residues near the active site such as D102N [75], Δ146-149e [76], Y225P [77], and N143P [78]. In MD simulations, WT thrombin adopts a similar occluded conformational state in a sodium-free environment [72]. When analyzing the effects of W215A, W215I, and F227V on the activity of thrombin towards substrates, we observed that the activity of W215I towards both chromogenic substrates was almost entirely abolished compared to the W215A mutant. The F227A mutant also could not self-activate and this could be due to a reconfiguration of the Trp215$_{CT}$ side chain into the active site preventing optimal activity. In contrast, the F227V mutant is able to self-activate, cleave fibrinogen, and activate PC with near WT activity. A consistent model that explains these data is that a Val at position 227$_{CT}$, as is found in all other coagulation proteases, is sufficient to stabilize the Trp215$_{CT}$ side chain from flipping into the active site whereas an Ala at position 227$_{CT}$ is not. Additionally, the lack of pi-stacking by Ile215$_{CT}$ with Phe227$_{CT}$ results in the repositioning of Ile215$_{CT}$ into the active site blocking activity. These data show the importance of introducing multiple conservative substitutions for understanding the role of specific enzyme residues as well as the importance of correlating data from HDXMS with enzyme activity.

The HDXMS data presented here show that the backbone amide of Trp215$_{CT}$ in WT thrombin does exchange with deuterated solvent, but at a rate far slower than nearly all other regions of the enzyme. The presence of Phe227$_{CT}$ in thrombin may be an evolutionarily significant event allowing the S1 site to more often be open for substrate binding. Consequently, the catalytic triad of thrombin would be stabilized to a greater degree than is observed for other chymotrypsin-like proteases.

Long-range effects of mutation of Trp215. Mutations at Trp215$_{CT}$ appeared to have a greater effect on deuterium exchange into the 220s$_{CT}$ loop than mutations at 227$_{CT}$ suggesting that the W215A mutation destabilized residues in the 220s$_{CT}$ loop to a greater extent than the F227A mutation. Although mutations at Phe227$_{CT}$ led to the increased exchange into the backbone amide of Trp215$_{CT}$, only mutations at Trp215$_{CT}$ appeared to notably affect amide exchange into the whole 220s$_{CT}$ loop.

Our HDXMS results also showed that the W215A mutant had significantly higher exchange into the N-terminus of the heavy chain, and this effect was greater than for any of the other mutants tested (Figure 3.6 and 3.8). The AMD simulations of the W215A mutant showed a transient structure in which the side chain of Phe227$_{CT}$ (residue 275) was rotated into the position that the Trp215$_{CT}$ side chain formerly occupied. In addition, the side chain of Arg173$_{CT}$ (residue 214) rotated to form a new interaction with Glu217$_{CT}$ (residue 265). Interestingly, the structure of the W215A/E217A double mutant thrombin [79, 80] showed the 214-219$_{CT}$ segment collapsed into the S1 pocket similar to the structures of D102N [75], Δ146-149e [76], Y225P [77], and N143P [78]. Our AMD results suggest that removal of the Trp215$_{CT}$ side chain transforms the backbone of residues 214-219$_{CT}$ into a much less structured segment, stabilized only when the side chain of Arg173$_{CT}$ makes contact with Glu217$_{CT}$. Kinetic analysis of R173A by Di Cera et al. showed no significant deviation of activity towards either procoagulative or anticoagulative substrates as compared to WT thrombin, but it is possible that the Arg173-Glu217$_{CT}$ interaction stabilizes the 214-219$_{CT}$ segment only when Trp215$_{CT}$ is also mutated. This would explain why the double W215A/E217A mutant shows a collapsed S1 pocket in X-

ray crystal structures [79]. Our results thus provide the first experimental evidence of the allosteric connections between position 215_{CT} and the active site first proposed by Di Cera [75, 79].

The AMD results show that the structural effects of the altered $214\text{-}219_{CT}$ segment are accompanied by a shift in the backbone hydrogen bonding to the N-terminal amino group of $Ile16_{CT}$ (residue 37) and a reorientation of the $Ile16_{CT}$ side chain. In addition, the side chains of $Asp194_{CT}$ (residue 240) and $Ser195_{CT}$ (residue 241) are altered resulting in improper alignment of the serine hydroxyl group with $His57_{CT}$ (residue 79) (Figure 3.6B). Finally, $Asp189_{CT}$ (residue 235) at the base of the S1 pocket is also rotated almost 180^{o} away from its position in the wild type enzyme and forms a new H-bond with $Arg187_{CT}$ (residue233) which is now located in the sodium binding pocket.

The work presented here identifies the distinct changes in the structure of thrombin that result from both changes in the concentration of NaCl and the disruption of the $Trp215_{CT}$-$Phe227_{CT}$ pi-stacking interaction. Our results explain how the $170s_{CT}$ loop, which makes up part of ABE2 may act as another potential regulatory region of thrombin. Additionally, the similar effects of NaCl concentration and the disruption of the $Trp215_{CT}$-$Phe227_{CT}$ pi interaction on the $170s_{CT}$ loop of thrombin opens the door for questions regarding whether sodium ions help modulate this pi interaction rather than the $220s_{CT}$ and $180s_{CT}$ loops. Most importantly, the combination of HDXMS, which provides evidence of structural changes that are difficult to elucidate by crystallographic methods alone, with AMD simulations, provides a clearer understanding of allostery in thrombin. Here we show

that mutation of $Trp215_{CT}$ rebalances the ensemble of states to populate structures in which the $170s_{CT}$ loop is unfolded and structures in which the catalytic triad and S1 pocket are perturbed. Future experiments that investigate the dynamics of thrombin will be imperative for developing a full picture regarding complex enzyme regulation.

E. Materials and Methods

Thrombin mutagenesis and Expression. All mutants were generated through site-directed mutagenesis using primers purchased from Integrated DNA Technologies. All thrombin constructs were expressed and refolded in *E. coli*, as previously described [15]. Activation of thrombin was achieved by diluting properly-folded thrombin, purified through ion exchange chromatography, to 50 mL with 50 mM Tris/HCl pH 7.4, 20 mM $CaCl_2$, 1 mg/mL PEG8000, 5% (v/v) glycerol, and 20 μg/mL *E. carinatus* venom (Sigma-Aldrich Car. # V8250) pretreated with AEBSF. Optimal activation times varied from 2-10hr at room temperature, determined by monitoring the conversion of pre-thrombin-2 to a-thrombin through ion exchange chromatography. Activated samples were loaded onto a MonoS cation exchange column (GE Healthcare Life Sciences), allowing for the separation of active a-thrombin from preactive (prethombin-2, meizothrombin) and autoproteolyzed forms (particularly γ-thrombin) using a gradient of 100 mM NaCl to 500 mM NaCl in 25 mM phosphate pH 6.5. Because of their inherent inactivity, thrombin mutants F227A and W215I were activated with 45 nM wild type α-thrombin present. Fully active α-thrombin is the latest eluting species from the MonoS column, however, all fully

active mutants eluted earlier than WT, allowing for effective purification of F227A and W215I from the WT thrombin added for activation. Fractions containing fully activated thrombin were pooled and stored at -80 C for no longer than 1 month before use. This method of thrombin purification, which avoids dialysis, has been shown previously to result in >95% active α-thrombin. Previous NMR analysis of isotopically labeled thrombin prepared this way, demonstrated that the species present was active a-thrombin [15, 34].

Thrombin activity assays. To account for the loss of A_{280} for all Trp mutants, enzyme concentrations were determined using BCA protein assays. Activity assay reactions occurred in 200 μL volumes containing 2.5 ng/mL human thrombin, 0.88 μM BSA, 2.93 mM $CaCl_2$, 20 mM Tris, 200 mM NaCl, and chromogenic substrate (Diapharma, West Chester, OH). Chromogenic substrate stocks at 12.5 mg/mL in H_2O were stored at -20 C, and were neutralized with Tris base before use. Chromogenic substrate dilutions were performed using a solution of 20 mM Tris and 200 mM NaCl. The thrombin-specific chromogenic substrate S-2238 was present at concentrations varying from 2.5 - 100 μM for WT, 6.25 - 200 μM for W215A, 1 - 100 μM for F227V, and 25 - 1000 μM for W215I. Activated PC (aPC)-specific chromogenic substrate S-2366 was present between 10 - 1000 μM for WT, 10 - 1000 μM for W215A, 50 - 1600 μM for F227V, and 50 - 1600 μM for W215I. All reactions were incubated at room temperature for 10 min following the addition of thrombin, before chromogenic substrate was added. Enzyme dilutions were made by diluting purified thrombin with a solution of 20 mM Tris pH 7.5, 200 mM NaCl, 5

mM $CaCl_2$, and 15 μM BSA. Each reaction was monitored via the linear increase in absorbance at 405 nm over time, corresponding to the release of p-nitroaniline following chromogenic substrate cleavage. From the rates measured, K_M and V_{max}, and thereby k_{cat}, values were determined for each substrate for each thrombin construct. All chromogenic substrate assays were repeated in triplicate.

Protein C assays were carried out as previously described [24]. The TM activation of thrombin towards protein C cleavage was first performed by incubating the TM construct TM456m with purified human α-thrombin before adding protein C (Hematologic Technologies, Essex Junction, VT). TM456m was purified as previously described [18]. Following a 20 min incubation with protein C, the thrombin was inactivated by addition of heparin/antithrombin-III, and the activated protein C was assayed by the addition of S-2366. Human thrombin was present at 17.4 ng/mL for each reaction, and TM456m was present at either 21.7 ng/mL, 43.5 ng/mL, 65.2 ng/mL, or 87.0 ng/mL. The rates measured in reactions from which thrombin and/or TM4546m were omitted were subtracted from the rates of the other reactions to account for any PC activation not catalyzed by the thrombin-thrombomodulin complex. The rates for each F227V reaction were divided by the rates for each WT thrombin reaction with the same amount of TM456m added, and all ratios calculated were averaged.

Fibrinogen clotting assays were performed as previously described [81]. Thrombin concentrations were determined by BCA assays. The concentrations of thrombin used correspond to the amount necessary for a clot to form between 18-22

sec after the addition of fibrinogen. All clotting assays were performed in triplicate, and the average time-to-clot was used in activity determination.

Hydrogen-Deuterium Exchange. All α-thrombin proteins were prepared for HDXMS from frozen aliquots (~7 μM). After being passed through a 0.2 micron filter, a portion was diluted to 5 μM, and 130 μL was saved for the HDXMS experiment. The remaining sample was concentrated to 10 μM using pre-rinsed 6 mL 10K MWCO Amicon concentrators, spinning at 3000 rpm in 5 min intervals at 4ºC to be used for peptide identification (50 μL). In the HDXMS experiment, the sample is diluted 12-fold (see below) resulting in a final α-thrombin concentration of 420 nM.

HDXMS was performed using a Waters Synapt G2Si system with HDX technology (Waters Corporation). Deuterium exchange reactions were prepared using a Leap HDX PAL autosampler (Leap Technologies, Carrboro, NC). D_2O buffer was prepared by lyophilizing 1 mL of 250 mM phosphate pH 6.5 and either 1 M NaCl for low salt experiments of 3 M NaCl for high salt experiments, before being resuspended in 10 ml 99.96% D_2O immediately before use. Under the conditions of the HDXMS experiment (420 nM thrombin), the sodium binding site should have been less than 80% occupied [69] at 100mM NaCl and over 90% occupied at 300 mM NaCl. Each deuterium exchange time point (0 min, 30 sec, 1 min, 2 min, 5 min) was measured in triplicate. For each deuteration time point, 5 μL of protein was held at 25ºC for 5 min before being mixed with 55 μL of D_2O buffer. The deuterium exchange was quenched for 1 min at 1ºC by combining 50 μL of the

deuteration reaction with 50 μL of 250 mM TCEP pH 2.5. The quenched sample was then injected in a 50 μL sample loop, followed by digestion on an in-line pepsin column (immobilized pepsin, Pierce, Inc.) at 15oC. The resulting peptides were captured on a BEH C18 Vanguard pre-column, separated by analytical chromatography (Acquity UPLC BEH C18, 1.7 μM, 1.0 x 50 mm, Waters Corporation) using a 7-85% acetonitrile in 0.1% formic acid over 7.5 min, and electrosprayed into the Waters Synapt G2Si quadrupole time-of-flight mass spectrometer. The mass spectrometer was set the collect data in the Mobility, ESI+ mode; mass acquisition range of 200-2,000 (m/z); scan time 0.4 s. Continuous lock mass correction was accomplished with infusion of leu-enkephalin (m/z = 556.277) every 30 s (mass accuracy of 1 ppm for calibration standard).

For peptide identification, the mass spectrometer was set to collect data in MS^E, ESI+ mode instead. Peptides masses were identified from triplicated analyses of 10 μM α-thrombin, and data were analyzed using PLGS 2.5 (Waters Corporation). Peptides masses were identified using a minimum number of 250 ion counts for low energy peptides and 50 ion counts for their fragment ions; the peptides also had to be larger than 1500 Da. The following cutoffs were used to filter peptide sequence matches: minimum products per amino acid of 0.2, minimum score of 7, maximum MH+ error of 5 ppm, a retention time RSD of 5%, and the peptides had to be present in two of the three ID runs collected. The peptides identified in PLGS were then analyzed in DynamX 3.0 (Waters Corporation). The relative deuterium uptake for each peptide was calculated by comparing the centroids of the mass envelopes of the deuterated samples with the undeuterated controls following previously published

methods [52]. To account for back-exchange, and systematic autosampler sample handling differences between shorter and longer deuteration times, the uptake and standard deviation values for the 30 sec and 1 min, and the 2 min and 5 min timepoints were divided by 0.67 and 0.64 respectively for every HDXMS experiment run. Data were plotted as number of deuterons incorporated vs. time (min). The Y-axis limit for each plot reflects the total number of amides within the peptide that can possible exchange. Each plot includes the peptide MH+ value, sequence, and sequential residue numbering.

AMD simulations. Atomic coordinates for WT thrombin were obtained from the Protein Data Bank (PDB) 1.9-A X-ray crystal structure (PDB ID: 1PBB) and the active-site inhibitor was removed from the structure. For the W215A mutant, residue 215_{CT} was manually converted from a tryptophan to an alanine residue. Each system was placed at the center of a periodically repeating box, and the simulation cell size was defined such that the distance between the edge of the simulation box and the surface of the solute was at least 12 Å. All AMD simulations were performed in explicit solvent with appropriate counter-ions to achieve cell neutrality. Bonds involving protons were constrained using the SHAKE algorithm. Electrostatic interactions were treated using the particle mesh Ewald method with a direct space sum limit of 10 Å. The ff14SB force-field was used for the solute residues, and the TIP3P water force-field was employed for solvent molecules. In the present work, we implemented a "dual boost" AMD approach [82], in which two acceleration potentials are simultaneously applied to the system: The first acceleration potential is

applied to the torsion terms only, and a second, weaker acceleration is applied across the entire potential. For both WT thrombin and the W215A mutant systems, the specific torsional acceleration parameters were defined as Eb(dih) - <V0(dih)> = [4.0 kcal/mol * Number of residues], and the acceleration parameter, □(dih), was set to one-fifth of this value. The total background acceleration parameters were fixed at Eb(tot) - <V0(tot)> = □(tot) = [0.16 kcal/mol * No. atoms in simulation cell]. The specific choice of these AMD parameters was based on a previous NMR/AMD study of thrombin:PPACK [15]. The results of this study suggested that these acceleration parameters afforded an effective speed up in conformational space sampling of 3-4 orders of magnitude, which is in line with other studies on different systems in which AMD simulations at a similar acceleration level were directly compared to long brute-force CMD simulations [65]. The average minimum energy potentials, V0(dih) and V0(tot), were obtained from 20-ns CMD simulations performed as part of the initial equilibration procedure. It should be noted that, given the similarity of the two systems, the acceleration parameters for WT thrombin and the W215A mutant are, to all intents and purposes, identical.

For each system (WT and W215A thrombin), two AMD simulations were performed for 750,000,000 steps with a (real time) time-step of 2-fs. This is computationally equivalent to performing a 1.5μs CMD simulation. Given an effective speed up in the rate of conformational space-sampling by 3 to 4 orders of magnitude due to the application of the bias potential, we anticipate that the configurational space sampling afforded in each of the AMD simulations is associated with slow time-scale dynamics occurring on time-scales of milliseconds

to tens of milliseconds, thereby identifying slow motions, including rare local unfolding/refolding events which can be experimentally probed by HDXMS in the fast limit. All simulations were performed using the AMBER14 simulation suite. For each AMD trajectory, a corrected canonical ensemble was obtained by performing the Boltzmann free energy reweighting protocol using a cumulant expansion to the second order [83].

Chapter III, in full, is a reprint that the dissertation author was the principal researcher and author of. The material appears in *Biochemistry*. **Peacock RB**, Davis JR, Markwick PRL, Komives EA. (2018). Dynamic Consequences of Mutation of Tryptophan 215 in Thrombin. *Biochemistry*. 57(18):2694-2703.

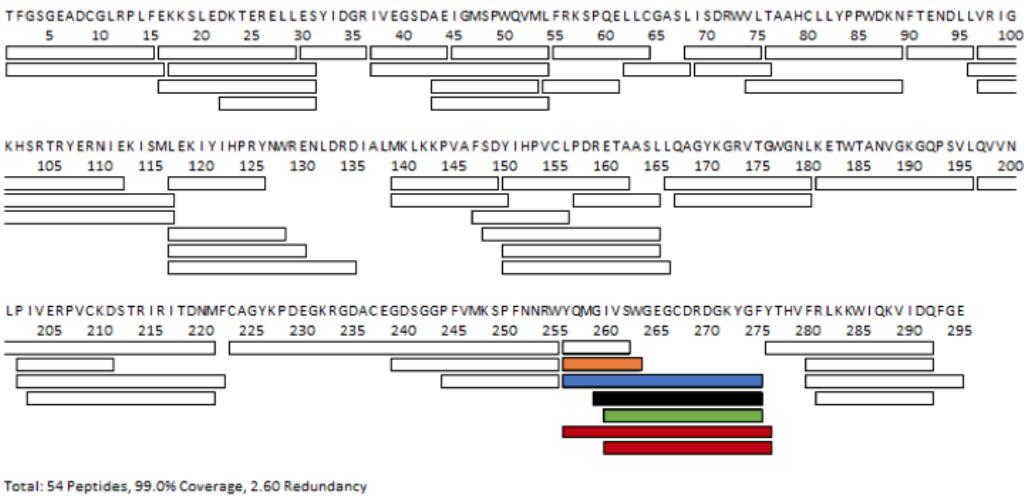

Figure 3.1. HDX-MS coverage map of all peptides analyzed for WT thrombin, W215A, W215I, F227A, and F227V. All white peptides were identified for all enzymes tested. Black peptides were identified in WT and W215A datasets only. Orange peptides were Identified in WT, F227A, and F227V datasets only. Blue peptides were identified in WT, F227A, and W215A datasets only. Green peptides were identified in WT, W215I, and W215A datasets only. Red peptides were identified in the F227V dataset only.

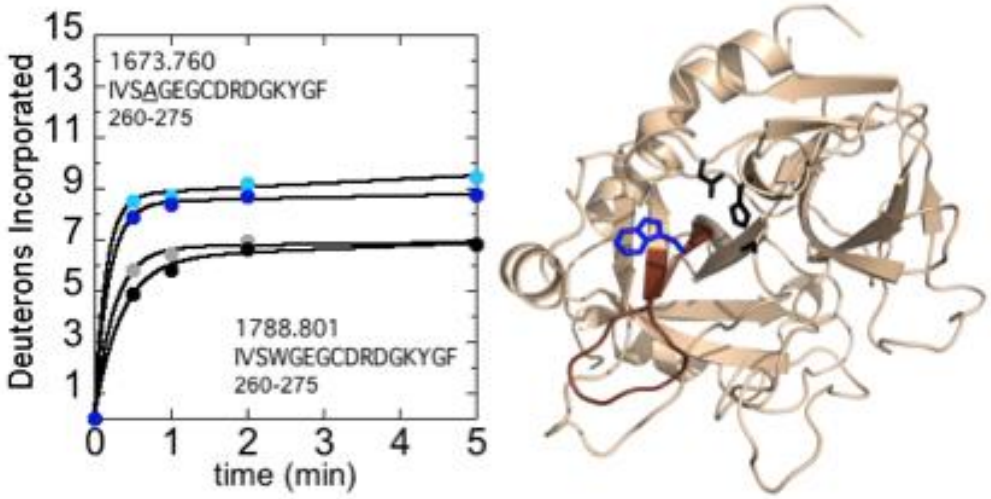

Figure 3.2. Deuterium incorporation into residues 212-227$_{CT}$ (residues 260-275; MH+ 1673.760 and 1788.801 for W215A and WT respectively) over 5 min is shown for WT thrombin at 100 mM NaCl (grey) and 300 mM NaCl (black), and for the W215A mutant at 100 mM NaCl (cyan) and 300 mM NaCl (blue)(left). The mutant residue, is underlined in the peptide sequence shown. Structure of WT thrombin (PDB 1PPB) highlighting residues 212-227$_{CT}$ (residues 260-275; brown)(right). The sidechains of Trp215$_{CT}$ (blue) and the catalytic triad (black) are shown as sticks.

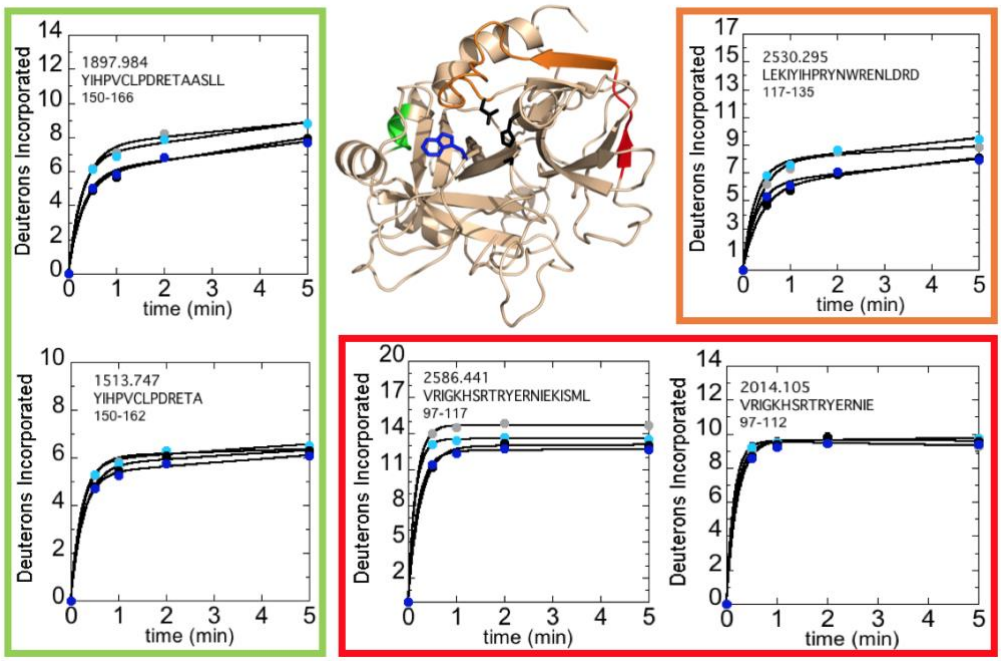

Figure 3.3. Structure of WT thrombin (PDB 1PPB) highlighting residues 81-85$_{CT}$ (residues 113-117; red), residues 86-102$_{CT}$ (residues 118-135; orange), and residues 129A-130$_{CT}$ (residues 163-166; green). Colored residues specify regions affected by the concentration of NaCl after subtraction of deuteron uptake of overlapping peptides 66-80$_{CT}$ (residues 97-112; MH+ 2014.105) from 66-85$_{CT}$ (residues 97-117; MH+ 2586.441) and 117-129$_{CT}$ (residues 150-162; MH+ 1513.747) from 117-130$_{CT}$ (residues 150-166; MH+ 1897.984) as well as residues 85-102$_{CT}$ (residues 117-135; MH+ 2530.295). The sidechains of Trp215$_{CT}$ (blue) and the catalytic triad (black) are shown as sticks. Deuteron incorporation into these residues over 5 min is shown for WT thrombin at 100 mM NaCl (grey) and 300 mM NaCl (black), and for the W215A mutant at 100 mM NaCl (cyan) and 300 mM NaCl (blue).

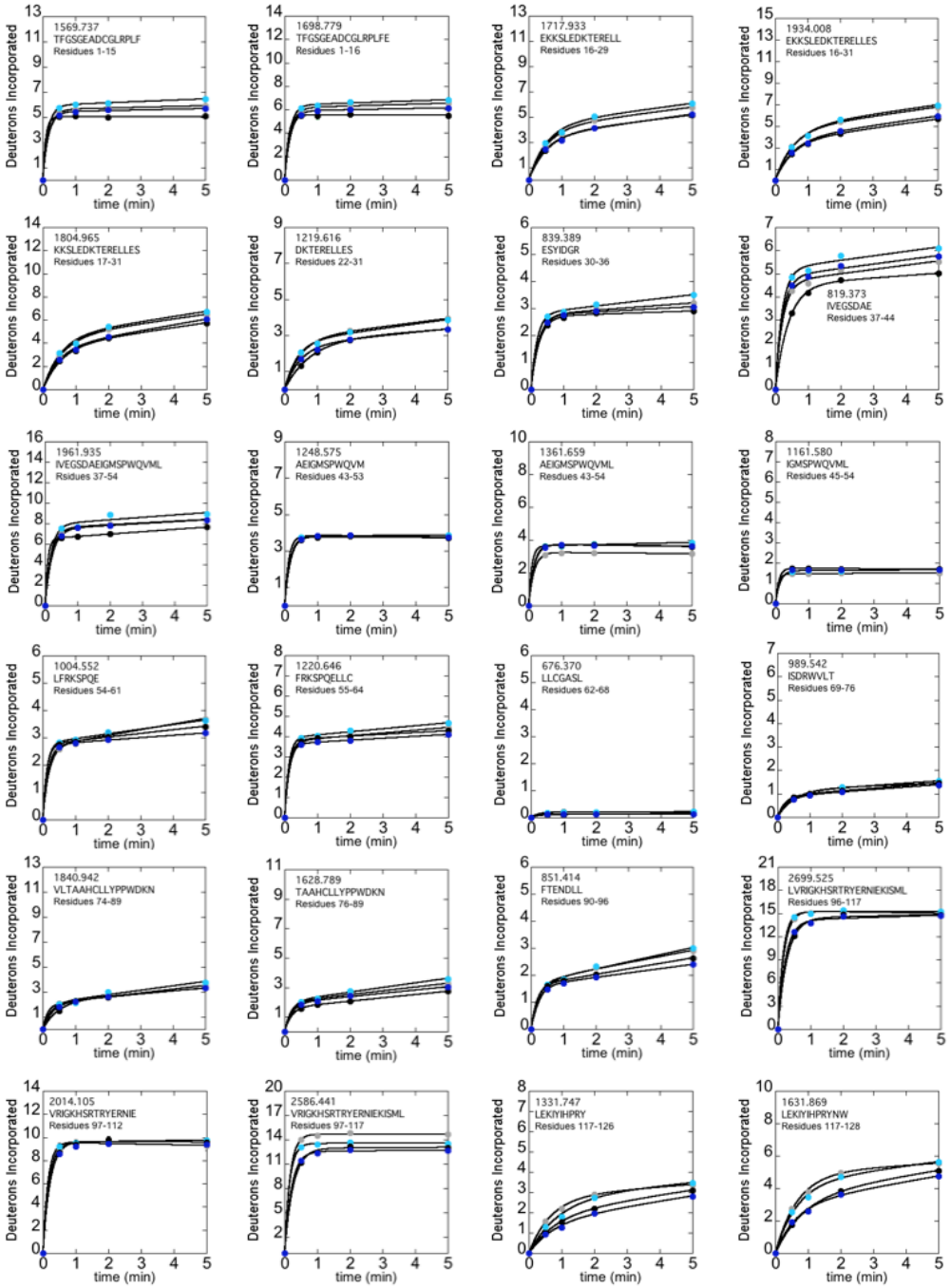

Figure 3.4. HDX-MS uptake plots showing deuterium uptake overtime for WT thrombin (grey) and W215A (cyan) at 100 mM NaCl, and for WT thrombin (black) and W215A (blue) at 300 mM NaCl. Mutations, if present, are underlined in the peptide sequence within the uptake plot. All Experiments were done in triplicate, and error are bars shown.

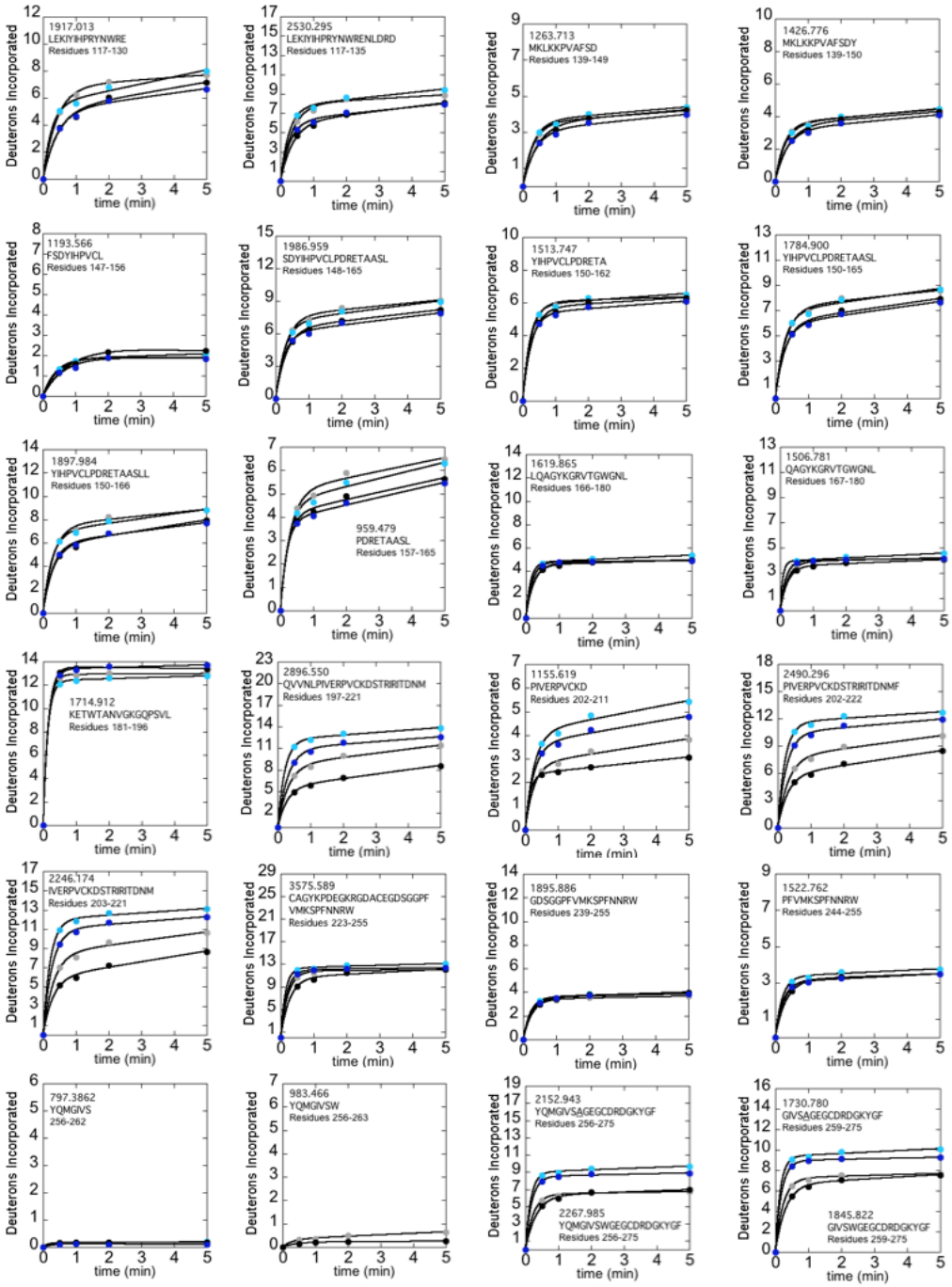

Figure 3.4 Continued. HDX-MS uptake plots showing deuterium uptake overtime for WT thrombin (grey) and W215A (cyan) at 100 mM NaCl, and for WT thrombin (black) and W215A (blue) at 300 mM NaCl. Mutations, if present, are underlined in the peptide sequence within the uptake plot. All Experiments were done in triplicate, and error are bars shown.

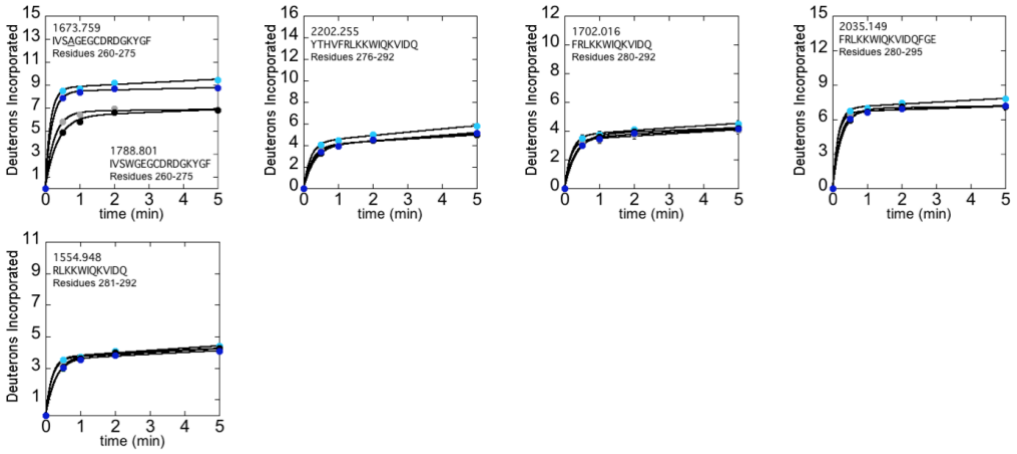

Figure 3.4 Continued. HDX-MS uptake plots showing deuterium uptake overtime for WT thrombin (grey) and W215A (cyan) at 100 mM NaCl, and for WT thrombin (black) and W215A (blue) at 300 mM NaCl. Mutations, if present, are underlined in the peptide sequence within the uptake plot. All Experiments were done in triplicate, and error are bars shown.

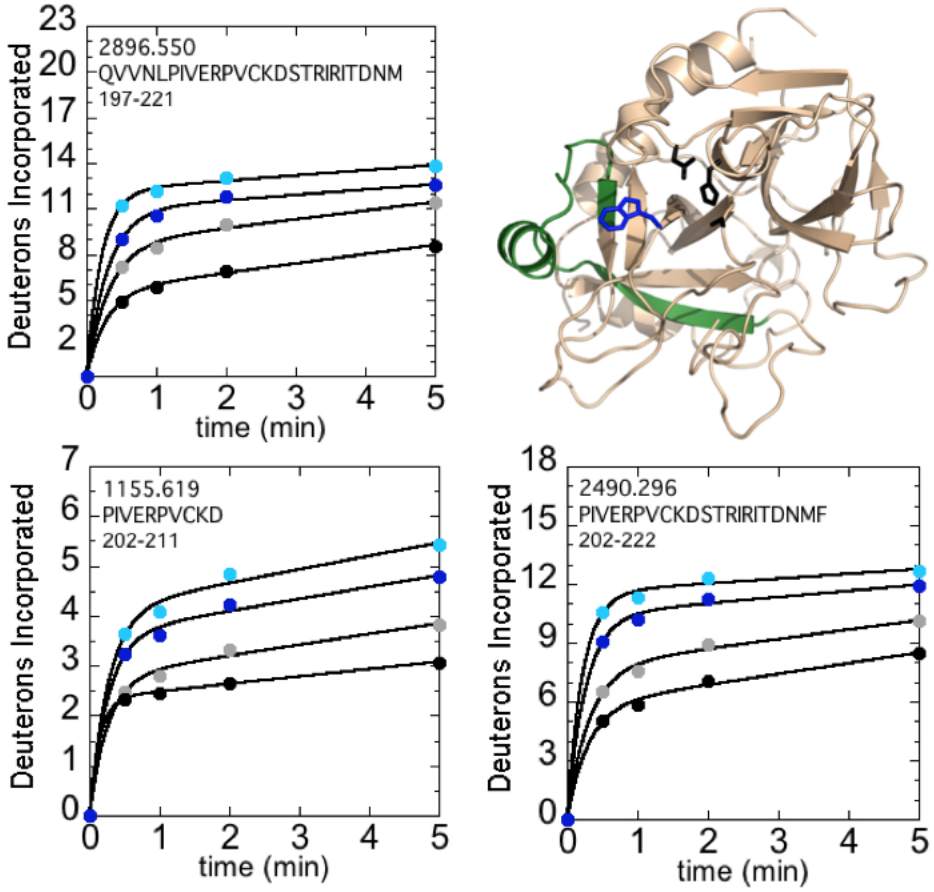

Figure 3.5. Structure of WT thrombin (PDB 1PPB) highlighting 156-181$_{CT}$ (residues 197-222; green). The sidechains of Trp215CT (blue) and the catalytic triad (black) are shown as sticks. Deuteron incorporation over 5 min into residues 156-180 $_{CT}$ (residues 197-221; MH+ 2896.550), 161-170$_{CT}$ (residues 202-211; MH+ 1155.619), and 161-181$_{CT}$ (residues 202-222; MH+ 2490.296) is shown for WT thrombin at 100 mM NaCl (grey) and 300 mM NaCl (black), and for the W215A mutant at 100 mM NaCl (cyan) and 300 mM NaCl (blue).

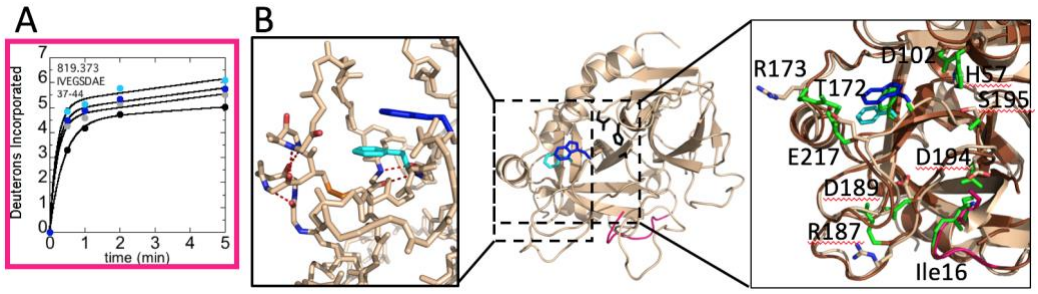

Figure 3.6. A) Deuterium incorporation over 5 min into residues 16-23$_{CT}$ (residues 36-44; MH+ 819.373) for WT thrombin at 100 mM NaCl (grey) and 300 mM NaCl (black), and for the W215A mutant at 100 mM NaCl (cyan) and 300 mM NaCl (blue). **B)** Structure of WT thrombin (wheat; PDB 1PPB) highlighting residues 16-23$_{CT}$ (pink). The sidechains of Trp215$_{CT}$ (blue), Phe227$_{CT}$ (cyan), and the catalytic triad (black) are shown as sticks. Accelerated MD simulations identified 5 H-bonds (red-dotted lines) within WT thrombin (left) that broke during simulations of W215A. The transient structure observed during the W215A simulation (brown) overlaying the structure of WT thrombin (right). The side chains of His57$_{CT}$, Asp102$_{CT}$, Thr172$_{CT}$, Arg173$_{CT}$, Arg 187$_{CT}$, Asp 189$_{CT}$, Asp194$_{CT}$, Ser195$_{CT}$, Trp215$_{CT}$ (blue), Glu217$_{CT}$, and Phe227$_{CT}$ (cyan). The 140s$_{CT}$ loop is hidden for clarity. The backbone of Ile16$_{CT}$ (pink) is also shown as sticks. The corresponding side chains in the W215A structure, including Ala215$_{CT}$, are colored green and are shown as sticks.

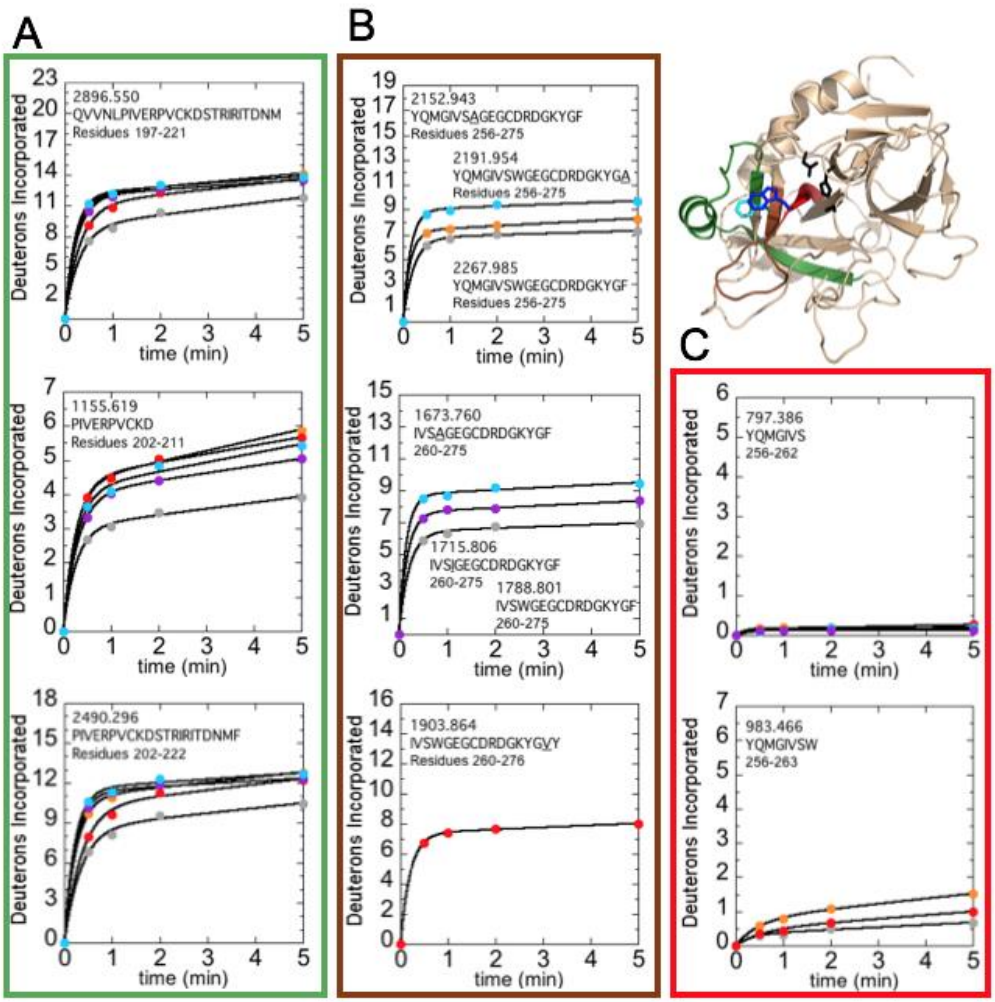

Figure 3.7. Structure of WT thrombin (PDB 1PPB) highlighting residues 156-181$_{CT}$ (residues 197-222; green), residues 208-215$_{CT}$ (residues 256-263; red), and residues 216-228$_{CT}$ (residues 264-276; brown). The sidechains of Trp215$_{CT}$ (blue), Phe227$_{CT}$ (cyan), and the catalytic triad (black) are shown as sticks. **A)** Uptake plots corresponding to residues 156-180$_{CT}$ (residues 197-221; MH+ 2896.550), 161-170$_{CT}$ (residues 202-211; MH+ 1155.619), and 161-181$_{CT}$ (residues 202-222; MH+ 2490.296). **B)** Uptake plots corresponding to residues 208-227$_{CT}$ (residues 256-275; MH+ 2152.943, MH+ 2191.954, and MH+ 2267.985 for W215A, F227A, and WT respectively), residues 212-227$_{CT}$ (residues 260-275; MH+ 1673.760, MH+ 1715.806, and MH+ 1788.801 for W215A, W215I, and WT respectively), and residues 212-228$_{CT}$ (residues 260-276; MH+ 1903.864 for F227V). The mutant residue, if present, is underlined in the peptide sequence shown. **C)** Uptake plots corresponding to residues 208-214$_{CT}$ (residues 256-262; MH+ 797.386) and 208-215$_{CT}$ (residues 256-263; MH+ 983.466). Deuterium incorporation over 5 min into the multiple peptides that cover these regions are shown for WT thrombin (grey) as well as the F227A (orange), F227V (red), W215A (cyan), and W215I (purple) mutants under experimental conditions of 100 mM NaCl.

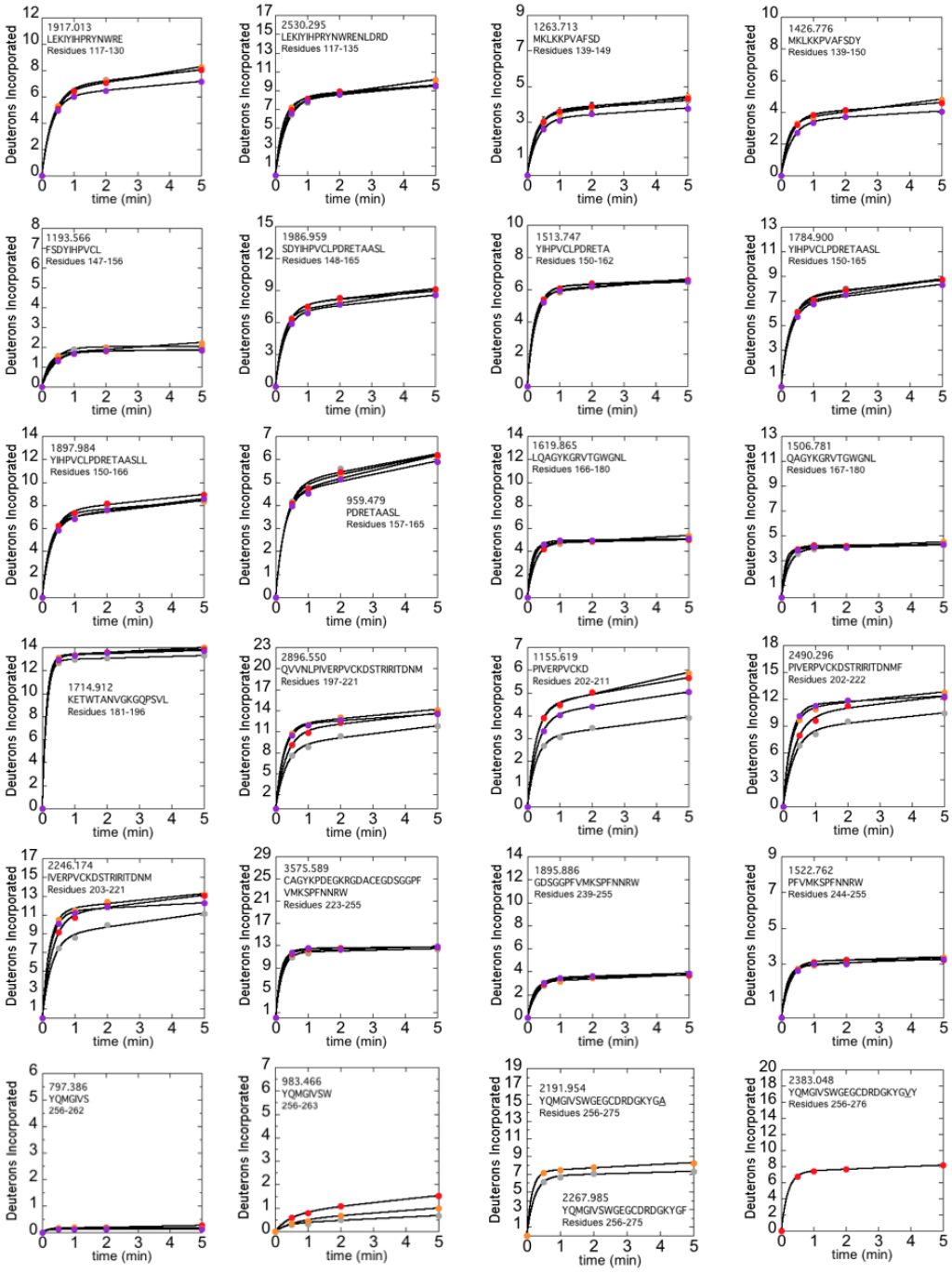

Figure 3.8. HDX-MS uptake plots showing deuterium uptake overtime for WT thrombin (grey), F227A (orange), F227V (red), and W215I (purple) at 100 mM NaCl. Mutations, if present, are underlined in the peptide sequence within the uptake plot. All Experiments were done in triplicate, and error are bars shown.

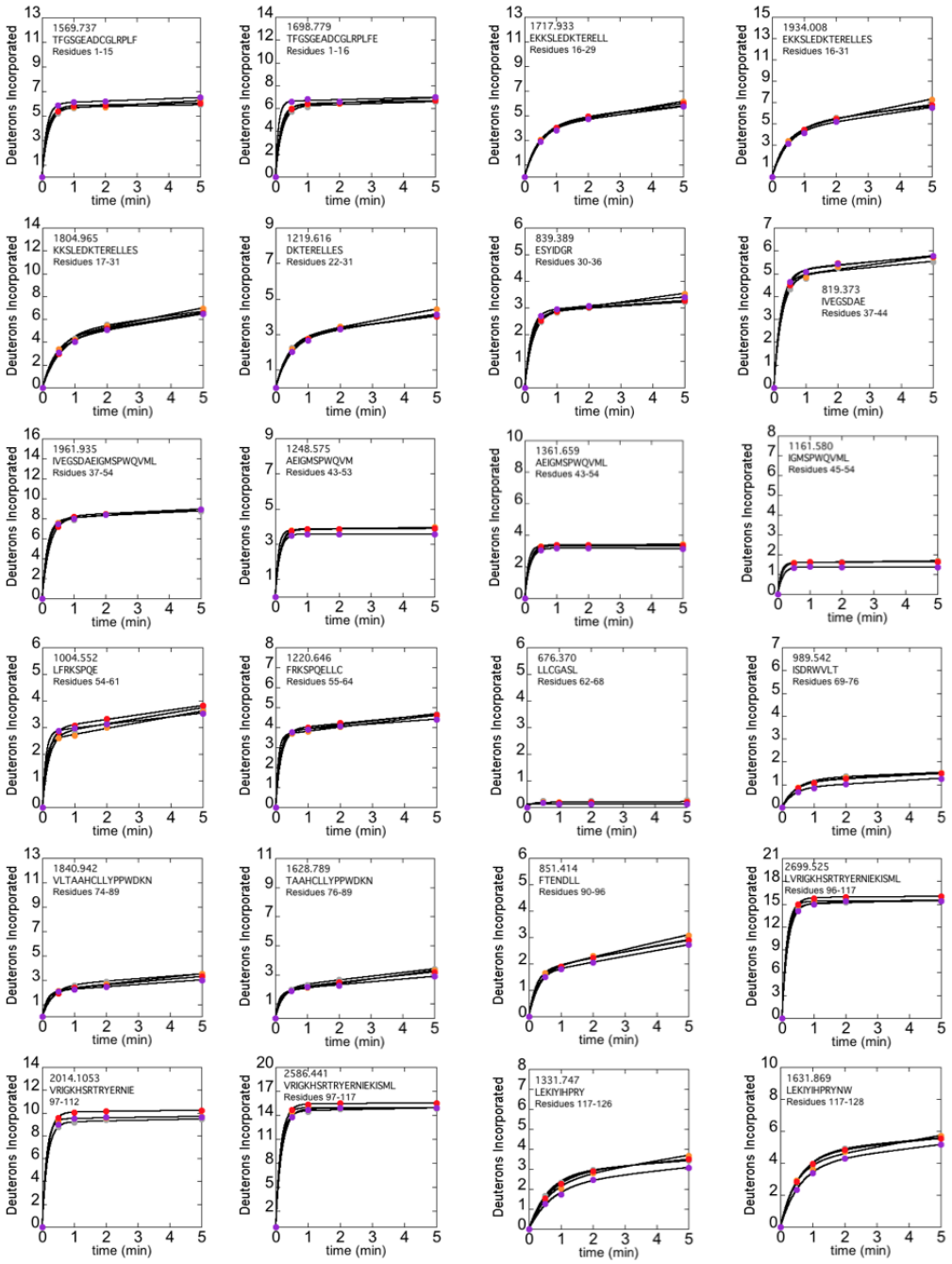

Figure 3.8 Continued. HDX-MS uptake plots showing deuterium uptake overtime for WT thrombin (grey), F227A (orange), F227V (red), and W215I (purple) at 100 mM NaCl. Mutations, if present, are underlined in the peptide sequence within the uptake plot. All Experiments were done in triplicate, and error are bars shown.

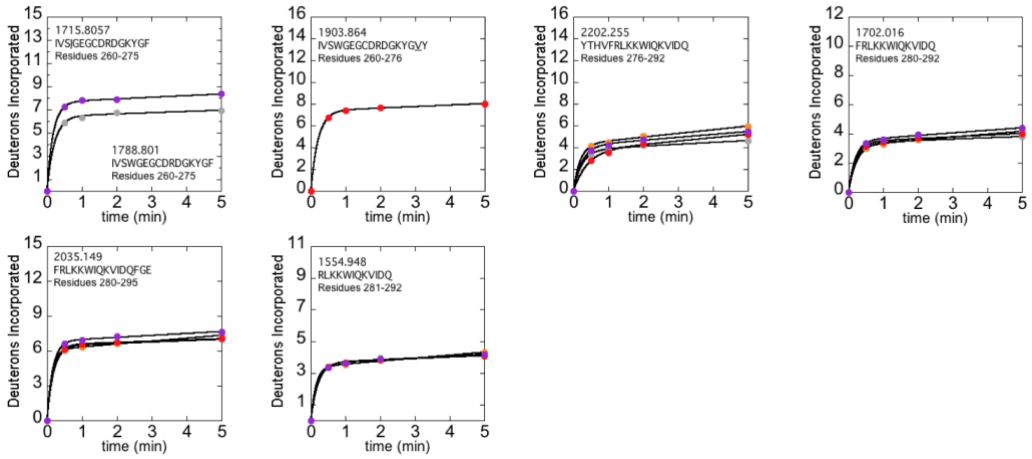

Figure 3.8 Continued. HDX-MS uptake plots showing deuterium uptake overtime for WT thrombin (grey), F227A (orange), F227V (red), and W215I (purple) at 100 mM NaCl. Mutations, if present, are underlined in the peptide sequence within the uptake plot. All Experiments were done in triplicate, and error are bars shown.

Table 3.1. Activity of the various thrombin mutants. s/s_{WT} is the ratio of k_{cat}/K_M for the mutant divided by the k_{cat}/K_M for the wild type. Fibrinogen activation units correspond to the amount of thrombin required to clot fibrinogen in 20 sec. This amount for WT thrombin is 100 ng or 3 pmol. Protein C activation was determined as described in the Methods section.

Construct	**Auto-Activating?**	**s/s_{WT} S-2238**	**s/s_{WT} S-2366**	**Fibrinogen Activation units relative to WT thrombin**	**Protein C activation rate relative to WT thrombin**
WT	Yes	1.00+/-0.16	1.00+/-0.03	1	1
W215A	Yes	0.053+/-0.007	0.038+/-0.003	0.032	n.d.
W215I	No	0.017+/-0.001	0.013+/-0.003	n.d.	n.d.
F227A	No	N/D	N/D	n.d.	n.d.
F227V	Yes	1.00+/-0.15	0.66+/-0.06	0.76	0.66

Chapter IV

Mutation of W215A/E217A in Thrombin Interrupts the Allosteric Activity of Thrombomodulin

Mutation of W215A/E217A in Thrombin Interrupts the Allosteric Activity of Thrombomodulin

Riley B. Peacock[1], Taylor McGrann[1] Sofia Zaragoza[1], Marco Tonelli[2], and Elizabeth A. Komives[1*]

[1]Department of Chemistry and Biochemistry, University of California, San Diego, 9500 Gilman Drive, La Jolla, CA 92093-0378.

[2] NMRFAM University of Wisconsin, 433 Babcock Drive, Madison, WI 53706.

*Corresponding author: Elizabeth A. Komives

Department of Chemistry and Biochemistry, University of California, San Diego, 9500 Gilman Drive, La Jolla, CA 92092-0378

Ph: (858) 534-3058

Email: ekomives@ucsd.edu

Keywords: serine protease, protein dynamics, hydrogen deuterium exchange, allostery

A. Abstract

The serine protease thrombin plays an essential regulatory role in blood clotting. Prothrombin is converted to the active α-thrombin in response to tissue damage, allowing the enzyme to cleave procoagulative substrates such as fibrinogen and PAR, enabling the formation of the clot. On the other hand, when thrombin binds its protein cofactor thrombomodulin (TM), the enzyme loses substrate specificity for procoagulative substrates, and engages the anticoagulative pathway by selectively targeting the substrate protein C for proteolytic activation. The W215A/E217A mutant has shown great promise as a thrombin species that retains the anticoagulative activity of thrombin yet loses much of the procoagulative activity of the enzyme, begging the question of whether TM binding recovers the effects of these mutations. The work presented here uses hydrogen-deuterium exchange mass spectrometry (HDXMS) to report the dynamics of W215A/E215A thrombin in the presence and absence of TM. We found that these mutations cause increased dynamics locally around the S1 pocket, as well as distally, reaching all the way to ABE1 where TM binds. TM binding could partially correct the increased dynamics induced by the W215A/E217A mutations near ABE1, but had no effect on the loops that make up the S1 pocket suggesting that these mutations do not affect the ability of thrombin to recognize protein C as a substrate.

B. Introduction

The serine protease, thrombin, circulates in the blood as the zymogen prothrombin. Vascular tissue damage triggers the clotting cascade, which ultimately converts prothrombin to α-thrombin via proteolytic cleavage near the site of the compromised tissue [84]. Activation of thrombin creates a new amino terminus at the N-terminus of the thrombin heavy chain that inserts itself into the Ile cleft of thrombin during the structural rearrangement associated with the formation of the catalytically active α-thrombin species [4]. Once activated, α-thrombin readily cleaves fibrinogen in the blood, initiating the procoagulative response that ultimately leads to the formation of a blood clot.

Thrombin is often described as a "dual-action" protease as this enzyme is also capable of stimulating the anticoagulative pathway by cleaving -and thereby activating- protein C [5]. The binding of the protein cofactor, thrombomodulin (TM), to thrombin is the key regulatory switch that toggles thrombin substrate specificity away from procoagulative substrates and towards protein C. Numerous studies over the years using a variety techniques such as X-ray crystallography [25], hydrogen-deuterium exchange mass spectrometry (HDX-MS) [18], and isothermal titration calorimetry (ITC)[20], surface plasmon resonance (SPR) [35], accelerated molecular dynamics simulations [16] have been conducted on the complex formed between thrombin and TM456 -the minimal fragment of TM necessary for triggering the anticoagulative activity of thrombin. However, only the recent publication of nuclear magnetic resonance (NMR) Carr-Purcell-Meiboom-Gill (CPMG) experiments

measuring the dynamics of thrombin-TM456 have been able to reveal the residue-level changes in thrombin that result when TM456 binds (Chapter II). Together, these experiments describe TM as a cofactor that allosterically prepares thrombin for the binding and cleavage of protein C by promoting the motions in thrombin residues that are necessary for effective catalytic function.

NMR CPMG experiments showed that TM456 binding limited the μs-ms motions exhibited by the $170s_{CT}$, $180s_{CT,}$ and $220s_{CT}$ loops, which are implicated in thrombin substrate recognition and binding (Chapter II). Residues Trp 215_{CT} (263_{seq}) and Glu 217 (265_{seq}) were highlighted as residues that link the $170s_{CT}$ and $220s_{CT}$ loops through sidechain interactions, and the mutation of residue 215_{CT} has been shown to induce disorder in the $170s_{CT}$ loop and increase the dynamics of the $220s_{CT}$ loop [8]. Furthermore, studies have shown the W215A and E217A mutations to cause a decrease in thrombin activity towards procoagulative substrates that is much more significant than the loss of activity towards protein C when TM is present, causing the thrombin W215A/E217A double mutant to be called an anticoagulant thrombin species [59, 85-87]. However, the presence of TM is a necessary requirement for W215A/E217A thrombin to exhibit activity against protein C [88, 89]. A crystallographic study suggested that the W215A/E217A mutation closes the primary substrate binding pocket of thrombin [79]. This provides an explanation for the lack of activity exhibited by W215A/E217A thrombin towards procoagulative substrates, but little evidence exists to explain why this mutant is capable of readily cleaving protein C in the presence of TM.

W215A/E217A thrombin has also been shown to act as a safe and efficacious anticoagulant intervention during *in vivo* studies [90-97], providing an important motivation for further investigation into the structural characteristics of this enzyme. In the experiments presented here, we utilized HDX-MS to evaluate the changes in thrombin dynamics induced by the W215A/E217A mutations in the absence and presence of TM456. We found that these mutations cause changes in dynamics that could be traced from the 170s$_{CT}$, 180s$_{CT,}$ and 220s$_{CT}$ loops of thrombin all the way to the anion binding exosite 1 (ABE1) that facilitates the interaction with TM. TM binding was able to reverse the effect of the W215A/E217A mutations to the same degree as seen for WT thrombin. Thus, the dynamic motions necessary for the catalytic activity of thrombin could still be induced by TM456 in some regions of thrombin when the W215A/E217A mutations were present, despite the changes these mutations caused in the primary substrate binding pocket.

C. Results

Amide exchange at the TM binding site differs between WT and the W215A/E217A mutant when TM is bound. HDX-MS experiments were conducted on WT and on W215A/E217A thrombin in the absence and when bound to TM. We were able to determine deuterium uptake for 99% of the α-thrombin sequence for both WT and the W215A/E217A mutant thrombin in all experiments (Figure 4.1), and all HDXMS plots collected are present in Figure 4.2. Consistent with the role of the thrombin 70s$_{CT}$ loop as part of the TM-binding site of thrombin, peptides spanning the 70s$_{CT}$ loop- residues 66-84$_{CT}$ (residues 97-116$_{seq}$; MH+ 2473.357)- of

both WT and W215A/E217A thrombin showed decreased exchange in the presence of TM (Figure 4.3). However, the degree in which TM provided protection from the exchange of deuterons at this binding interface region was impacted by the presence of the W215A/E217A mutations.

The presence of the W215A/E217A mutations did not affect the degree of exchange of residues 66-84$_{CT}$ (residues 97-116$_{seq}$) which was ~12 deuterons for both WT and the W215A/E217A mutant in the absence of TM. In the presence of TM, however, this region of WT thrombin exchanged ~ 4 fewer deuterons at 30 sec whereas the W215A/E217A mutant thrombin exchanged only ~2 fewer deuterons. Despite the changes induced by the W125A/E217A mutations to the thrombin 70s loop, residues 106-114$_{CT}$ (139-147$_{seq}$; MH+ 1061.654), which link ABE1 to the catalytic Asp 102$_{CT}$ (135$_{seq}$)(Chapter II), remained unaffected by these mutations (Figure 4.2).

Allosteric effects at the N-terminus of the heavy chain when TM is bound. We previously showed that the N-terminus of the heavy chain exchanges substantially in WT thrombin, but that TM binding allosterically decreases exchange of this region likely stabilizing the catalytically active form of thrombin [18]. We were able to analyze this same region in the W215A/E217A mutant thrombin. The peptide spanning residues 16-23$_{CT}$ (residues 37-44$_{seq}$; MH+ 819.373), which contains the N-terminus of the heavy chain, exchanged significantly more in the W215A/E217A mutant thrombin than in WT (4 deuterons in the W215A/E217A mutant vs. 3 deuterons in WT thrombin). Upon TM binding, this region showed a substantial decrease in exchange of ~1.5 deuterons for WT thrombin within 1 min of exchange.

The decrease in exchange observed for the W215A/E217A mutant with TM present was only ~0.5 deuterons bringing it to the same level of exchange for WT thrombin in the absence of TM (Figure 4.4). This region is remote, ~29 Å away from the $70s_{CT}$ loop where TM binds, and ~12 Å away from the W215A/E217A mutations.

The W215A/E217A mutations destabilize the $170s_{CT}$, $180s_{CT}$ and $220s_{CT}$ loops of thrombin. HDX-MS revealed dramatically increased exchange, ~5 deuterons more, for residues $161\text{-}180_{CT}$ (residues $202\text{-}221_{seq}$; MH+ 2343.227), which span the $170s_{CT}$ loop, in the W215A/E217A mutant thrombin as compared to WT thrombin (Figure 4.5). Similarly, deuterium uptake into residues $182\text{-}207_{CT}$ (residues $223\text{-}255_{seq}$; MH+ 3575.589) was ~2 deuterons higher in the W215A/E217A mutant compared to WT. Subtraction of the deuterium uptake into residues 198-207 (residues $244\text{-}255_{seq}$; MH+ 1522.762), from that into residues $182\text{-}207_{CT}$ (residues $223\text{-}255_{seq}$; MH+ 3575.589) allowed localization of the difference in uptake to residues $182\text{-}198_{CT}$, which encompasses the $180s_{CT}$ loop of thrombin. The presence of TM causes a decrease in uptake of ~1 deuteron in residues $161\text{-}180_{CT}$ (residues $202\text{-}221_{seq}$; MH+ 2343.227), and a decrease in uptake of ~2 deuterons in residues $198\text{-}207_{CT}$ (residues $244\text{-}255_{seq}$; MH+ 1522.762) (i.e. residues $182\text{-}198_{CT}$) in WT thrombin. In contrast, the presence of TM had no effect on the deuterium uptake on the W215A/E217 mutant thrombin in either the $170s_{CT}$ or the $180s_{CT}$ loop.

A comparison of the peptides identified that cover the $220s_{CT}$ loop, residues $212\text{-}227_{CT}$ (residues $260\text{-}275_{seq}$; MH+ 1615.753 for W215A/E217A; MH+ 1788.801 for WT)showed that the W215A/E217A mutant exchanged by ~3 deuterons more as compared to WT thrombin (Figure 4.6). Similar to the peptides covering the $170s_{CT}$

and 180s$_{CT}$ loops, the 220s$_{CT}$ loop, residues 212-227 (residues 260-275$_{seq}$; MH+ 1615.753 for W215A/E217A; MH+ 1788.801 for WT), exchanged less when TM is present only for WT thrombin. TM did not appear to affect this region in the W215A/E217A mutant. Thus, the peptides spanning the 170s$_{CT}$, 180s$_{CT}$, and 220s$_{CT}$ loops all exchanged more in the W215A/E217A mutant as compared to WT thrombin, and the mutations make these regions unable to respond allosterically to TM-binding.

D. Discussion

Long-range destabilization caused by the combined W215A and E217A mutations. In a previous study, we showed that mutation of W215A alone causes changes in thrombin dynamics that extend as far as the residues at the N-terminus of the thrombin heavy chain [8]. However, the experiments described here show that the combined W215A and E217A mutations cause increased backbone dynamics in thrombin that extend past the N-terminus of the heavy chain and impact the 70s$_{CT}$ loop of the TM binding site. Gandhi et al. used isothermal titration calorimetry to show that the W215A/E217A mutations had little effect on association constant and enthalpy of binding of hirugen to AEB1, providing evidence that the binding of thrombin substrates to AEB1 is not appreciably hindered by the presence of these mutations [80].

Kinetics experiments conducted by Tanaka et al. showed that the direct thrombin inhibitor bivalirudin, which the authors suggest primarily interacts with thrombin at ABE1, could inhibit WT thrombin activity towards H-D-Phe-Pro-Arg-*p*-

nitroanilide with a K_i of 9.2 nmol/L, yet bivalirudin showed no inhibitory effect on the W215A/E217A mutant [88]. Unlike most other thrombin substrates, H-D-Phe-Pro-Arg-*p*-nitroanilide binds to thrombin only at the active site, so the inhibitory effect of bivalirudin must be allosteric in nature.

The HDX results shown here clearly show that TM binding induces the hallmark decrease in dynamics of the $70s_{CT}$ loop and the N-terminus of the heavy chain that has been observed in previous experiments [18] for both WT and -to a lesser extend- the W215A/E217A mutant. However, the effects of TM binding on the $170s_{CT}$, $180s_{CT}$, and $220s_{CT}$ loops were only observed for WT thrombin. Together, this data suggest that the W215A/E217A mutations do not markedly affect the ability of TM to bind to thrombin, but rather, they disrupt the conformational response to these molecules binding at ABE1. Thus, the inhibitory effect caused by bivalirudin and the anticoagulative activity of the thrombin-TM complex are likely reduced for the W215A/E217A thrombin mutant because these mutations interrupt the allosteric pathway used by both bivalirudin and TM to illicit changes in the thrombin active site.

Trp 215_{CT} and Glu 217_{CT} are key to the allosteric communication between the thrombin substrate binding pocket and bound TM. The $170s_{CT}$, $180a_{CT,}$ and $220s_{CT}$ loops that participate in the formation of the primary substrate binding pocket of thrombin showed the greatest changes in HD exchange when the W215A/E217A mutations were present. It is expected that residues $212\text{-}227_{CT}$ ($260\text{-}275_{seq}$) of the thrombin $220s_{CT}$ loop would show a difference between WT and the W215A/E217A mutant, because these mutations remove a large hydrophobic side chain and an

acidic side chain, which both have different intrinsic exchange rates compared to Ala [98]. However, the differences in intrinsic exchange rates are <1 deuteron between the WT and mutant residues, and as a result cannot provide an explanation for the ~3 deuteron difference in exchange within residues 212-227$_{CT}$ (260-275$_{seq}$) between the mutant and WT thrombin. Similarly, the side chains of Trp 215$_{CT}$ and Glu 217$_{CT}$ make contacts with Ile 172$_{CT}$ and Thr 174$_{CT}$ in the crystal structures of both WT thrombin in the absence and presence of TM456 [25, 27], so it is unsurprising that the thrombin 170s$_{CT}$ and 220s$_{CT}$ loops showed increased dynamics with the W215A/E217A mutations. However, the observation that the 180s$_{CT}$ loop was also affected by these mutations suggests that these three loops are structurally linked.

There is significant evidence demonstrating that the WT thrombin residues in the 170s$_{CT}$, 180s$_{CT}$, and 220s$_{CT}$ loops are important to the structural and functional integrity of this region of thrombin. Crystal structures of thrombin containing Y225P, D221A/D222K, and W215A/E217A mutations showed dramatic changes in the architecture of these two loops such as the closing of the S1 pocket, and mutations in these loops showed a loss of Na^+ binding between the 180$_{CT}$ and 220s$_{CT}$ loops [9, 31, 77, 99]. Similarly, HDX-MS experiments measuring the changes that result from the mutation of Trp 215$_{CT}$ alone showed that the 170s$_{CT}$ and 220s$_{CT}$ loops exhibit increased dynamics when a residue with less hydrophobic character than Trp is present at position 215$_{CT}$ [8].

An analysis of both the WT thrombin crystal structure without TM456 (PDB ID: 1PPB[4]) and with TM456 (PDB ID: 1DX5[25]) identified side chain interactions involving residues 172$_{CT}$ (213$_{seq}$), 174$_{CT}$ (215$_{seq}$), 187$_{CT}$ (233$_{seq}$), 215$_{CT}$ (263$_{seq}$),

217_{CT} (265_{seq}), 221_{CT} (268_{seq}), 222_{CT} (270_{seq}), and 224_{CT} (272_{seq}) that link the $170s_{CT}$, $180a_{CT,}$ and $220s_{CT}$ loops. We recently used NMR CPMG experiments to identify the residue-specific changes in µs-ms motions that occur in thrombin when TM456 binds (chapter II), and the results identified residues 172_{CT} (213_{seq}), 174_{CT} (215_{seq}), 187_{CT} (233_{seq}), 189_{CT} (235_{seq}), 217_{CT} (265_{seq}), 219_{CT} (266_{seq}), 221_{CT} (268_{seq}), and 222_{CT} (270_{seq}) as moving less on the µs-ms timescale when TM456 was present compared to apo-thrombin (Figure 4.7). The results of these CPMG experiments suggest that TM binding allosterically stabilizes the dynamics of the $170s_{CT}$, $180a_{CT,}$ and $220s_{CT}$ loops through the sidechain interactions formed by residues in these loops, which is in agreement with the HDX-MS results for WT thrombin presented here. Ala scanning mutagenesis showed significant increases in the Na^+ binding affinity of thrombin when residues 172_{CT} (213_{seq}), 187_{CT} (233_{seq}), 189_{CT} (235_{seq}), 215_{CT} (263_{seq}), 217_{CT} (265_{seq}), 222_{CT} (270_{seq}), and 224_{CT} (272_{seq}) were mutated [9], which suggests that the $180s_{CT}$ and $220s_{CT}$ loops experience dramatic structural changes as a result of these mutations. Thus, mutation of the residues that link the $170s_{CT}$, $180a_{CT,}$ and $220s_{CT}$ loops appears to reduce the structural integrity of these loops, while the binding of TM to thrombin reduces their conformational flexibility in preparation for the binding of protein C.

TM binding partially recovers the destabilizing effects of the W215A/E217A mutations. The crystal structure of W215A/E217A thrombin shows a collapsed S1 pocket [79], suggesting that the destabilizing effect of these mutations establishes a different ground-state structure than WT thrombin. This provides an explanation for why W215A/E217A thrombin shows poor activity towards procoagulative

substrates, but does not explain why this mutant retains notable activity towards protein C [89]. Multiples studies have shown that the W215A/E217A thrombin mutant requires the presence of TM to exhibit anticoagulative activity [88, 89, 95], indicating that the binding of TM must recover the catalytic activity of this mutant thrombin. Though NMR CPMG experiments showed TM binding stabilizes the $170s_{CT}$, $180a_{CT,}$ and $220s_{CT}$ loops of WT thrombin, the HDX-MS results presented here show that the W215A/E217A mutations render these thrombin loops insensitive to TM binding.

The question of how TM binding can promote the catalytic function of thrombin despite the W215A/E217A mutations may be answered by looking at the regions of this mutant that remain sensitive to TM binding. Residues $16\text{-}23_{CT}$ ($37\text{-}44_{seq}$) at the N-terminus of the heavy chain showed increased protection from H/D exchange when TM456 was present, though the degree of protection was less for the W215A/E217A mutant than for WT thrombin. The N-terminal residue of the heavy chain, Ile 16_{CT} (37_{seq}), is known to play an important role in preparing thrombin for its catalytic role through its insertion into the Ile cleft following the proteolytic conversion of prothrombin to α-thrombin [28, 29]. Ile 16_{CT} (37_{seq}) interacts with the backbone of Asp 189_{CT} (235_{seq}), and participates in sidechain interactions with the residues that make up the hydrophobic core of the C-terminal β-barrel in both the crystal structure of thrombin (PDB ID: 1PPB[4]) and of thrombin-TM456 (PDB ID: 1DX5[25]). The amine at the N-terminus of the heavy chain is also known to help coordinate the formation of the oxyanion hole through interactions with the sidechain of Asp 194_{CT} (240_{seq}) [28-30]. The residues at the N-terminus of the heavy chain have been shown to be relatively dynamic, but these residues show a

protection from H/D exchange when TM456 is bound [18] both in WT thrombin and in the W215A/E217A mutant. Thus, the allosteric effect of TM on the thrombin active site is not abolished by the W215A/E217A mutations, allowing TM to continue mediate the structural organization of the thrombin active site.

Residues 66-84$_{CT}$ (97-116$_{seq}$) spanning the 70s loop and residues 106-114$_{CT}$ (139-147$_{seq}$) (Figure 4.2; MH+ 1061.654) of the N-terminal β-barrel also demonstrated a sensitivity to TM456 binding to thrombin. While the W215A/E217A mutations affected the dynamics of residues 66-84$_{CT}$ (97-116$_{seq}$) in response to TM456 binding, residues 106-114$_{CT}$ (139-147$_{seq}$) were not at all perturbed by these mutations. NMR CPMG experiments showed that residues from both of these regions were participants in a second allosteric pathway utilized by TM to impart changes in the dynamics from the 70s$_{CT}$ loop to the thrombin active site (Chapter II). The results presented here suggest that TM456 binding allosterically stabilizes residues 106-114$_{CT}$ (139-147$_{seq}$) of both WT and W215A/E217A thrombin. NMR CPMG results showed that TM456 also induces motions on multiple timescales through the β-strand containing residues 105-108$_{CT}$ (139-141$_{seq}$) to the catalytic Asp 102$_{CT}$ (135$_{seq}$). We proposed that the residue dynamics induced by TM456 in this region were important for the conformational flexibility required by the thrombin active site to follow through with the diverse steps of the serine protease catalytic mechanism, suggesting that TM is a key catalytic activator of thrombin (Chapter II).

Though TM binding is able to allosterically enhance the catalytic function of thrombin through its effect on the N-terminus of the heavy chain and the N-terminal β-barrel despite the W215A/E217A mutations, this explanation for the activity of

W215A/E217A mutant thrombin towards protein C cannot reconcile the presence of a closed S1 pocket in the W215A/E217A crystal structure [79]. The data presented here show that TM binding does not influence the loops that compose the S1 pocket of the W215A/E217A mutant. The fact that the double mutant has markedly increased dynamics in this region disagrees with a model that suggests these mutations stabilize a state containing a closed S1 pocket.

Instead, the loss in activity of the W215A/E217A mutant towards fibrinogen compared to WT thrombin appears to mostly be the result of the mutation of W215A, which by itself causes a 500-fold loss in activity towards fibrinogen [89]. The W215A and W215A/E217A mutants are described as anticoagulative thrombin mutants because they only result in a 3-fold and 7-fold loss in activity towards protein C despite the much larger impact of these mutations on the activity of thrombin towards fibrinogen. If these mutations stabilized a closed S1 pocket as suggested by the crystal structure of W215A/E217A, then the expectation would be that the activity towards all thrombin substrates would be similarly impacted. More importantly, a collapsed structure would be expected to have reduced HD exchange whereas we observed increased HD exchange in the $170s_{CT}$, $180a_{CT,}$ and $220s_{CT}$ loops due to the mutations. When taken together, the dramatic loss of activity towards fibrinogen is likely the result of the removal of Trp 215_{CT} (265_{seq}) as a key residue involved in the recognition of these thrombin substrates [60], rather than a collapse of the active site. The 7-fold loss in activity of the W215A/E217A mutant towards protein C is likely the result of the increased disorder of the $170s_{CT}$, $180a_{CT,}$

and $220s_{CT}$ loops due to the loss of the structurally-stabilizing side chains of Trp 215_{CT} (265_{seq}) and Glu 217_{CT} (267_{seq}).

E. Materials and Methods

Thrombin expression and purification. The W215A/E217A mutant thrombin plasmid was created through site-directed mutagenesis using primers from Integrated DNA Technologies. W215A/E217A and WT thrombin plasmids were expressed and refolded from *E. coli* as previously described [15, 17]. The final step is purification of the refolded pre-thrombin on a HiLoadS column with an NaCl gradient. After diluting the resulting thrombin solution to 50 mL with 50 mM Tris/HCl pH 7.4, 20 mM $CaCl_2$, 1 mg/mL PEG8000, and 5% (v/v) glycerol, activation of WT thrombin was facilitated by the addition of *E. carinatus* venom (Sigma-Aldrich Car. #V8250) for 2-10 hr at room temperature. To activate W215A/E217A thrombin, the pooled HiLoadS fractions corresponding to correctly-folded W215A/E217A was diluted by a factor of 2 with 50 mM Tris/HCl pH 7.4, 20 mM $CaCl_2$, 1 mg/mL PEG8000, and 5% (v/v) glycerol before the *E. carinatus* venom was added. After the W215A/E217A sample was left to rock for 3 hr with *E. carinatus* venom, previously purified α-thrombin was added to a molar ratio of 1:30 WT:W215A/E217A and was left to rock for 12-16 hr at 30 ºC to convert the meizothrombin species formed to α-thrombin. After activation, the WT α-thrombin was inhibited with biotinyl-PPACK (Haematologic Technologies) followed by the addition of streptavidin resin (Thermo Scientific), and the biotinyl-PPACK-α-thrombin complex was removed via filtration.

The activated thrombin samples were loaded onto a MonoS cation exchange column (GE Healthcare Life Sciences), which was used to purify the α-thrombin species from the pre-thrombin-2 and meizothrombin as well as autopreoteolyzed (γ-thrombin) species using a gradient of 100 mM – 500 mM NaCl in 25 mM phosphate pH 6.5. The fully-active WT thrombin species (α-thrombin) eluted last off the MonoS column. WT α-thrombin eluted off the MonoS at ~340 mM NaCl, and W215A/E217A α-thrombin eluted at ~310 mM NaCl. Fractions containing the target α-thrombin species were pooled and stored at -80 ºC for no longer than 1 month before use. This method of thrombin purification has been shown to result in >95% α-thrombin, and previous NMR analysis of isotopically labeled thrombin prepared this way demonstrated that the species present was α-thrombin[15, 34].

Production of TM456. A modified TM456 species used for all thrombin-TM456 experiments described here. TM456m was generated from the TM456 gene, which had been previously synthesized using *E. coli*-optimized codons [24]. PCR mutagenesis was used to introduce a stop codon to terminate the protein sequence at G449 and to change Cys448 to Ser. Details of the expression vectors, transformation, and transformant selection of *Pichia pastoris* clones were all carried out as previously described [18, 24]. In brief, freshly purified TM456m-containing pPic9K expression plasmid was linearized using BglII, and introduced into spheroplasts of the *P. pastoris* protease resistant strain, SMD1168, to achieve multicopy insertion of the expression plasmid into the chromosomal DNA resulting in stable transformants. The multicopy transformants were selected by replica

plating on G418, a kanamycin analog that penetrates *P. pastoris*. The SMD1168 transformants that produced the highest levels of TM expression were stored as glycerol freezes at −80 °C.

P. pastoris transformant glycerol stocks were used to start growths in baffled shake-flasks according to previously published methods [24]. The TM456m proteins are secreted into the media, and initially captured by anion-exchange chromatography using a QAE Sephadex A-50 gravity column (4cm x 50 cm) at 4 ^{o}C using a gradient of 100-1000mM NaCl in 50 mM MES, pH 6.5. The protein is then further purified on a HiLoad 26/10 Q Sepharose High Performance column NEED Buffers etc. followed by reverse-phase C-18 HPLC using an acetonitrile gradient from 10 – 50% in 20mM NH_4OAc pH 5.65. The protein was lyophilized before being reconstituted in MilliQ H_2O and purified by Superdex 75 size-exclusion chromatography in 50 mM Tris 150 mM NaCl pH 7.4. Protein C activation assays (described below) were used at each step in the purification strategy to determine the highest activity fractions to be taken to the next step.

Protein C Activation Assays. Protein C activation assays were performed as previously described [24]. Briefly, a discontinuous assay for TM activation of thrombin towards protein C cleavage was performed by first incubating TM with human α-thrombin (Hematologic Technologies, Essex Junction, VT) for 10 min before adding human protein C (Hematologic Technologies, Essex Junction, VT). Following a 20 min incubation with protein C, the thrombin was inactivated by addition of heparin/antithrombin-III, and the activated protein C was assayed by addition of the

chromagenic substrate, S-2366 (Diapharma, West Chester, OH). The cleavage of the chromogenic substrate results in a linear increase in absorbance at 405 nm over time, which is proportional to the amount of activated protein C. TM is an essential activator of thrombin.

Hydrogen-Deuterium Exchange Mass Spectrometry. Purified WT and W215A/E217A α-thrombin samples were concentrated to 5 µM using pre-rinsed 6 mL 10K MWCO Vivaspin concentrators, spinning at 1000 x g in 5 min intervals at 4 ^{o}C. These apo-thrombin samples were passed through a 0.2 micron filter, and 130 µL of each was saved for the HDX-MS experiment. The remaining apo-thrombin samples were then concentrated to 10 µM, and 50 µL was used for peptide identification. To make the α-thrombin-TM456m complex for HDX-MS, purified TM456m was added to purified WT and W215A/E217A α-thrombin samples at a molar ratio of 1:10 thrombin:TM456m, which ensured 99% of thrombin would be bound to TM456m at the concentrations used in these experiments. These samples were left at 4 ^{o}C for 12-16 hr before being concentrated to 5 µM and 10 µM for the HDX-MS and ID runs respectively using 6 mL 3K MWCO Vivaspin concentrators, spinning at 3000 rpm in 15 min intervals at 4 ^{o}C.

HDX-MS was performed using a Waters Synapt G2Si system with HDX technology (Waters Corporation) [52]. Deuterium exchange reactions were prepared using a Leap HDX PAL autosampler (Leap technologies, Carrboro, NC). D_2O buffer was prepared by lyophilizing 1 mL of 250 mM phosphate pH 6.5 along with 850 mM NaCl for the apo-thrombin experiments and 1000 mM NaCl for the thrombin-

TM456m experiments, before being resuspended in 10 mL 99.96% D_2O immediately before use. Each deuterium exchange time point (0 min, 30 sec, 1 min, 2 min, and 5 min) was measured in triplicate. For each deuteration time point, 5 µL of protein was help at 25 ^oC for 5 min before being mixed with 55 µL of D_2O buffer, which ensured a concentration of 100 mM NaCl for both the apo and TM456-bound samples at the time of the HDX experiments. The NaCl concentration of 100 mm was selected because we found that HDX was more sensitive to thrombin dynamics at this concentration.

The deuterium exchange was quenched for 1 min at 1 ^oC by combining 50 µL of the deuteration reaction with 50 µL of 250 mM TCEP pH 2.5. The quenched sample was then injected into a 50 µL sample loop, followed by digestion and an in-line pepsin column (immobilized pepsin, Pierce, Inc.) at 15^oC. The resulting peptides were captured on a BEH C18 Vanguard pre-column, separated by analytical chromatography (Acquity UPLC BEH C18, 1.7 µM, 1.0 x 50 mm, Waters Corporation) using a 7-85% acetonitrile in 0.1% formic acid over 7.5 min, and electrosprayed into the Waters Synapt G2Si quadrupole time-of-flight mass spectrometer. The mass spectrometer was set to collect data in the Mobility, ESI^+ mode; mass acquisition range 200-2,000 (m/z); scan time 0.4 s. Continuous lock mass correction was accomplished with infusion of leu-enkephalin every 30 s (mass accuracy of 1 ppm for calibration standard). For peptide identification, the mass spectrometer was set to collect data in MS^E, mobility ESI+ mode instead. Peptides masses were identified from triplicate analyses of 10 µM α-thrombin, and data were analyzed using PLGS 2.5 (Waters Corporation). Peptides masses were identified

using a minimum number of 250 ion counts for low energy peptides and 50 ion counts for their fragment ions.

The peptides identified in PLGS were then analyzed in DynamX 3.0 (Waters Corporation). Additional filters in DynamX 3.0 included a cut-off score of 7, minimum products per amino acid of 0.2, maximum MH+ error tolerance of 5 ppm, retention time standard deviation of 5%, and requiring that the peptide be present in at least 2 of the 3 peptide identification runs. The final identified peptide data was then used to analyze the deuteration data. The deuterium uptake for each peptide was calculated by comparing the centroids of the mass envelopes of the deuterated samples vs. the undeuterated controls. For all HDX-MS data, at least 2 biological replicates were analyzed, each with 3 technical replicates. Data are represented as mean values +/- SEM of 3 technical replicates due to processing software limitations, however biological replicates were highly reproducible due to use of the LEAP robot for all experiments. The deuterium uptake was corrected for back-exchange using a global back exchange correction factor (typically 25%) determined from the average percent exchange measured in disordered termini of various proteins. ANOVA analyses and t tests with a p value cutoff of 0.05 implemented in the program, DECA, were used to determine the significance of differences between HDX data points [53].

The peptides reported on the coverage maps are actually those from which deuterium uptake data were obtained. Deuterium uptake plots were generated in DECA (github.com/komiveslab/DECA) and the data are fitted with an exponential curve for ease of viewing. Data were plotted in DECA as number of deuterons

incorporated vs. time (min). The Y-axis limit for each plot reflects the total possible number of amides within the peptide that can exchange. Each plot includes the peptide MH+ value, sequence, and sequential residue numbering. The HDX-MS data for WT apo-thrombin and thrombin-TM456 reported here are the same as reported in another study (Chapter II).

Chapter IV, in full, is a reprint that the dissertation author was the principal researcher and author of. The material has been submitted to *Biochemsitry*. Peacock RB, McGrann T, Zaragoza S, Komives EA. (2020). Mutation of W215A/E217A in Thrombin Interrupts the Allosteric Activity of Thrombomodulin. *Biochemistry*. (Submitted).

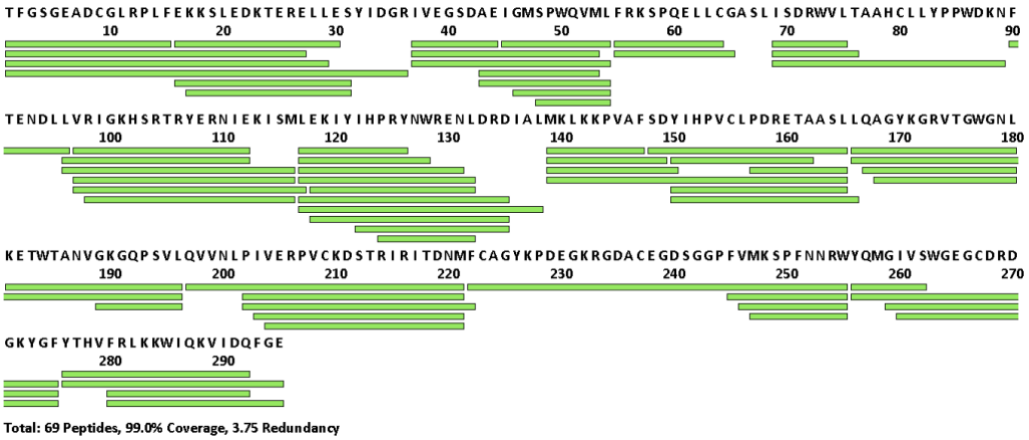

Figure 4.1. Coverage map showing the peptides identified and evaluated during HDX-MS experiments on WT thrombin and thrombin-TM456. The peptides identified are the same as those in Chapter 3.

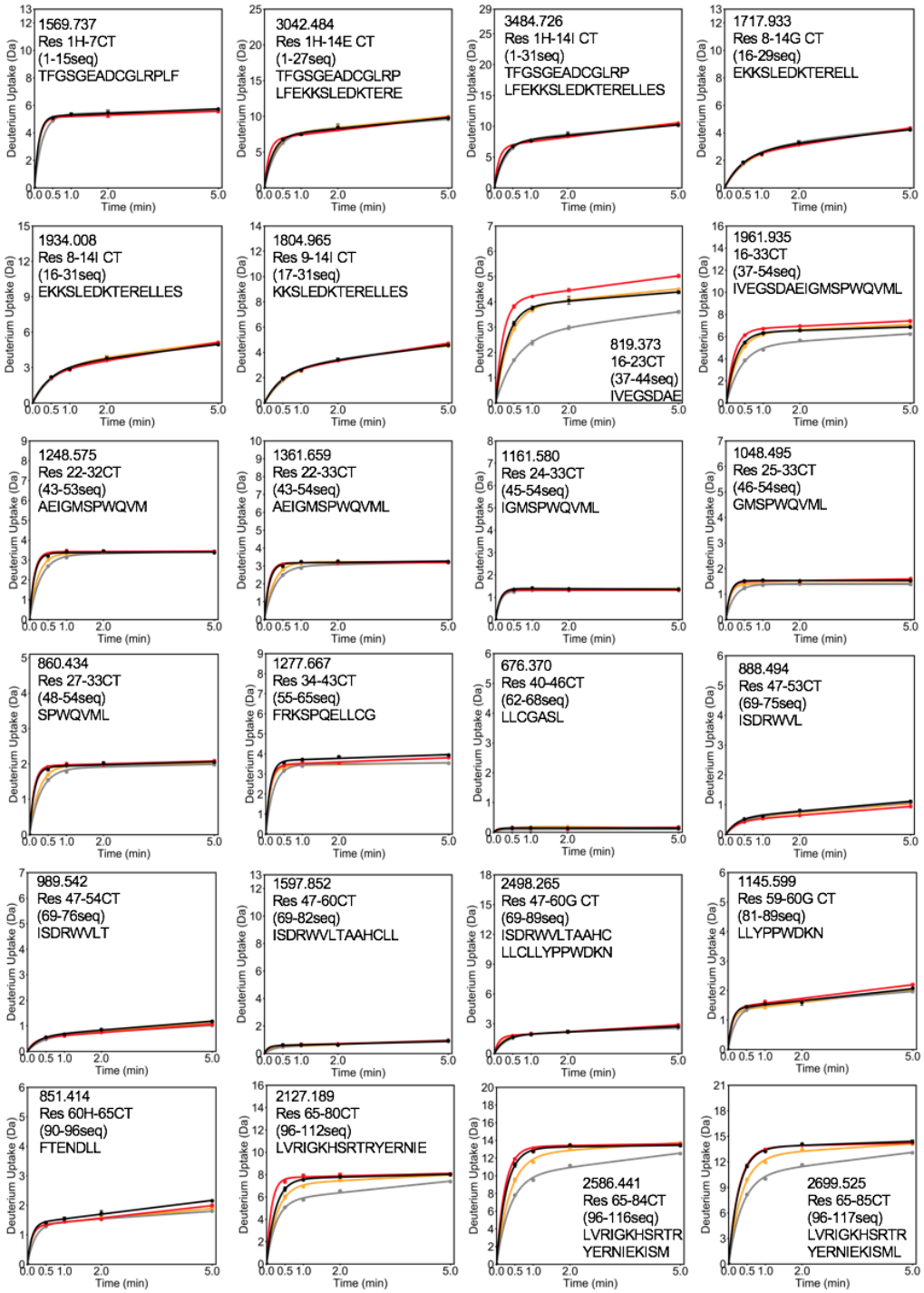

Figure 4.2. Relative deuterium uptake plots for all peptides identified through HDXMS on WT and W215A/E217A thrombin in the presence and absence of TM456. The red and orange curves are the results from W215A/E217A thrombin in the absence and presence of TM456 respectively, and the black and grey curves are WT thrombin in the absence and presence of TM456 respectively. Each HDS timepoint was run in triplicate, and error bars are shown.

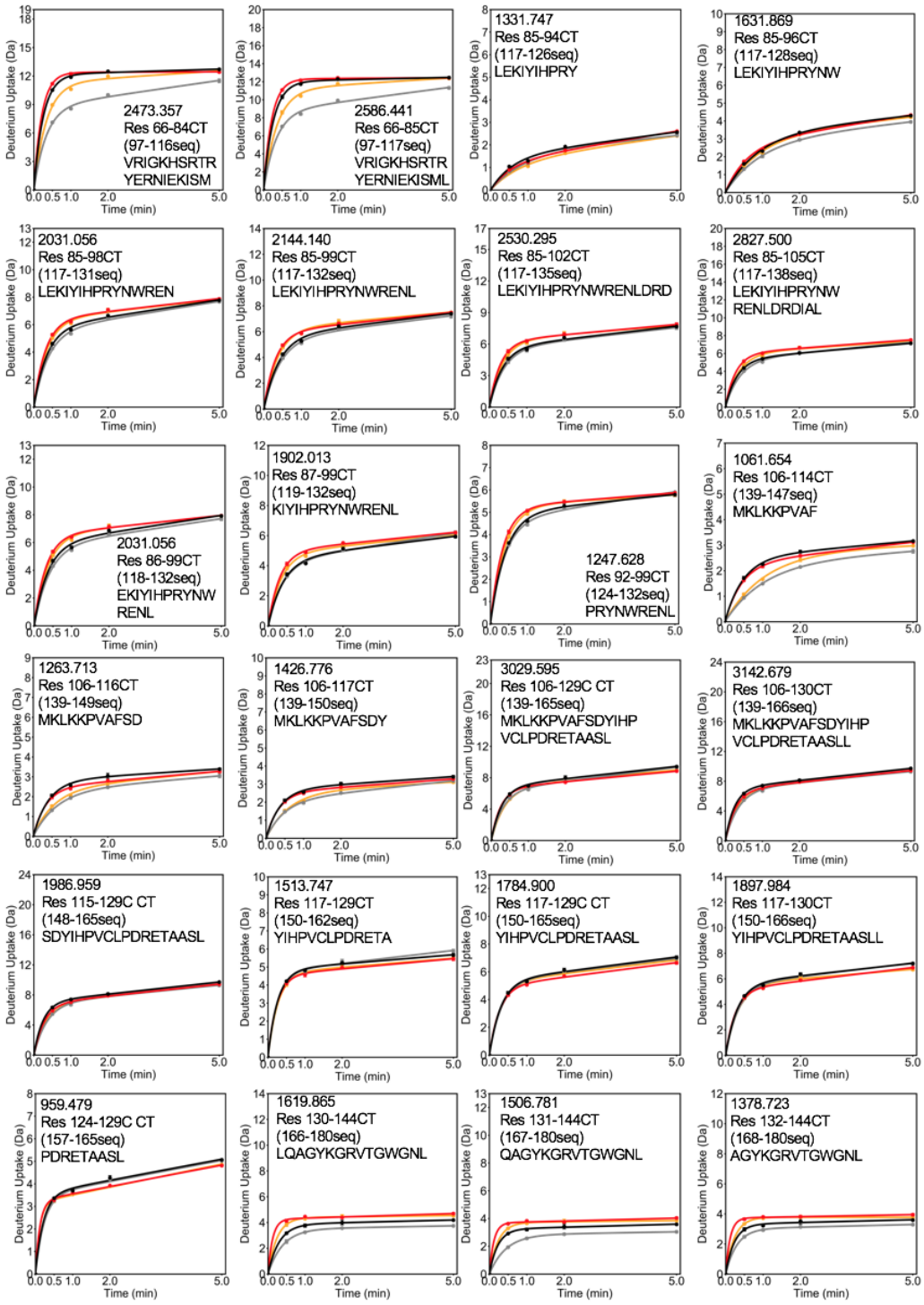

Figure 4.2 Continued. Relative deuterium uptake plots for all peptides identified through HDXMS on WT and W215A/E217A thrombin in the presence and absence of TM456. The red and orange curves are the results from W215A/E217A thrombin in the absence and presence of TM456 respectively, and the black and grey curves are WT thrombin in the absence and presence of TM456 respectively. Each HDS timepoint was run in triplicate, and error bars are shown.

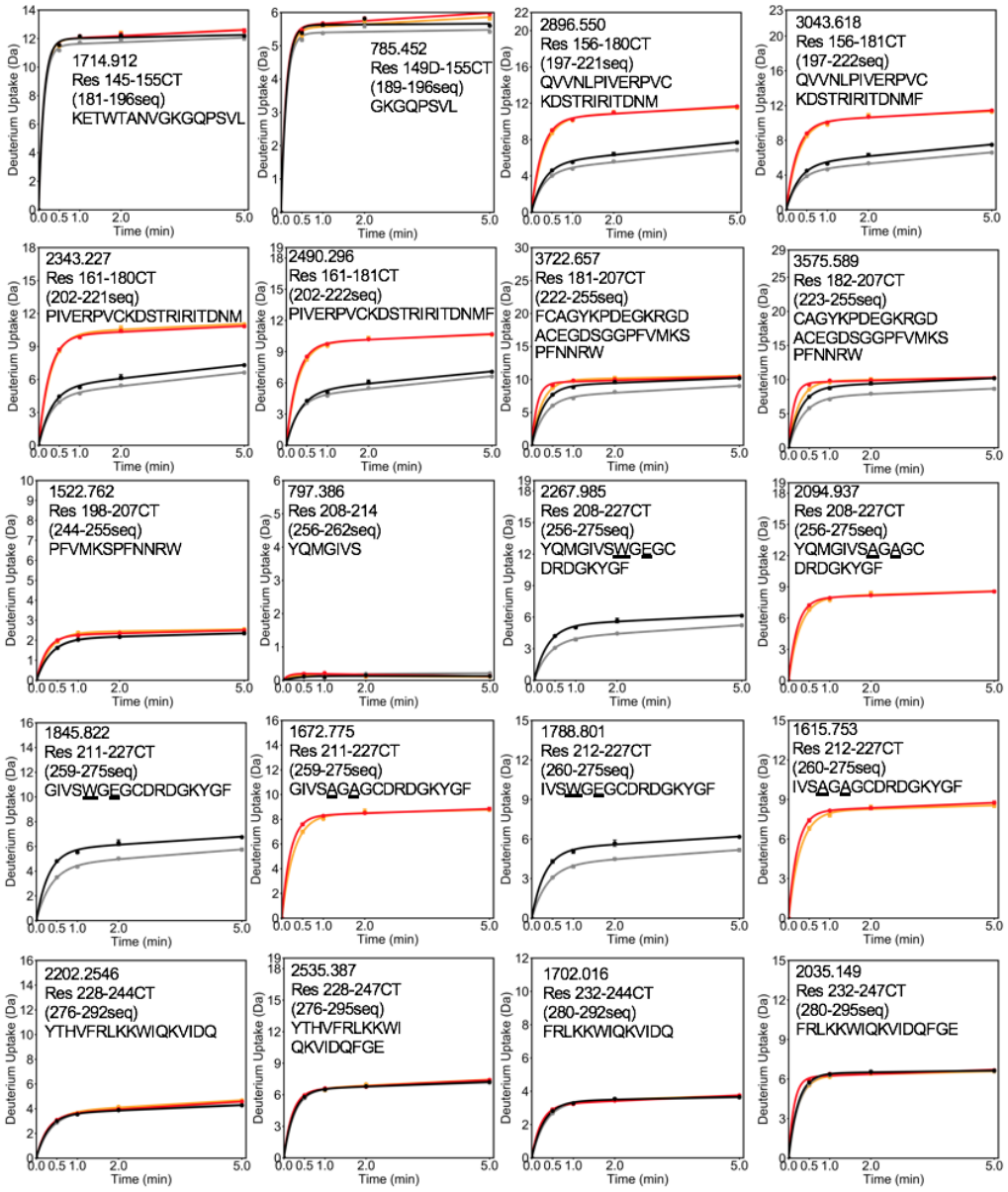

Figure 4.2 Continued. Relative deuterium uptake plots for all peptides identified through HDXMS on WT and W215A/E217A thrombin in the presence and absence of TM456. The red and orange curves are the results from W215A/E217A thrombin in the absence and presence of TM456 respectively, and the black and grey curves are WT thrombin in the absence and presence of TM456 respectively. Each HDS timepoint was run in triplicate, and error bars are shown.

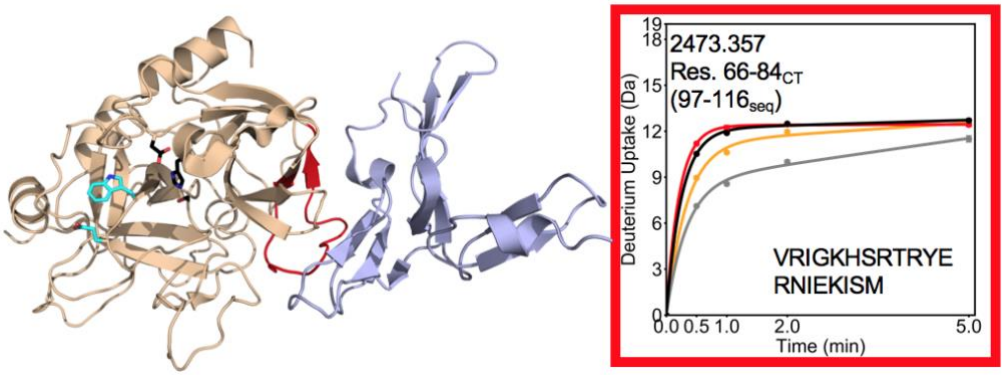

Figure 4.3. Crystal structure of thrombin (wheat) bound to TM456 (light blue) [PDB ID: 1DX5], and the HDXMS deuterium uptake plot for residues 66-84$_{CT}$ (97-116$_{seq}$; MH+ 2473.357) colored red on the structure. Sidechains are shown for the catalytic triad (black), and for Trp 215 and Glu 217 (cyan). The black and grey curves correspond to WT thrombin and WT thrombin-TM456, and the red and orange curved correspond to W215A/E217A thrombin and W215A/E217A-TM456 respectively. HDXMS error bars are shown.

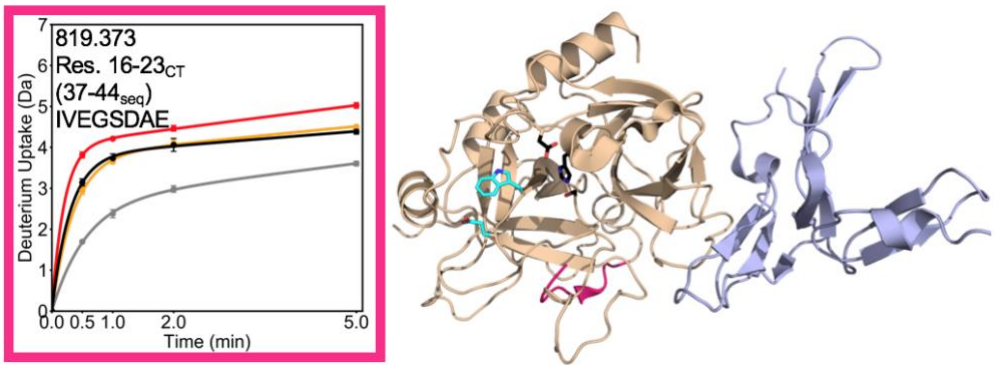

Figure 4.4. Crystal structure of thrombin (wheat) bound to TM456 (light blue) [PDB ID: 1DX5], and the HDXMS deuterium uptake plot for residues 16-23_{CT} (37-44_{seq}; MH+ 819.373) colored pink on the structure. Sidechains are shown for the catalytic triad (black), and for Trp 215 and Glu 217 (cyan). The black and grey curves correspond to WT thrombin and WT thrombin-TM456, and the red and orange curved correspond to W215A/E217A thrombin and W215A/E217A-TM456 respectively. HDXMS error bars are shown.

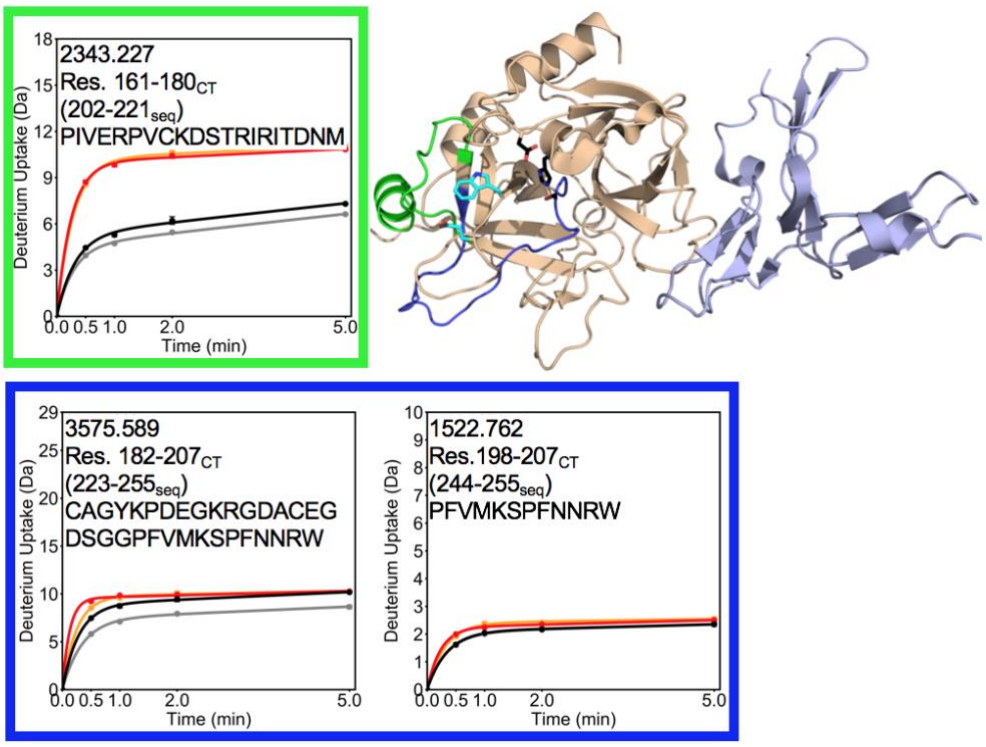

Figure 4.5. Crystal structure of thrombin (wheat) bound to TM456 (light blue) [PDB ID: 1DX5], and the HDXMS deuterium uptake plot for residues 161-180$_{CT}$ (202-221$_{seq}$; MH+ 2343.227) colored green and residues 182-197 (223-243$_{seq}$) are colored dark blue on the structure. Residues 182-197 (223-243$_{seq}$) correspond to the region of thrombin that showed an uptake difference between experiments when peptide subtraction is applied to residues 182-207$_{CT}$ (223-255$_{seq}$; MH+ 3575.589) and 198-207$_{CT}$ (244-255$_{seq}$; MH+ 1522.762). Sidechains are shown for the catalytic triad (black), and for Trp 215 and Glu 217 (cyan). The black and grey curves correspond to WT thrombin and WT thrombin-TM456, and the red and orange curved correspond to W215A/E217A thrombin and W215A/E217A-TM456 respectively. HDXMS error bars are shown.

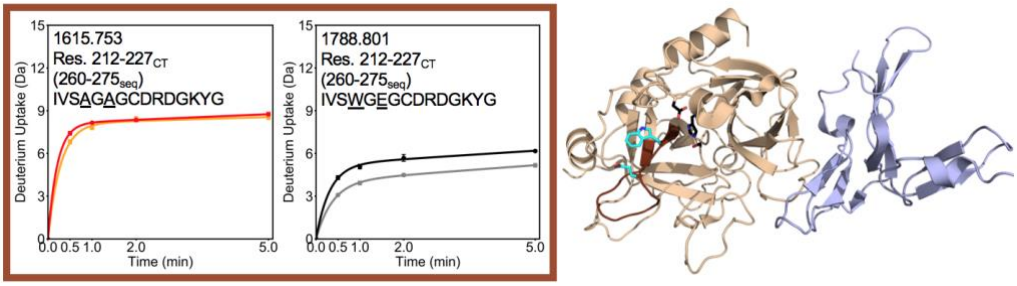

Figure 4.6. Crystal structure of thrombin (wheat) bound to TM456 (light blue) [PDB ID: 1DX5], and the HDXMS deuterium uptake plot for residues 212-227$_{CT}$ (260-275$_{seq}$) are colored brown on the structure. Because this region of thrombin contains residues 215 and 217, the uptake plots for WT (MH+ 1788.801) and W215A/E217A (MH+ 1615.553) are shown separately. Sidechains are shown for the catalytic triad (black), and for Trp 215 and Glu 217 (cyan). The black and grey curves correspond to WT thrombin and WT thrombin-TM456, and the red and orange curved correspond to W215A/E217A thrombin and W215A/E217A-TM456 respectively. HDXMS error bars are shown.

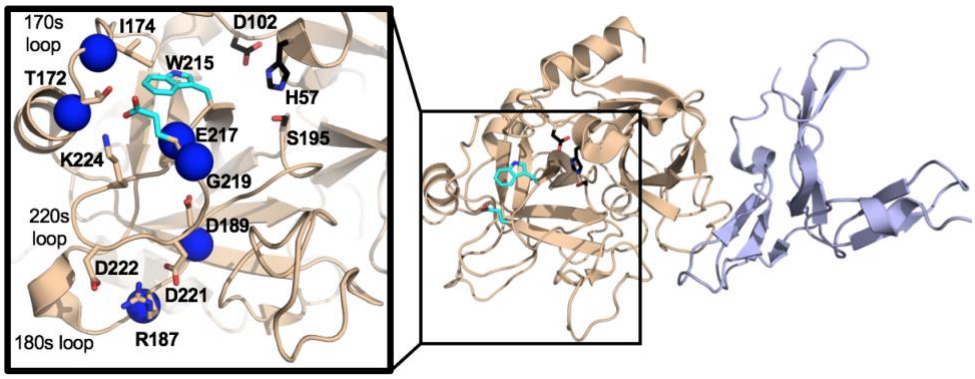

Figure 4.7. Crystal structure of Crystal structure of thrombin (wheat) bound to TM456 (light blue) [PDB ID: 1DX5] with a close-up view of the $170s_{CT}$, $180s_{CT}$, and $220s_{CT}$ loops (labeled). The sidechains of the catalytic triad (black) and $Trp215_{CT}$ $Glue217_{CT}$ (cyan) are shown as sticks. The sidechains of each residue involved in sidechain contacts between these loops are also shown as sticks. The backbone amides of residues that showed decreased μs-ms motions in CPMG experiments on thrombin with TM456 present compared to apo-thrombin are shown as blue spheres see Chapter 3. The residues with sidechains showing are labeled using the CT system. Residue 221_{CT} (268_{seq}) could not be assigned to HSQC resonances in the apo-thrombin nor thrombin-TM456 spectra, and the resonances for residues 215_{CT} (263_{seq}) and 222_{CT} (270_{seq}) were overlapped with other resonances in the thrombin-TM456m spectrum, so CPMG data could not be analyzed for these three residues. Residue 224_{CT} (272_{seq}) did not have an $R_{ex} > 6$ in the CPMG experiments on thrombin-TM456 nor apo-thrombin and was not considered a key residue involved in the allosteric communication between TM and the thrombin primary substrate binding pocket.

Chapter V

Final Thoughts and Future Directions

Utilizing NMR experiments to investigate the residue-specific changes in thrombin dynamics induced by TM was key to revelations that resulting from the work presented here. Investigations into the effect of substrate binding at ABE1 would offer key insights in distinguishing the effects of TM binding and the binding of procoagualtive thrombin substrates would be quite informative if probed using NMR methodologies. However, the difficulty in generating enough isotopically-labeled thrombin for an NMR sample remains a significant limitation to the proactive study of this enzyme by NMR. HDXMS experiments are significantly easier to perform when studying a protein that cannot be produced in mass quantities easily, but HDXMS results are complimentary to those produced by NMR and cannot replace the resolution offered by the later technique. Thus, future investigations into the modulation of thrombin dynamics and allostery by substrate binding should be designed with the use of both NMR and HDX methodologies in mind.

The model of thrombin-TM allostery presented as a result of this work is well informed by decades of published literature on thrombin and TM. However, more work is needed to define the limitations and amendments needed to more accurately describe the phenomena related to the thrombin-TM interaction. If, in fact, the s^{-1} dynamics observed throughout thrombin as a result of TM binding are in fact the consequence of subdomain conformational fluctuations, then single molecule fluorescence resonance energy transfer (FRET) experiments would be very informative. Donor/acceptor fluorescence probes strategically placed on the

thrombin subdomains would report on any conformational changes that result in differing motions between the subdomains.

The work presented here only investigated the role of Trp 215_{CT} and Glu 217_{CT} as residues involved in the allosteric communication between thrombin and TM. However, the NMR experiments conducted identified a number of other residues that should be probed for their contributions to thrombin allostery. Because the allosteric pathway linking the 70s loop to the catalytic Asp 102_{CT} is a novel discovery, the evaluation of mutant residues within this region would be an ideal set of follow-up experiments.

Lastly, the model presented through this work suggests that the motions induced in thrombin by TM are likely indicative of the motions required for a serine protease to effectively move through the reaction coordinate. To provide a clear comparison between the dynamics observed in thrombin when TM is present to the dynamics of less-regulated serine proteases, HDX and NMR experiments should be conducted on other proteases. These results would allow for the thrombin-specific dynamics to be distinguished from the generic serine protease dynamics, and would provide a clearer picture regarding the regulatory elements of the structure and sequence of thrombin.

References

[1] Krem, M. M., and Di Cera, E. (2001) Molecular markers of serine protease evolution, *Embo j 20*, 3036-3045.

[2] Di Cera, E. (2008) Thrombin, *Mol Aspects Med 29*, 203-254.

[3] Palta, S., Saroa, R., and Palta, A. (2014) Overview of the coagulation system, *Indian J Anaesth 58*, 515-523.

[4] Bode, W., Mayr, I., Baumann, U., Huber, R., Stone, S. R., and Hofsteenge, J. (1989) The refined 1.9 A crystal structure of human alpha-thrombin: interaction with D-Phe-Pro-Arg chloromethylketone and significance of the Tyr-Pro-Pro-Trp insertion segment, *Embo j 8*, 3467-3475.

[5] Esmon, C. T. (1992) The protein C anticoagulant pathway, *Arterioscler Thromb 12*, 135-145.

[6] Hedstrom, L. (2002) Serine Protease Mechanism and Specificity, *Chemical Reviews 102*, 4501-4524.

[7] Bah, A., Chen, Z., Bush-Pelc, L. A., Mathews, F. S., and Di Cera, E. (2007) Crystal structures of murine thrombin in complex with the extracellular fragments of murine protease-activated receptors PAR3 and PAR4, *Proc Natl Acad Sci U S A 104*, 11603-11608.

[8] Peacock, R. B., Davis, J. R., Markwick, P. R. L., and Komives, E. A. (2018) Dynamic Consequences of Mutation of Tryptophan 215 in Thrombin, *Biochemistry 57*, 2694-2703.

[9] Pineda, A. O., Carrell, C. J., Bush, L. A., Prasad, S., Caccia, S., Chen, Z. W., Mathews, F. S., and Di Cera, E. (2004) Molecular dissection of Na+ binding to thrombin, *J Biol Chem 279*, 31842-31853.

[10] Di Cera, E., Page, M. J., Bah, A., Bush-Pelc, L. A., and Garvey, L. C. (2007) Thrombin allostery, *Phys Chem Chem Phys 9*, 1291-1306.

[11] Lechtenberg, B. C., Freund, S. M., and Huntington, J. A. (2012) An ensemble view of thrombin allostery, *Biol Chem 393*, 889-898.

[12] Banfield, D. K., Irwin, D. M., Walz, D. A., and MacGillivray, R. T. (1994) Evolution of prothrombin: isolation and characterization of the cDNAs encoding chicken and hagfish prothrombin, *J Mol Evol 38*, 177-187.

[13] Süel, G. M., Lockless, S. W., Wall, M. A., and Ranganathan, R. (2003) Evolutionarily conserved networks of residues mediate allosteric communication in proteins, *Nat Struct Biol 10*, 59-69.

[14] Fuglestad, B., Gasper, P. M., McCammon, J. A., Markwick, P. R., and Komives, E. A. (2013) Correlated motions and residual frustration in thrombin, *J Phys Chem B 117*, 12857-12863.

[15] Fuglestad, B., Gasper, P. M., Tonelli, M., McCammon, J. A., Markwick, P. R., and Komives, E. A. (2012) The dynamic structure of thrombin in solution, *Biophys J 103*, 79-88.

[16] Gasper, P. M., Fuglestad, B., Komives, E. A., Markwick, P. R. L., and McCammon, J. A. (2012) Allosteric networks in thrombin distinguish procoagulant vs. anticoagulant activities, *Proceedings of the National Academy of Sciences 109*, 21216-21222.

[17] Handley, L. D., Fuglestad, B., Stearns, K., Tonelli, M., Fenwick, R. B., Markwick, P. R. L., and Komives, E. A. (2017) NMR reveals a dynamic allosteric pathway in thrombin, *Scientific Reports 7*, 39575.

[18] Handley, L. D., Treuheit, N. A., Venkatesh, V. J., and Komives, E. A. (2015) Thrombomodulin Binding Selects the Catalytically Active Form of Thrombin, *Biochemistry 54*, 6650-6658.

[19] Lechtenberg, B. C., Johnson, D. J., Freund, S. M., and Huntington, J. A. (2010) NMR resonance assignments of thrombin reveal the conformational and dynamic effects of ligation, *Proc Natl Acad Sci U S A 107*, 14087-14092.

[20] Treuheit, N. A., Beach, M. A., and Komives, E. A. (2011) Thermodynamic Compensation upon Binding to Exosite 1 and the Active Site of Thrombin, *Biochemistry 50*, 4590-4596.

[21] Xu, H., Bush, L. A., Pineda, A. O., Caccia, S., and Di Cera, E. (2005) Thrombomodulin changes the molecular surface of interaction and the rate of complex formation between thrombin and protein C, *J Biol Chem 280*, 7956-7961.

[22] Lane, D. A., Philippou, H., and Huntington, J. A. (2005) Directing thrombin, *Blood 106*, 2605-2612.

[23] Kurosawa, S., Stearns, D. J., Jackson, K. W., and Esmon, C. T. (1988) A 10-kDa cyanogen bromide fragment from the epidermal growth factor homology domain of rabbit thrombomodulin contains the primary thrombin binding site, *J Biol Chem 263*, 5993-5996.

[24] White, C. E., Hunter, M. J., Meininger, D. P., White, L. R., and Komives, E. A. (1995) Large-scale expression, purification and characterization of small fragments of thrombomodulin: the roles of the sixth domain and of methionine 388, *Protein Eng 8*, 1177-1187.

[25] Fuentes-Prior, P., Iwanaga, Y., Huber, R., Pagila, R., Rumennik, G., Seto, M., Morser, J., Light, D. R., and Bode, W. (2000) Structural basis for the anticoagulant activity of the thrombin-thrombomodulin complex, *Nature 404*, 518-525.

[26] Truhlar, S. M., Croy, C. H., Torpey, J. W., Koeppe, J. R., and Komives, E. A. (2006) Solvent accessibility of protein surfaces by amide H/2H exchange MALDI-TOF mass spectrometry, *J Am Soc Mass Spectrom 17*, 1490-1497.

[27] Matthews, B. W., Sigler, P. B., Henderson, R., and Blow, D. M. (1967) Three-dimensional structure of tosyl-alpha-chymotrypsin, *Nature 214*, 652-656.

[28] Bode, W., Schwager, P., and Huber, R. (1978) The transition of bovine trypsinogen to a trypsin-like state upon strong ligand binding. The refined crystal structures of the bovine trypsinogen-pancreatic trypsin inhibitor complex and of its ternary complex with Ile-Val at 1.9 A resolution, *J Mol Biol 118*, 99-112.

[29] Huber, R., and Bode, W. (1978) Structural basis of the activation and action of trypsin, *Accounts of Chemical Research 11*, 114-122.

[30] Stojanovski, B. M., Chen, Z., Koester, S. K., Pelc, L. A., and Di Cera, E. (2019) Role of the I16-D194 ionic interaction in the trypsin fold, *Sci Rep 9*, 18035.

[31] Dang, Q. D., Guinto, E. R., and Cera, E. D. (1997) Rational engineering of activity and specificity in a serine protease, *Nature Biotechnology 15*, 146-149.

[32] Esmon, N. L., Owen, W. G., and Esmon, C. T. (1982) Isolation of a membrane-bound cofactor for thrombin-catalyzed activation of protein C, *J Biol Chem 257*, 859-864.

[33] Kurosawa, S., Galvin, J. B., Esmon, N. L., and Esmon, C. T. (1987) Proteolytic formation and properties of functional domains of thrombomodulin, *J Biol Chem 262*, 2206-2212.

[34] Baerga-Ortiz, A., Rezaie, A. R., and Komives, E. A. (2000) Electrostatic dependence of the thrombin-thrombomodulin interaction, *J Mol Biol 296*, 651-658.

[35] Baerga-Ortiz, A., Bergqvist, S., Mandell, J. G., and Komives, E. A. (2004) Two different proteins that compete for binding to thrombin have opposite kinetic and thermodynamic profiles, *Protein Sci 13*, 166-176.

[36] Giladi, M., and Khananshvili, D. (2020) Hydrogen-Deuterium Exchange Mass-Spectrometry of Secondary Active Transporters: From Structural Dynamics to Molecular Mechanisms, *Front Pharmacol 11*, 70.

[37] Konermann, L., Pan, J., and Liu, Y. H. (2011) Hydrogen exchange mass spectrometry for studying protein structure and dynamics, *Chem Soc Rev 40*, 1224-1234.

[38] Kleckner, I. R., and Foster, M. P. (2011) An introduction to NMR-based approaches for measuring protein dynamics, *Biochim Biophys Acta 1814*, 942-968.

[39] Farber, P. J., and Mittermaier, A. (2015) Relaxation dispersion NMR spectroscopy for the study of protein allostery, *Biophys Rev 7*, 191-200.

[40] Huntington, J. A. (2008) How Na+ activates thrombin--a review of the functional and structural data, *Biol Chem 389*, 1025-1035.

[41] Lai, M. T., Di Cera, E., and Shafer, J. A. (1997) Kinetic pathway for the slow to fast transition of thrombin. Evidence of linked ligand binding at structurally distinct domains, *J Biol Chem 272*, 30275-30282.

[42] Adams, T. E., Li, W., and Huntington, J. A. (2009) Molecular basis of thrombomodulin activation of slow thrombin, *J Thromb Haemost 7*, 1688-1695.

[43] Mandell, J. G., Baerga-Ortiz, A., Akashi, S., Takio, K., and Komives, E. A. (2001) Solvent accessibility of the thrombin-thrombomodulin interface, *Journal of molecular biology 306*, 575-589.

[44] Vindigni, A., White, C. E., Komives, E. A., and Di Cera, E. (1997) Energetics of thrombin-thrombomodulin interaction, *Biochemistry 36*, 6674-6681.

[45] Myles, T., Church, F. C., Whinna, H. C., Monard, D., and Stone, S. R. (1998) Role of thrombin anion-binding exosite-I in the formation of thrombin-serpin complexes, *J Biol Chem 273*, 31203-31208.

[46] Rezaie, A. R., Cooper, S. T., Church, F. C., and Esmon, C. T. (1995) Protein C inhibitor is a potent inhibitor of the thrombin-thrombomodulin complex, *J Biol Chem 270*, 25336-25339.

[47] Rezaie, A. R., He, X., and Esmon, C. T. (1998) Thrombomodulin increases the rate of thrombin inhibition by BPTI, *Biochemistry 37*, 693-699.

[48] De Cristofaro, R., and Landolfi, R. (1999) Allosteric modulation of BPTI interaction with human alpha- and zeta-thrombin, *Eur J Biochem 260*, 97-102.

[49] van de Locht, A., Bode, W., Huber, R., Le Bonniec, B. F., Stone, S. R., Esmon, C. T., and Stubbs, M. T. (1997) The thrombin E192Q-BPTI complex reveals gross structural rearrangements: implications for the interaction with antithrombin and thrombomodulin, *Embo j 16*, 2977-2984.

[50] Zeymer, C., Werbeck, N. D., Zimmermann, S., Reinstein, J., and Hansen, D. F. (2016) Characterizing Active Site Conformational Heterogeneity along the Trajectory of an Enzymatic Phosphoryl Transfer Reaction, *Angew Chem Int Ed Engl 55*, 11533-11537.

[51] Berliner, L. J., Sugawara, Y., and Fenton, J. W. (1985) Human .alpha.-thrombin binding to nonpolymerized fibrin-sepharose: evidence for an anionic binding region, *Biochemistry 24*, 7005-7009.

[52] Wales, T. E., Fadgen, K. E., Gerhardt, G. C., and Engen, J. R. (2008) High-speed and high-resolution UPLC separation at zero degrees Celsius, *Anal Chem 80*, 6815-6820.

[53] Lumpkin, R., and Komives, E. A. (2019) DECA, a comprehensive, automatic post-processing program for HDX-MS data, *Molecular & Cellular Proteomics*, mcp.TIR119.001731.

[54] Takeda, M., Hallenga, K., Shigezane, M., Waelchli, M., Löhr, F., Markley, J. L., and Kainosho, M. (2011) Construction and performance of an NMR tube with a sample cavity formed within magnetic susceptibility-matched glass, *J Magn Reson 209*, 167-173.

[55] Carver, J., and Richards, R. (1972) A general two-site solution for the chemical exchange produced dependence of T2 upon the Carr-Purcell pulse separation, *Journal of Magnetic Resonance (1969) 6*, 89-105.

[56] Sugase, K., Konuma, T., Lansing, J. C., and Wright, P. E. (2013) Fast and accurate fitting of relaxation dispersion data using the flexible software package GLOVE, *J Biomol NMR 56*, 275-283.

[57] Bode, W. (2006) Structure and interaction modes of thrombin, *Blood Cells Mol Dis 36*, 122-130.

[58] Esmon, C. T. (2000) Regulation of blood coagulation., *Biochim Biophys Acta 1477*, 349-360.

[59] Arosio, D., Ayala, Y. M., and Di Cera, E. (2000) Mutation of W215 compromises thrombin cleavage of fibrinogen, but not of PAR-1 or protein C, *Biochemistry 39*, 8095-8101.

[60] Marino, F., Pelc, L. A., Vogt, A., Gandhi, P. S., and Di Cera, E. (2010) Engineering thrombin for selective specificity toward protein C and PAR1, *J Biol Chem 285*, 19145-19152.

[61] Ayala, Y., and Di Cera, E. (1994) Molecular recognition by thrombin. Role of the slow-->fast transition, site-specific ion binding energetics and thermodynamic mapping of structural components., *J Mol Biol 235*, 733-746.

[62] Koeppe, J. R., Seitova, A., Mather, T., and Komives, E. A. (2005) Thrombomodulin tightens the thrombin active site loops to promote protein C activation, *Biochemistry 44*, 14784-14791.

[63] Handley, L. D., Treuheit, N. A., Venkatesh, V. J., and Komives, E. A. (2015) Thrombomodulin binding selects the catalytically active form of thrombin, *Biochemistry 54*, 6650-6658.

[64] Cervantes, C. F., Markwick, P. R., Sue, S. C., McCammon, J. A., Dyson, H. J., and Komives, E. A. (2009) Functional dynamics of the folded ankyrin repeats of I kappa B alpha revealed by nuclear magnetic resonance., *Biochemistry 48*, 8023-8031.

[65] Kamenik, A. S., Kahler, U., Fuchs, J. E., and Liedl, K. R. (2016) Localization of millisecond dynamics: Dihedral entropy from accelerated MD., *J Chem Theory Comput 12*, 3449-3455.

[66] Hamelberg, D., Mongan, J., and McCammon, J. A. (2004) Accelerated molecular dynamics: a promising and efficient simulation method for biomolecules., *J Chem Phys 120*, 11919-11929.

[67] Markwick, P. R., and McCammon, J. A. (2011) Studying functional dynamics in bio-molecules using accelerated molecular dynamics., *Phys Chem Chem Phys 13*, 20053-20065.

[68] Markwick, P. R. L., Peacock, R. B., and Komives, E. A. (2019) Accurate Prediction of Amide Exchange in the Fast Limit Reveals Thrombin Allostery, *Biophys J 116*, 49-56.

[69] Di Cera, E., Guinto, E. R., Vindigni, A., Dang, Q. D., Ayala, Y. M., Wuyi, M., and Tulinsky, A. (1995) The Na+ binding site of thrombin, *J Biol Chem 270*, 22089-22092.

[70] Zhang, E., and Tulinsky, A. (1997) The molecular environment of the Na+ binding site of thrombin, *Biophys Chem 63*, 185-200.

[71] Kurisaki, I., Takayanagi, M., and Nagaoka, M. (2015) Toward Understanding Allosteric Activation of Thrombin: A Conjecture for Important Roles of Unbound Na+ Molecules around Thrombin, *J Phys Chem B 119*, 3635-3642.

[72] Xiao, J., Melvin, R. L., and Salsbury, F. R. (2017) Mechanistic insights into thrombin's switch between “slow” and “fast” forms, *Phys Chem Chem Phys 19*, 24522-24533.

[73] Kromann-Hansen, T., Lange, E. L., Sørensen, H. P., Hassanzadeh-Ghassabeh, G., Huang, M., Jensen, J. K., Muyldermans, S., Declerck, P. J., Komives, E. A., and Andreasen, P. A. (2017) Discovery of a novel conformational equilibrium in urokinase-type plasminogen activator, *Sci Rep 7*, 3385.

[74] Plattner, N., and Noé, F. (2015) Protein conformational plasticity and complex ligand-binding kinetics explored by atomistic simulations and Markov models, *Nat commun 6*.

[75] Gandhi, P. S., Chen, Z., Mathews, F. S., and Di Cera, E. (2008) Structural identification of the pathway of long-range communication in an allosteric enzyme, *Proc Natl Acad Sci U S A 105*, 1832-1837.

[76] Bah, A., Carrell, C. J., Chen, Z., Gandhi, P. S., and Di Cera, E. (2009) Stabilization of the E* form turns thrombin into an anticoagulant, *J Biol Chem 284*, 20034-20040.

[77] Niu, W., Chen, Z., Gandhi, P. S., Vogt, A. D., Pozzi, N., Pelc, L. A., Zapata, F., and Di Cera, E. (2011) Crystallographic and kinetic evidence of allostery in a trypsin-like protease, *Biochemistry 50*, 6301-6307.

[78] Niu, W., Chen, Z., Bush-Pelc, L. A., Bah, A., Gandhi, P. S., and Di Cera, E. (2009) Mutant N143P reveals how Na+ activates thrombin, *J Biol Chem 284*, 36175-36185.

[79] Pineda, A. O., Chen, Z. W., Caccia, S., Cantwell, A. M., Savvides, S. N., Waksman, G., Mathews, F. S., and Di Cera, E. (2004) The anticoagulant thrombin mutant W215A/E217A has a collapsed primary specificity pocket, *J Biol Chem 279*, 39824-39828.

[80] Gandhi, P. S., Page, M. J., Chen, Z., Bush-Pelc, L., and Di Cera, E. (2009) Mechanism of the anticoagulant activity of thrombin mutant W215A/E217A, *J Biol Chem 284*, 24098-24105.

[81] Fenton, J. W. (1986) Thrombin, *Annals New York Acad Sci 485*, 5-15.

[82] Hamelberg, D., de Oliveira, C. A., and McCammon, J. A. (2007) Sampling of slow diffusive conformational transitions with accelerated molecular dynamics., *J Chem Phys 127*, 155102.

[83] Miao, Y., Sinko, W., Pierce, L., Bucher, D., Walker, R. C., and McCammon, J. A. (2014) Improved Reweighting of Accelerated Molecular Dynamics Simulations for Free Energy Calculation., *J Chem Theory Comput 10*, 2677-2689.

[84] Fenton II, J. W. (1981) THROMBIN SPECIFICITY*, *Annals of the New York Academy of Sciences 370*, 468-495.

[85] Gibbs, C. S., Coutré, S. E., Tsiang, M., Li, W. X., Jain, A. K., Dunn, K. E., Law, V. S., Mao, C. T., Matsumura, S. Y., Mejza, S. J., and et al. (1995) Conversion of thrombin into an anticoagulant by protein engineering, *Nature 378*, 413-416.

[86] Tsiang, M., Jain, A. K., Dunn, K. E., Rojas, M. E., Leung, L. L., and Gibbs, C. S. (1995) Functional mapping of the surface residues of human thrombin, *J Biol Chem 270*, 16854-16863.

[87] Tsiang, M., Paborsky, L. R., Li, W. X., Jain, A. K., Mao, C. T., Dunn, K. E., Lee, D. W., Matsumura, S. Y., Matteucci, M. D., Coutré, S. E., Leung, L. L., and Gibbs, C. S. (1996) Protein engineering thrombin for optimal specificity and potency of anticoagulant activity in vivo, *Biochemistry 35*, 16449-16457.

[88] Tanaka, K. A., Gruber, A., Szlam, F., Bush, L. A., Hanson, S. R., and Di Cera, E. (2008) Interaction between thrombin mutant W215A/E217A and direct thrombin inhibitor, *Blood Coagul Fibrinolysis 19*, 465-468.

[89] Cantwell, A. M., and Di Cera, E. (2000) Rational design of a potent anticoagulant thrombin, *J Biol Chem 275*, 39827-39830.

[90] Gruber, A., Cantwell, A. M., Di Cera, E., and Hanson, S. R. (2002) The thrombin mutant W215A/E217A shows safe and potent anticoagulant and antithrombotic effects in vivo, *J Biol Chem 277*, 27581-27584.

[91] Gruber, A., Fernández, J. A., Bush, L., Marzec, U., Griffin, J. H., Hanson, S. R., and E, D. I. C. (2006) Limited generation of activated protein C during

infusion of the protein C activator thrombin analog W215A/E217A in primates, *J Thromb Haemost 4*, 392-397.

[92] Gruber, A., Marzec, U. M., Bush, L., Di Cera, E., Fernández, J. A., Berny, M. A., Tucker, E. I., McCarty, O. J., Griffin, J. H., and Hanson, S. R. (2007) Relative antithrombotic and antihemostatic effects of protein C activator versus low-molecular-weight heparin in primates, *Blood 109*, 3733-3740.

[93] Feistritzer, C., Schuepbach, R. A., Mosnier, L. O., Bush, L. A., Di Cera, E., Griffin, J. H., and Riewald, M. (2006) Protective signaling by activated protein C is mechanistically linked to protein C activation on endothelial cells, *J Biol Chem 281*, 20077-20084.

[94] Berny, M. A., White, T. C., Tucker, E. I., Bush-Pelc, L. A., Di Cera, E., Gruber, A., and McCarty, O. J. (2008) Thrombin mutant W215A/E217A acts as a platelet GPIb antagonist, *Arterioscler Thromb Vasc Biol 28*, 329-334.

[95] Vicente, C. P., Weiler, H., Di Cera, E., and Tollefsen, D. M. (2012) Thrombomodulin is required for the antithrombotic activity of thrombin mutant W215A/E217A in a mouse model of arterial thrombosis, *Thromb Res 130*, 646-648.

[96] Tucker, E. I., Verbout, N. G., Markway, B. D., Wallisch, M., Lorentz, C. U., Hinds, M. T., Shatzel, J. J., Pelc, L. A., Wood, D. C., McCarty, O. J. T., Di Cera, E., and Gruber, A. (2020) The protein C activator AB002 rapidly interrupts thrombus development in baboons, *Blood 135*, 689-699.

[97] Berny-Lang, M. A., Hurst, S., Tucker, E. I., Pelc, L. A., Wang, R. K., Hurn, P. D., Di Cera, E., McCarty, O. J., and Gruber, A. (2011) Thrombin mutant W215A/E217A treatment improves neurological outcome and reduces cerebral infarct size in a mouse model of ischemic stroke, *Stroke 42*, 1736-1741.

[98] Bai, Y., Milne, J. S., Mayne, L., and Englander, S. W. (1993) Primary structure effects on peptide group hydrogen exchange, *Proteins 17*, 75-86.

[99] Pineda, A. O., Zhang, E., Guinto, E. R., Savvides, S. N., Tulinsky, A., and Di Cera, E. (2004) Crystal structure of the thrombin mutant D221A/D222K: the Asp222:Arg187 ion-pair stabilizes the fast form, *Biophys Chem 112*, 253-256.